WAVE SPECTRAL TRANSFORMATION IN SHALLOW WATER

by

Yun-Hai Chen

and

Hsiang Wang

Technical Report No. 10

Contract No. N00014-81-K-0297

with the OFFICE OF NAVAL RESEARCH GEOGRAPHY PROGRAMS

Research Report CE-82-23

OCEAN ENGINEERING PROGRAM

DEPARTMENT OF CIVIL ENGINEERING
UNIVERSITY OF DELAWARE
NEWARK, DELAWARE
19711

WAVE SPECTRAL TRANSFORMATION

IN SHALLOW WATER

by

Yun-Hai Chen

and

Hsiang Wang

June, 1982

Technical Report No. 10

Contract No. N00014-81-K-0297

with the OFFICE OF NAVAL RESEARCH GEOGRAPHY PROGRAMS

Research Report CE-82-23

OCEAN ENGINEERING PROGRAM

DEPARTMENT OF CIVIL ENGINEERING
UNIVERSITY OF DELAWARE
NEWARK, DELAWARE
19711

TABLE OF CONTENTS

ACKNOWLEDGMENTS iii

LIST OF FIGURES vii

KEY TO SYMBOLS AND ABBREVIATIONS x

ABSTRACT xiii

CHAPTER 1

1. INTRODUCTION 1

1.1 Literature Review 2

1.2 Objectives 7

2. THEORY OF WAVE SPECTRAL TRANSFORMATION . . 10

2.1 Description of a Wave Field 10

2.2 Conservation of Energy Flux in Wave Spectral Transformation 16

2.3 Basic Equations for Wave Spectral Transformation 17

2.3.1 Wave Kinematics 17

2.3.2 Wave Dynamics 22

2.4 Specification of the G Functions . . 24

2.4.1 Wave Generation 24

2.4.1.1 Phillips' Resonant Mechanism . 25

2.4.1.2 Miles' Instability Mechanism . 28

2.4.2 Wave Dissipation 35

2.4.2.1 Bottom Friction 35

2.4.2.2 Wave Breaking 40

3. NUMERICAL SCHEME OF STATIONARY WAVE SPECTRAL TRANSFORMATION 43

3.1 Basic Equations for Stationary wave Spectral Transformation 43

3.2 Numerical Procedures 45

3.2.1 Wave Kinematics and Boundary Conditions 47

3.2.2 Wave Dynamics and Boundary Condition 53

3.3 Examples 55

3.3.1 Energy Flux Conservation Case . . 57

3.3.2 Bottom Friction Case 60

3.3.3 Local Wind Generation Case . . . 63

4. NUMERICAL SCHEME OF NON-STATIONARY WAVE SPECTRAL TRANSFORMATION 68

4.1 Basic Equations for Non-stationary Wave Spectral Transformation 68

4.2 Method of Solution 70

4.2.1 Two-Step Lax-Wendroff Scheme . . 70

4.2.2 Stability Analysis 73

4.2.2.1 Homogeneous Equation 73

4.2.2.2 Non-Homogeneous Equation . . 76

4.2.3 Numerical Dissipation and Dispersion Analysis 80

4.3 Numerical Analysis for Wave Conservation Equation 86

4.3.1 Numerical Procedures 86

4.3.2 Stability Analysis 90

4.3.3 Initial Condition and Boundary Conditions 91

4.4 Numerical Analysis for Energy Transport Equation 92

4.4.1 Numerical Procedures 92

4.4.2 Stability Analysis 94

4.4.3 Initial Condition and Boundary Conditions 96

4.5 Application in Monochromatic Wave . . 96

4.5.1 One-Dimensional Case 98

4.5.2 Two-Dimensional Case 105

5. RANDOM WAVE MODEL FOR NON-STATIONARY WAVE SPECTRAL TRANSFORMATION 112

5.1 Swell Wave Model 112

5.2 Wind Wave Model 116

5.3 Hybrid Wave Model 119

5.4 Comparison with the North Sea Field Data 122

6. SUMMARY AND CONCLUSIONS 135

REFERRENCES 142

LIST OF FIGURES

Figure 1.1 Schematic View of Ocean Environment

Figure 2.1 Schematic View of Nearshore Beach Terminology

Figure 2.2 Onshore Wind Blows over a Sloping Bottom

Figure 2.3 Offshore Wind Blows over a Sloping Bottom

Figure 2.4 Wind Blows over a Deep Uniform Bottom

Figure 3.1 Full Grid and Local Grid Description

Figure 3.2 Schematic View of Ocean Environment

Figure 3.3 Variation of Energy Spectrum in Energy Flux Conservation Case at Boundary, Location 5II and Location 2II

Figure 3.4 Variation of Energy Spectrum in Energy Flux Conservation Case at Boundary, Location 5II and Location 2II

Figure 3.5 Percentage Error of Spectral Density vs. Deviations of Wave Directions

Figure 3.6 Comparison between Energy Spectrum with and without Bottom Friction at Location 5II

Figure 3.7 Comparison between Energy Spectrum with and without Bottom Friction at Location 2II

Figure 3.8 Energy Spectrum of Local Wind at Location 5II and Location 2II

Figure 3.9 Comparison of Energy Spectrum of Local Wind at Location 5II and 2II with Pierson-Moskowitz Spectrum

Figure 4.1 Initial Lax-Friedrichs and the First Leap-Frog Scheme Solution Steps

Figure 4.2 General Leap-Frog Solution Scheme

Figure 4.3 Comparison between Exact and Approximate Solutions with Non-Homogeneous Term in nth Time Level in Leap-Frog Scheme

Figure 4.4 Comparison between Exact and Approximate Solutions with Non-Homogeneous Term in (n-1)th Time Level in Leap-Frog Scheme

Figure 4.5 Comparison of Exact and Numerical Solution for r=1/2

Figure 4.6 Dissipation and Dispersion for the Lax-Friedrichs Scheme

Figure 4.7 Dissipation and Dispersion for the Leap-Frog Scheme

Figure 4.8 Schematic View of a Two Dimensional Case

Figure 4.9 Variation of Wave Energy Decreasing with T=10sec, $\theta=0^\circ$ at Boundary, Location 5III and Location 2III

Figure 4.10 Variation of Wave Energy Decreasing with T=2.5sec, $\theta=0^\circ$ at Boundary, Location 5III and Location 2III

Figure 4.11 Variation of Wave Energy Increasing with T=10sec, $\theta=0^\circ$ at Boundary, Location 5III and Location 2III

Figure 4.12 Variation of Wave Energy Decreasing with T=10sec, $\theta=20^\circ$ at Boundary, Location 5III and Location 2III

Figure 4.13 Variation of Wave Angle Decreasing with T=10sec, $\theta=20^\circ$ at Location 5III and Location 2III

Figure 4.14 Variation of Wave Angle Decreasing with T=10sec, $\theta=-20^\circ$ at Location 5III and Location 2III

Figure 4.15 Variation of Wave Energy Increasing with T=10sec, $\theta=20^\circ$ at Boundary, Location 5III and Location 2III

Figure 4.16 Variation of Wave Angle Increasing with T=10sec, θ=20° at Location 5III and Location 2III

Figure 5.1 Schematic View of Ocean Environment

Figure 5.2 Variation of Energy Spectrum Decreasing due to Swell at Boundary, Location 5II and Location 2II

Figure 5.3 Variation of Energy Spectrum Increasing due to Swell at Boundary, Location 5II and location 2II

Figure 5.4 Time Changes of Wave Energy Spectrum in the Decrease of Swell of a Typhoon (After Ijima, 1957)

Figure 5.5 Variation of Energy Spectrum Increasing due to Wind Generation at Location 5II and Location 2II

Figure 5.6 Variation of Energy Spectrum due to Decrease of Swell and Increase of Wind Wave at Location 5II and Location 2II

Figure 5.7 Frequency Spectrum Indicating Wind Sea and Swell Peaks (After Long and Hasselmann, 1979)

Figure 5.8 MARSEN Wave Measurement Stations

Figure 5.9 Nearshore Field Instrument Arrangement

Figure 5.10 Wind Speed and Direction on september 24, 1979

Figure 5.11 Energy Spectrum and Mean Wave Direction at Deep Water at 12:14, September 24, 1979

Figure 5.12 Grid System used in the Computation

Figure 5.13 Comparison between Swell Wave Model from 13:14, Wind Wave Model from 8:00 and Field Data at 14:00 at Location 1225m

Figure 5.14 Comparison between Hybrid Wave Model and Field Data at 14:00 at Location 1225m

KEY TO SYMBOLS AND ABBREVIATIONS

$A(f)$	Frequency spectral density function
$A(f,\theta)$	Directional frequency spectral density function
a	Wave amplitude
B	Coefficient of Phillips' equilibrium spectrum
$B(\vec{r},\sigma)$	Cross spectral density function
C	Wave celerity
C_g	Wave group velocity
c_f	Bottom friction coefficient
c_o	Co spectrum
E	Total energy per unit surface area
$F(\vec{k})$	Wave number spectral density function
$F(k,\theta)$	Directional wave number spectral density function
f	frequency
G	Wave generation or dissipation function
g	Acceleration of gravity
h	Mean water depth
i	Mesh point in x-axis
j	Mesh point in y-axis
k	Wave number
L	Wave length

M	Number of space steps in x-axis
N	Number of space steps in y-axis
n	Mesh point in time axis
P	Pressure
$P(\vec{k},\sigma)$	Three dimensional spectrum of the random atomospheric pressure fluctuation
q	Quadrature spectrum
R	Co-variance function
$\vec{r}$	Vector space
Sxx	Radiation stress in xx direction
Sxy	Radiation stress in xy direction
Syy	Radiation stress in yy direction
T	Wave period
t	Time
Δt	Time step
U	Current velocity in x direction
Uc	Convection velocity of the the turbulent eddies with wave number k
u_b	Horizontal water partical velocity at the bottom
V	Current velocity in y direction
W	Wind velocity
x	Horizontal axis toward offshore direction
Δx	space step in x-axis
y	Horizontal axis toward alongshore direction
Δy	space step in y-axis

z	Vertical axis toward upward
θ	Wave direction
ρ_a	Density of air
ρ_w	Density of water
σ	Wave angular frequency
$\overline{\sigma}$	Wave angular frequency for stationary reference frame
ϕ	Phase function
δ	Angle between wind and wave
α	Phillips' resonant spectrum
β	Miles' instability spectrum
α'	Coefficient of Pierson-Moskowitz spectrum
β'	Coefficient of Pierson-Moskowitz spectrum
Φ	Total bottom friction of the wave field
η	Water surface displacement
τ	Time lag
τ_b	Bottom friction
Θ	Angular Distribution
μ	Coefficient for breaking
ϵ	Representation shown in Eq. (2.44)
Γ	Kitaigorodskii's modification factor

ABSTRACT

The purpose of this study is to develop a numerical method to compute shallow water wave spectral transformation both for stationary and non-stationary cases.

A numerical model for stationary wave spectral transformation has been developed by Shiau and Wang (1977) and further amplified by Wang and Yang (1981). The present work extends the model to add bottom friction and local wind generation. This model is applicable to wave spectral transformation under stationary meterological conditions. If the meterological condition is non-stationary in the generating area or the local wind effect in the domain of consideration can no longer be neglected, such as when a hurricane or storm sweeps through offshore of a coastal region, the wave spectral transformation in shallow water should also be treated as non-stationary. A non-stationary wave spectral transformation model is thus developed to handle these cases.

The non-stationary model consists of three sub-models; dealing respectively, with 1) swell transformation due to offshore wind variation without local wind generation, 2) wind wave transformation due to local wind generation, 3) hybrid condition that combines the swell and the wind wave transformations. The numerical results were compared with North Sea field data.

CHAPTER 1

INTRODUCTION

The need for a more realistic representation and accurate prediction to shallow water environment is increasing for both scientific and engineering purposes. It is also an accepted opinion that wave spectrum utilizing the ensemble of random surface oscillations provide a more realistic, and perhaps more accurate representation of ocean waves than a monochromatic wave train of single frequency. In the past, considerable efforts have been devoted to the development of deepwater wave spectra, to the extent that reasonable confidence can be placed in its applicability to describe wind generated ocean waves. To establish the wave climate in the coastal zone, as is often necessary for scientific and engineering purposes, the deepwater wave environment needs to be transformed into shallow water. It is in this area that both knowledge and effort are conspicuously lacking, although, odd as it may seem, the transformation of monochromatic wave trains is a

well-studied topic.

1.1 Literature Review

There exist a few attempts in the development of theoretical concepts and numerical techniques concerning wave spectral transformation from deep to shallow water.

Longuet-Higgins (1956,1957) considered the refraction of a wave spectrum having just two components. In one case, the two components consisted of two regular wave trains of the same wave number and travelling in slightly different directions. The effects of refraction on each other tend to increase the crest lengths, and to decrease the wave heights and the angle between the two components. Another case considered by Longuet-Higgins was a two component spectrum where the components were of slightly different wave numbers and both travelling in the same direction in deep water. In this case, the wave pattern which originally was long crested becomes short crested due to the different refraction of the two components.

Based on the radiative transfer equation, Barnett (1968) developed a method to predict the two-dimensional wind wave spectrum in the North Atlantic Ocean. The model takes account of wave generation by both resonance and instability mechanisms and wave dissipation by breaking. However, the shallow water effects such as refraction, bottom dissipation and the non-stationary wave conservation phenomenon are not involved. Therefore, the model is applicable to deep water only.

Based on the conservation of energy flux, Karlsson (1969) developed a method to compute spectral transformation for refraction over parallel bottom contours. The governing equation for the distribution of the continuous directional wave spectrum under steady state conditions in water of any depth was derived and its solution by finite difference techniques was presented.

Collins (1972) extended the work to the inclusion of bottom frictional effects and mentioned the application to an irregular bottom topography. However, his numerical scheme traced wave energy along wave rays, which made the computational procedure quite

impractical to determine shallow water wave spectra at designated locations in an area of irregular offshore bottom configuration.

Based on a geometrical-optical approximation, Krasitskiy (1974) has derived explicit analytical solutions for the spectral transformation over two-dimemsional parallel bottom contours. The solution he achieved took account of refraction and was applied to problems of spectral transformation due to diffractions.

Hasselmann (1976) developed a parametric model within which non-linear interactions are implicitly taken into account through the assumed shape of the spectrum represented by a limited number of parameters. Although the parametrization of the non-linear wave-wave interactions had been considered, shallow water phenomenon due to the interaction of surface waves with the bottom was not taken into account.

Shiau and Wang (1977) developed a numerical model to compute the stationary wave spectral transformation over irregular bottom topographies. It is based on the assumption that wave energy associated with a narrow frequency band stays within the band on

refraction when waves propagate from deep into shallow water.

Longuet-Higgins (1957), assuming a horizontal bottom, obtained an approximate solution of monochromatic wave in shoaling water. Yang and Chen (1979) further improved the solution by incorporating wave statistics. They showed that the transformation formula of random wave spectrum, based upon the asymptotic solution of Friedrichs' (1948) small beach slope case, was consistent with the approximation theory by Longuet-Higgins. In addition, they extended Stoker's (1947) sloping bottom solution from deterministic wave to a random wave field. Their solution was based on the consideration of stationary case only; the non-stationary case was not considered.

Gunther (1979) developed a numerical wave prediction model incorporating a parametrical wind-sea model and a characteristic swell model. However, the model doesn't include the shallow water effects such as refraction, bottom dissipation and also can not handle the changing wind effect.

Wang and Yang (1981) compared field results with the numerical computations for energy transformation in shallow water, based on the numerical model developed by Shiau and Wang (1977). The results suggested that, prior to wave breaking, the transformation of wave components is mainly influenced by shoaling and refraction. The bottom frictional effect could also be important in the energy-containing range. After breaking, turbulent generation due to wave instability seems to be the dominant mechanism of energy dissipation.

Based on the ray technique, Cavaleri and Rizzoli (1981) developed a wind wave prediction model in shallow water which included wave refraction, shoaling, generation, and dissipation (breaking and bottom friction). However, without considering the wave conservation equation, the swell condition can not be handled.

Vincent (1982) attempted to summarize the start state of art on shallow-water wave modeling by examining various factors that have been and that should be included in the model. The review was restricted to models using wave-ray methods. He

observed that a complete shallow water wave model should include 1) propagation with refraction and shoaling, 2) source mechanism due to atmosphereic input, 3) sink mechanism including bottom dissipation, bottom percolation and wave breaking and 4) non-linear wave-wave interactions.

1.2 Objectives

A major motivation of the present study is to develop an accurate method to predict wave spectral transformation in shallow water environment. The region of interest is depicted in Figure 1.1 which begins from the point shoreward of the generating area to the point before breaking. Two different approaches are used in the present work. The first method is based on Noda's (1974) relaxation finite difference scheme to solve the stationary wave spectral transformation in shallow water with the inclusion of bottom dissipation and local wind generation effects. The second method is using two-step Lax-Wendroff scheme to solve the non-stationary case of wave spectral transformation in shallow water.

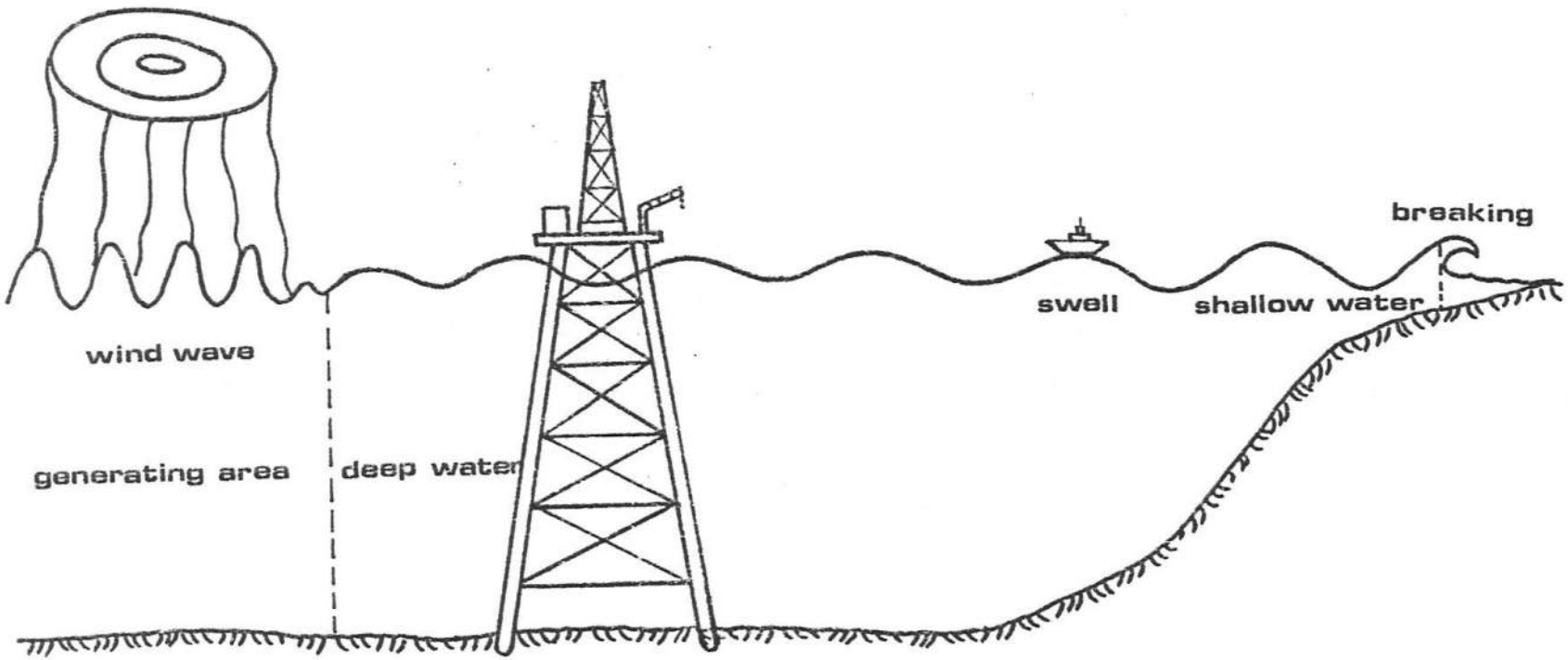

Figure 1.1 Schematic View of Ocean Environment

The stationary wave spectral transformation method is applicable to the energy spectral transformation under stationary meterological condition. However, if the meterological condition is non-stationary in the generating area and/or in the wave transformation area, the non-stationary wave spectral transformation method should be applied.

For the non-stationary wave spectral transformation method, it consists of three sub-models : 1) the swell model which handles non-stationary swell transformation without local wind generation, 2) the wind wave model which deals with the wave transformation due to wind generation effect, 3) the hybrid wave model that combines the swell wave model and the wind wave model to handle the mixed conditions. A set of field data recently collected along North Sea was compared with the numerical results.

CHAPTER 2

THEORY OF WAVE SPECTRAL TRANSFORMATION

As ocean surface waves propagate from deep to shallow water, significant changes occur in their characteristics. These changes include both wave kinematic and dynamic properties. Kinematically, the wave form obeys wave conservation, dispersion relation and wave refraction phenomena. Dynamically, the wave energy, hence the wave height, changes due to wave refraction, wave shoaling, wave generation, and wave dissipation. Thus, in considering wave transformation in shallow water, both wave kinematic and wave dynamic properties should conform to governing equations which are developed in this chapter.

2.1 Description of A Wave Field

The waves appearing on the surface of the sea are almost always random in the sense that the detailed configuration of the surface varies in an irregular manner in both space and time. Only the various

statistical measures of the motion can be regarded as significant observationally or predictable theoretically. Of these, the fundamental measure is the joint probability density of the variables concerned. In a homogeneous and stationary wave field, all the joint probability densities are spatially and time invariant except the addition of a constant space vector or a constant time scalar. If $\eta_1, \eta_2 \ldots, \eta_n$ are the ocean surface variations at n points, then the probability density function of η_s can be expressed as

$$\int_{-\infty}^{\infty} \cdots\cdots \int_{-\infty}^{\infty} P(\eta_1, \eta_2 \cdots \eta_n)\, d\eta_1\, d\eta_2 \cdots d\eta_n = 1 \qquad (2.1)$$

where

$P(\eta_1, \eta_2 \ldots \eta_n)$ is the probability density of the surface displacement.

$P(\eta_1, \eta_2 \ldots \eta_n)\, d\eta_1 d\eta_2 \ldots d\eta_n$ represents the probability that the surface displacements at the points $(x_1, t_1) \ldots (x_n, t_n)$.

i.e. the total probability is equal to 1.

It is usually convenient to measure the displacement η from the mean free surface level, so that the first moment (mean) of the probability density $P(\eta_r)$ becomes

$$\eta_r = \int_{-\infty}^{\infty} \eta_r\, P(\eta_r)\, d\eta_r = 0 \qquad (2.2)$$

for all r

where the overbar is used to denote the ensemble average.

The second moment (covariance) of the probability density $P(\eta_1, \eta_2)$ becomes

$$R(\vec{x}, \vec{r}; t, \tau) = \int_{-\infty}^{\infty} \int_{-\infty}^{\infty} \eta_1 \eta_2 P(\eta_1, \eta_2) \, d\eta_1 \, d\eta_2$$

$$= \overline{\eta(\vec{x}, t) \, \eta(\vec{x}+\vec{r}, t+\tau)} \qquad (2.3)$$

where the points 1,2 are taken as $(\vec{x},t)$, $(\vec{x}+\vec{r},t+\tau)$, respectively. In particular, the mean square surface displacement can be expressed by the covariance when both $\vec{r}=0$ and $\tau=0$, i.e.,

$$\overline{\eta^2}(x,t) = R(\vec{x}, o; t, o) = \int_{-\infty}^{\infty} \eta_1^2 \, p(\eta_1) \, d\eta_1 \qquad (2.4)$$

The wave spectrum $\chi(\vec{k}, \sigma)$ and the covariance $R(\vec{r},\tau)$ form a Fourier transform pair:

$$\chi(\vec{k},\sigma) = (2\pi)^{-3} \iint_{r\,\tau} R(\vec{r},\tau) \exp\left\{-i(\vec{k}\cdot\vec{r} - \sigma t)\right\} d\vec{r} \, d\tau \qquad (2.5)$$

and

$$R(\vec{r},\tau) = \iint_{\vec{k}\,\sigma} \chi(\vec{k},\sigma) \exp\left\{ i(\vec{k}\cdot\vec{r} - \sigma t)\right\} d\vec{k} \, d\sigma \qquad (2.6)$$

Equations (2.4) and (2.6) lead to

$$\overline{\eta^2} = \iint \chi(\vec{k},\alpha)\, d\vec{k}\, d\alpha = E \qquad (2.7)$$

where

$\vec{k}$ is wave number vector, $|\vec{k}| = k = \frac{2\pi}{L}$

$\alpha = 2\pi/T$, is wave angular frequency(rad/sec),

L is wave length,

T is wave period,

$E = \overline{\eta^2} = 1/2a^2$ (except for a factor ρg) is the total energy per unit surface area,

a is wave amplitude.

Therefore, $\chi(\vec{k},\alpha)$ can be interpretated as the spectral density function per unit surface area of wave number and angular frequency.

Reduced spectral density functions can be obtained from $\chi(\vec{k},\alpha)$ by integration over α or over $\vec{k}$. The wave number spectral density function is given by

$$F(\vec{k}) = \int_{-\infty}^{\infty} \chi(\vec{k},\alpha)\, d\alpha \qquad (2.8)$$

The angular frequency spectral density function is given by

$$A(\alpha) = \int \chi(\vec{k},\alpha)\, d\vec{k} \qquad (2.9)$$

The spectral density function $F(\vec{k})$ and $A(\sigma)$ can be considered as a descriptor of the sea in space (x,y) and time t, respectively. $F(\vec{k})$, for instance, is a five dimensional variables $F(k_1, k_2, x, y, t)$. The angular frequency spectral density function is also a five dimensional variables, $A(\sigma, \theta, x, y, t)$ with θ being the directional angle. Alternate forms of the energy density function can be shown as follows:

In directional wave-number spectrum,

$$F(k, \theta) = k F(k_1, k_2) \tag{2.10}$$

where

$$k_1 = k \cos\theta \quad \text{and} \quad k_2 = k \sin\theta$$

$$k = (k_1^2 + k_2^2)^{1/2} \quad \text{and} \quad \theta = \tan^{-1}\left(\frac{k_2}{k_1}\right)$$

In directional angular frequency spectrum

$$A(\sigma, \theta) = \frac{1}{C_g} F(k, \theta) \tag{2.11}$$

where $C_g = \frac{\partial \sigma}{\partial k}$ is the group velocity.

The directional frequency spectrum is

$$A(f,\theta) = 2\pi\, A(\sigma,\theta) \tag{2.12}$$

where f is wave frequency and $\sigma = 2\pi f$.

The one dimensional wave spectrum is:

$$A(f) = \int_{-\pi}^{\pi} A(f,\theta)\, d\theta \tag{2.13}$$

Therefore, the transformation between wave number spectrum and directional frequency spectrum becomes

$$F(k_1,k_2) = F(k) = \frac{C_g}{2\pi k}\, A(f,\theta) \tag{2.13a}$$

It is also noted that by definition.

$$\eta^2 = \int_{k_1}\int_{k_2} F(k_1,k_2)\, dk_1\, dk_2$$

$$= \int_f \int_\theta A(f,\theta)\, df\, d\theta \tag{2.13b}$$

Where $\overline{\eta^2}$ is the value of the mean square sea surface fluctuation. The directional frequency spectrum will be used throughout this text since it is easy to

calculate.

2.2 Conservation of Energy Flux in Wave Spectral Transformation

Let subscript O denote the reference state (deepwater condition is usually conveniently selected), the conservation equation of energy flux transformation is established. From equation (2.13), we have

$$A(f,\theta) = \frac{[K F(\vec{k})\, d\vec{k}]}{[K F(\vec{k})\, d\vec{k}]_o} [A(f,\theta)\, df]_o \qquad (2.14)$$

For steady state condition, the frequency f is invariant in space, the above equation simplifies to

$$A(f,\theta) = \frac{[K F(\vec{k})\, d\vec{k}]}{[K F(\vec{k})\, d\vec{k}]_o} A_o(f,\theta) \qquad (2.15)$$

since $F(\vec{k})d\vec{k}$ approximates the incremental of wave energy over the wave number band $d\vec{k}$, it is plausible to write

$$dE = F(\vec{k})\, d\vec{k} \qquad (2.16)$$

Substituting equation (2.16) into equation (2.15) results in

$$A(f,\theta) = \frac{[K\, dE]}{[K\, dE]_o} A_o(f,\theta) \qquad (2.17)$$

This transformation equation is not valid when wave generation and dissipation are involved. Also, it cannot be applied to unsteady state case because f is no longer space invariant. More details will be shown in the following sections.

2.3 Basic Equations for Wave Spectral Transformation

The basic equations for wave spectral transformation consist two parts: one is wave kinematics and the other is wave dynamics. In the derivations, wave reflection and non-linear wave-wave interactions are neglected.

2.3.1 Wave Kinematics

Starting with a progressive linear gravity wave, the free surface can be written as

$$\eta(x,y,t) = a(x,y,t)\cos\left\{\phi(x,y,t)\right\}$$

where a is the wave amplitude and $\phi = \vec{k}\cdot\vec{x} - \bar{\sigma}t$ is phase function.

A wave number vector can be defined as

$$\vec{k} = \vec{\nabla}\phi \qquad (2.18)$$

and a wave frequency scalar can be defined as

$$\bar{\sigma} = -\frac{\partial \phi}{\partial t} \tag{2.19}$$

Assuming $\phi(x,y,t)$ is continuous, then the order of differentiation are interchangeable;

$$\frac{\partial}{\partial t}(\vec{\nabla}\phi) = \vec{\nabla}\frac{\partial \phi}{\partial t} \tag{2.20}$$

Substituting Equation (2.18) and (2.19) into the above expression, it is found that

$$\frac{\partial \vec{k}}{\partial t} + \vec{\nabla}\bar{\sigma} = 0 \tag{2.21}$$

which is the classical conservation of wave equation. If no new waves are being created by a local disturbance, the rate of change of wave number is balanced by the convergence of the frequency, the number of wave crests passing a point per unit time, or the flux of waves. In a random wave field of linearly superposed waves, Equation (2.21) holds for each Fourier component but the simple geometrical interpretation is not possible. If the wave field is constant in time, then $\vec{\nabla}\bar{\sigma}=0$, or, the wave period does

not change with space. It remains constant even as the water depth changes.

In the presence of a steady current $\vec{u}=U\vec{i}+V\vec{j}$, it can be shown that the scalar frequency with respect to a stationary reference frame is

$$\overline{\sigma} = \sigma + \vec{k}\cdot\vec{u} \tag{2.22}$$

The wave frequency σ with respect to a moving reference frame is given by the dispersion relation,

$$\sigma^2 = gk \tanh kh \tag{2.23}$$

If it is also assumed that the wave number field changes slowly with time then from Equation(2.21)

$$\vec{\nabla}(\sigma + \vec{k}\cdot\vec{u}) = 0$$

or

$$\sigma + \vec{k}\cdot\vec{u} = \text{constant} \tag{2.24}$$

This constant can be evaluated for the case where $\vec{u}=0$ in which case $\sigma=2\pi/T$ where T is the wave period.

Equation (2.24) becomes

$$\sigma + \vec{k} \cdot \vec{u} = \frac{2\pi}{T}$$

or

$$(gk \tanh kh)^{1/2} + Uk\cos\theta + Vk\sin\theta = \frac{2\pi}{T} \qquad (2.25)$$

for the coordinate system shown in Figure 2.1. Here U and V are current velocity components in the x and y directions, respectively; is the wave approach angle measured from the positive x-axis.

Using the mathematical property that the curl of a gradient is identically zero, it is shown that

$$\vec{\nabla} \times \vec{\nabla} \phi = 0 \qquad (2.26)$$

which implies that

$$\vec{\nabla} \times \vec{k} = 0 \qquad (2.27)$$

This equation states that the wave number vector is irrotational. Using the coordinate in Figure 2.1, Equation (2.27) can be further decomposed to

$$\frac{\partial(k\cos\theta)}{\partial y} - \frac{\partial(k\sin\theta)}{\partial x} = 0 \qquad (2.28)$$

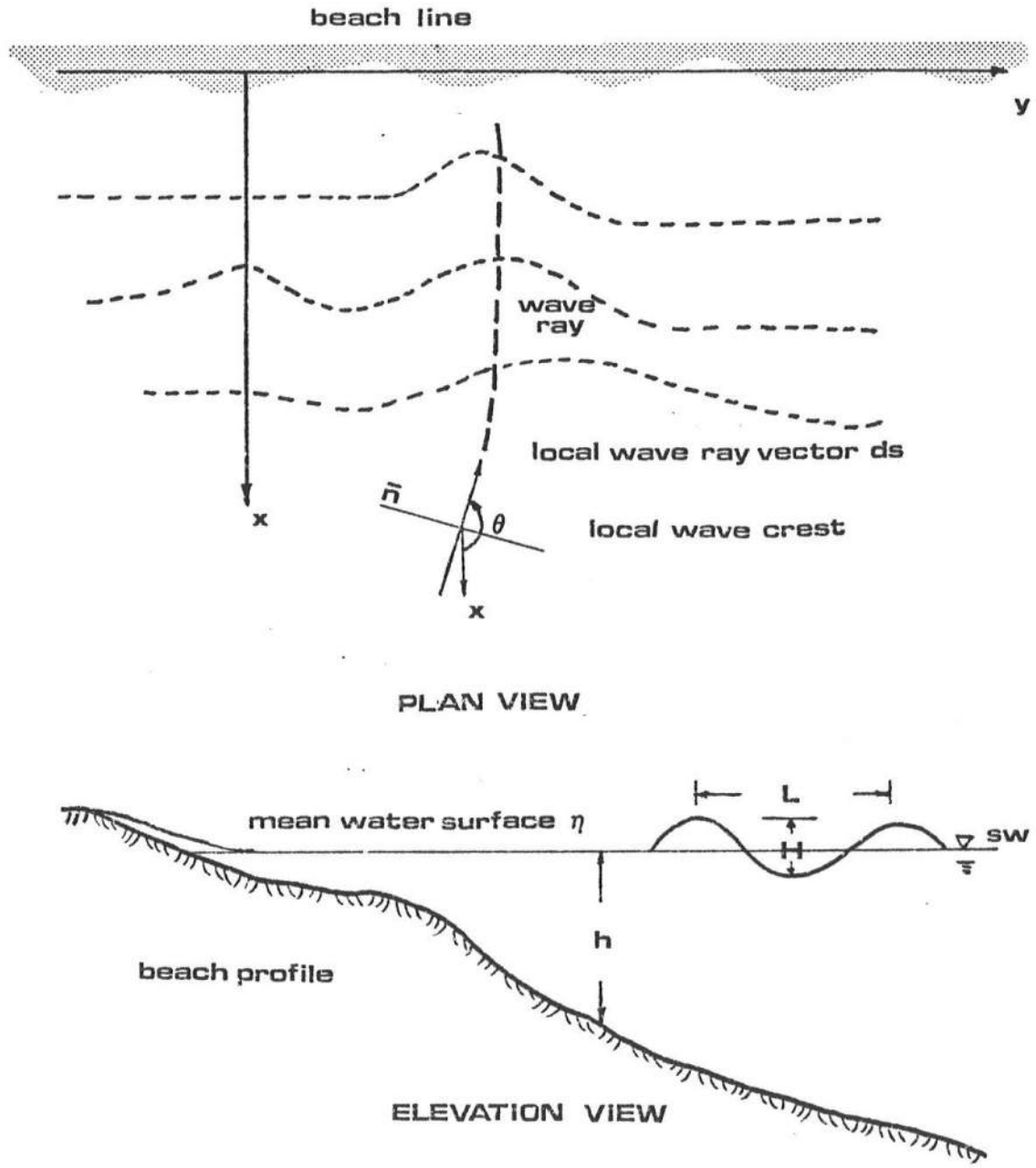

Figure 2.1 Schematic View of Nearshore Beach Terminology

For a shore line where the alongshore variations in the y direction of all variables are zero, that is, there are straight and parallel offshore contours, this equation yields Snell's law.

With known U, V, and h, the three unknown wave number k, angular frequency σ, and wave direction θ can be solved through Equations (2.21), (2.25) and (2.28). However, the kinematic conditions can not represent energy spectrum unless the dynamic condition is also considered.

2.3.2 Wave Dynamics

To determine the variation of A, the assumption is made that the wave energy associated with a certain frequency band stays within this band so that the linear superposition can be used. This assumption denies energy transfer among different frequencies and is compatible only when non-linear effects are negligible.

Gelci, et al. (1956), Hasselmann (1960), and Groves and Melcer (1961) have all independently proposed a transport equation which takes into account wave propagation as well as the processes of generation

and dissipation. However, the shoaling of waves is also affected by the interactions of waves and currents. The energy transport equation presented by Longuet-Higgins and Stewart (1960,1961) for the fluctuating motion of waves with a superimposed current system is

$$\frac{\partial A}{\partial t} + \frac{\partial}{\partial x}\left[A(U + C_g \cos\theta)\right] + \frac{\partial}{\partial y}\left[A(V + C_g \sin\theta)\right]$$

$$+ S_{xx}\frac{\partial U}{\partial x} + S_{xy}\frac{\partial U}{\partial y} + S_{yx}\frac{\partial V}{\partial x} + S_{yy}\frac{\partial V}{\partial y}$$

$$= \sum_{i=1}^{3} G_i \qquad (2.29)$$

where

A = A(f,θ,x,y,t) is directional frequency spectrum

G = G(f,θ,x,y,t) is a general representation of all processes which are adding or subtracting energy from the spectrum

Cg is the group velocity expressed as

$$C_g = nC = \frac{1}{2}\left(1 + \frac{2kh}{\sinh(2kh)}\right)$$

$C = \left(\frac{g}{k}\tanh kh\right)^{1/2}$ is the wave celerity

$S_{\alpha\beta}$ are the radiation stresses such that:

$S_{xx} = A((2n-1/2)\cos^2\theta + (n-1/2)\sin^2\theta) = A\Delta_{xx}$

$$Syy = A((2n-1/2)\sin^2\theta + (n-1/2)\cos^2\theta) = A\sigma yy$$

$$Sxy = Syx = An\cos\theta\sin\theta = A\sigma xy$$

The Equations (2.21), (2.25), (2.28) and (2.29) are the basic equations for wave spectral transformation.

2.4 Specification of the G-Functions

In Equation (2.29), G-Function represents all processes which are adding energy to or subtracting energy from the spectrum, i.e., source or sink function. The processes can be categorized into linear and nonlinear mechanism. The details are as follows.

2.4.1 Wave Generation

Based on the dynamics of the surface boundary layer, both the surface pressure and shear stress variations influence wave growth. One can see intuitively that the pressure fluctuations on the surface are of two kinds: those produced by the turbulent eddies in the wind and those induced by the air flow over the irregular water surface. At present, there are two prominant postulations on wind wave generations.

2.4.1 Phillips' Resonant Mechanism

In the resonance theory proposed by Phillips (1957), the turbulent atmospheric pressure fluctuations are seen as prime wave generators. It is first assumed that the ocean and the atmosphere are an uncoupled system. Provided the turbulent pressure spectrum is reasonably isotropic, the main condition for resonance is that $U_c \cos\delta = C(\sigma)$, where C is the phase velocity of wave with angular frequency σ, δ is the angle between wind and waves and U_c is the convection velocity of the turbulent eddies with wave number $\vec{k}$. This velocity is generally considered to be about equal to the mean wind velocity $\vec{W}$ at a distance $2\pi/k$ above the sea surface.

The Phillips mechanism calls for wave energy to grow linearly with time and should be particularly important for waves moving with approximately the same speed and direction as the wind. The coefficient of this linear growth will be denoted by the parameter $\alpha = \alpha(f, \theta, x, y, t)$. It has been shown by Hasselmann (1960) that

$$\alpha = \frac{4\pi^2 k \sigma^3}{\rho_w^2 g^3} P(\vec{k}, \sigma) \qquad (2.30)$$

where $P(\vec{k},\sigma)$ is the three dimensional spectrum of the random atmospheric pressure fluctuation, ρ_w is the density of sea water, g is gravitational acceleration and α has unit of $(\text{length})^2$. Barnett (1968) has proposed a suitable function for $P(\vec{k},\sigma)$ based on the work of Priestley (1965). The procedures are as follows.

Let $P(\vec{x},t)$ be the fluctuating static pressure at time t and point (x,y). Define the co-variance function

$$R(\vec{r},\tau) = \langle P(\vec{x},t)\, P(\vec{x}+\vec{r},t+\tau) \rangle \qquad (2.31)$$

where the brackets denote an ensemble average.
The quantity desired is

$$P(\vec{k},\sigma) = (2\pi)^{-3} \int_{\vec{r}} \int_{\tau} R(\vec{r},\tau) \cos(\vec{k}\cdot\vec{r} + \sigma\tau)\, d\vec{r}\, d\tau \qquad (2.32)$$

Priestley defines the cross spectral density as

$$B(\vec{r},\sigma) = (2\pi)^{-1} \int_{-\infty}^{\infty} R(\vec{r},\tau) \exp(-i\sigma\tau)\, d\tau$$

$$= C_o(\vec{r},\sigma) + i\, Q(\vec{r},\sigma) \qquad (2.33)$$

where c_o and q are referred to as the Co-and Quadrature-spectrum, respectively. Priestley eventually arrives at emprical representations for c_o and q as

$$C_o(\vec{r},\alpha) = \varphi(\alpha)\exp\left\{-\nu_1|r_1| - \nu_2|r_2|\right\}\cos\Lambda r_1 \tag{2.34}$$

and

$$q(\vec{r},\alpha) = \varphi(\alpha)\exp\left\{-\nu_1|r_1| - \nu_2|r_2|\right\}\sin\Lambda r_1 \tag{2.35}$$

where

$\Lambda = \frac{\alpha}{W}$ (1/m)

W is wind speed (m/sec)

$\nu_1 = 0.33\,\Lambda^{1.28}$ (1/m)

$\nu_2 = 0.52\,\Lambda^{0.95}$ (1/m)

$\varphi(\alpha) = 6.13 \times 10^{-4} W^6/\alpha^2$

is pressure power spectrum (m -sec)

r_1 and r_2 are distance associated with unit vectors

$\hat{r}_1$ and $\hat{r}_2$ directed downwind and crosswind,. respectively.

Substituting Equation (2.33), (2.34) and (2.35) into (2.32) and choosing the real part of P, then

$$P(\vec{k},\alpha) = \frac{\varphi(\alpha)}{4\pi^2}\int_{-\infty}^{\infty}\int \exp\left\{-\nu_1|r_1| - \nu_2|r_2|\right\}\cos(\vec{k}\cdot\vec{r} - \Lambda r_1)\,d\vec{r} \tag{2.36}$$

Direct integration yields

$$P(\vec{K},\alpha) = \frac{6.13\times10^{-4} W^6}{\pi^2 \alpha^2} \left[\frac{\nu_2}{\nu_2^2 + (K\sin\delta)^2}\right]\left[\frac{\nu_1}{\nu_1^2 + (K\cos\delta - \Lambda)^2}\right] \tag{2.37}$$

where δ is angle between wind and wave vectors. Barnett also compared the α value with experimental data which fit reasonably well.

This resonance mechanism, as the name implies, should be of particular importance for waves moving approximately in the same direction with the same speed as the wind field. We have found, as will be shown later that while this mechanism is important in the initial stage of wave generation and also contributes a large portion of the energy in the eventual spectral peak. It cannot account for the energy growth for the rest of the spectrum.

2.4.1.2 Miles' Instability Mechanism

Miles (1957, 1959a,1959b,1962) explains the energy transfer from the wind to the waves by hypothesizing a coupling between the existing waves and their induced surface pressure fluctuations. The waves

grow exponentially in time with the spectral peak shifting toward lower frequency. Of critical importance in this particular theory is the curvature of the wind profile at a height above the sea surface where W = C. The coefficient of this exponential growth is denoted by the parameter $\beta = \beta(f,\theta,x,y,t)$. Unfortunately, the theoretical prediction of Miles' theory did not agree with the measurements. Snyder and Cox (1966) recommended a modified expression of β.

$$\beta = s\,(\vec{k}\cdot\vec{W} - \sigma) \tag{2.38}$$

where s is the ratio of the densities of air and water, and $\vec{W}$ is the wind velocity measured one wave length above the mean sea surface. Barnett (1968) recommended a slight change in the ratio to yield

$$\beta = 5sf\left[W\cos\left(\frac{\delta}{c}\right) - 0.90\right] \tag{2.39}$$

where the wind W is considered 19.5 m above the sea surface. One can make an argument to the effect that most instability theories require waves moving faster than the wind, i.e., $\frac{W}{C} < 1$, either to experience no growth or to be attenuated. The dot product

representation in (2.38) and subsequent form of (2.39) are just simple mathematical expressions to fulfill this requirement. However, after the waves have moved away from the generating area, the actual form of β for $\frac{W}{C}<1$ then becomes important. If β is relatively large and negative, substantial dissipation would occur continuously outside the generating region. A similar circumstance would occur under head wind conditions, (i.e., $\pi/2 < \delta < 3\pi/2$), on the other hand, if β is small but generally positive, as has been suggested by Phillips (1966), then slow but continual growth would be expected in the presence of light, favorable winds. To make a choice between the two possibilities, it would be necessary to observe the behavior of spectral components over great distance or time. The measurements of Snodgrass et al. (1966) indicated that for long waves, at least, the damping is negligible. It is to be assumed that $\beta=0$ for $W\cos(\frac{\delta}{C})<0.90$.

Both wave growth mechanisms suggested above are for deepwater waves. It is not clear whether they are applicable for shallow water case. In the present model the combined Phillips' and Miles' mechanism is used anyhow for lack of a better model, that is,

$$G_1 + G_2 = \alpha + \beta A$$

To illustrate these two mechanisms, $\alpha+\beta A$, a simple case is tested here for a steady state, one dimensional, zero current, and frictionless situation. Equation (2.29) then becomes

$$C_g \cos\theta \frac{d}{dx} A(f,\theta) = \alpha + \beta A(f,\theta) \qquad (2.40)$$

Equation (2.40) is a linear boundary value problem. The solution can be easily obtained with given boundary condition. Here, the boundary condition is set as $A(f,\theta)=0$ at $x=0$. The solution for the spectral component along the x-axis, $A(f,0)$ is simply

$$A(f,o) = \frac{\alpha}{\beta}\left[\exp\frac{\beta x}{C_g} - 1\right] \qquad (2.41)$$

Three different conditions are illustrated here.

1) Onshore wind blows over a sloping bottom at right angle to the shore line. First of all, the growth of a specific wave component (T=8sec) with respect to fetch is examined. Here as shown in Figure 2.2(a), the growth of each component will undergo three stages. In the initial stage, wave will grow linearly with respect to distance and then grow exponentially. Eventually, the wave will reach the equilbrium range. Figure

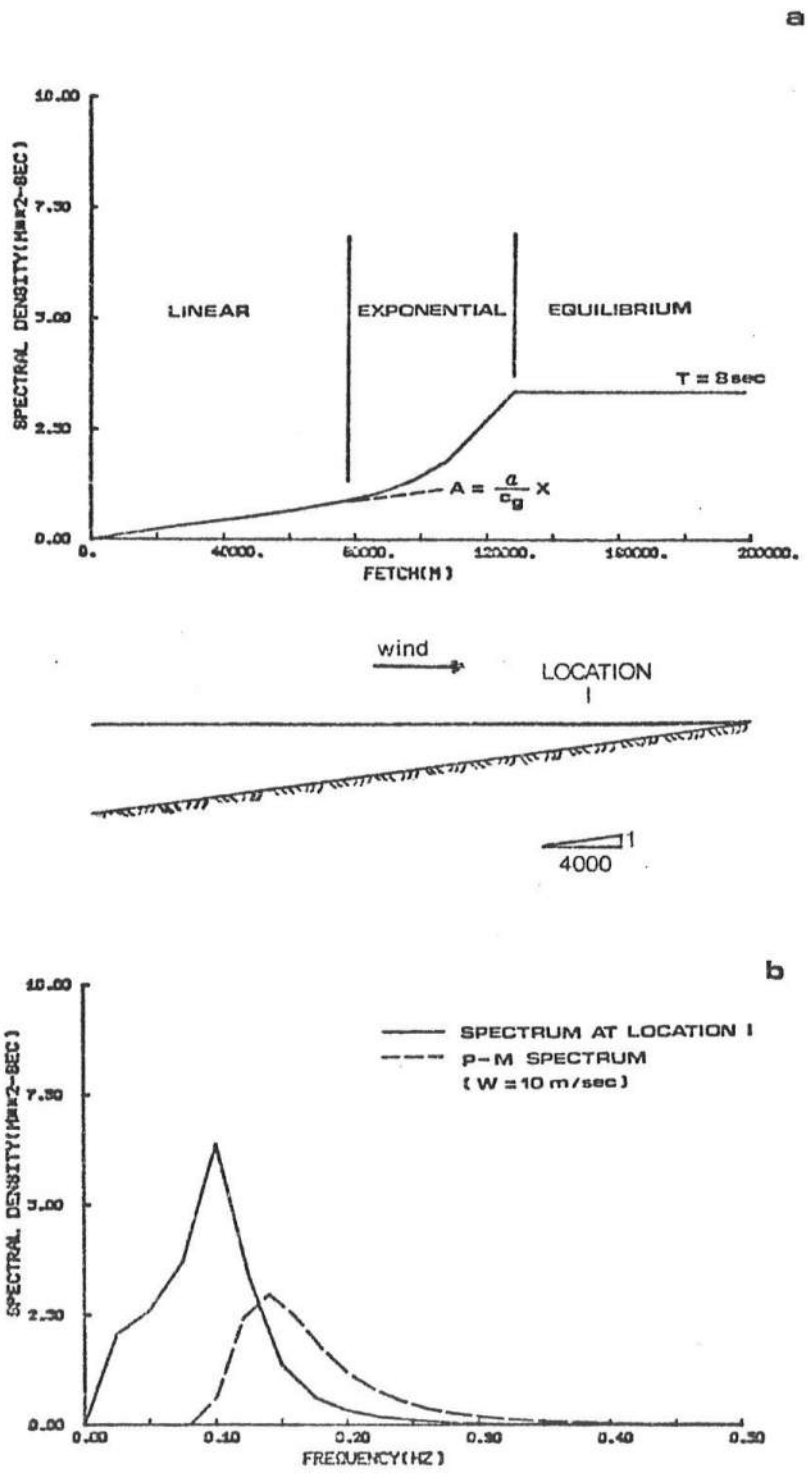

Figure 2.2 Onshore Wind Blows over a Sloping Bottom

2.2(b) illustrates the fully developed spectrum in shoaling water at location "I" based upon the combined Phillips' and Miles' mechanism. The major peak of the spectrum shifts toward the wind frequency f_w ($f_w=g/2\pi W$). After reaching f_w, it then shifts slowly toward even lower frequency. The light bump near f=0.02 HZ is due to the discontinuous 'cut off' of the Miles instability mechanism. While such a sharp cut-off is unrealistic, it will not significantly affect subsequent results. The fully developed P-M spectrum for the same wind condition is also shown in Figure 2.2(b) for comparison purposes. The Phillips' and Miles' mechanisms allow for a certain amount of growth in long wave components which do not appear in the fully developed P-M spectrum.

2) offshore wind blows over a sloping bottom as shown in Figure 2.3. The growth of a specific wave component with respect to fetch still maintains the three growing stages but the full spectrum at the location "I" is quite different from the above case for lack of shoaling effect. The comparison between the fully developed P-M spectrum and the spectrum generated by Phillips' and Miles' actually have very similar shape. The peak-energy frequencies also coincide with each

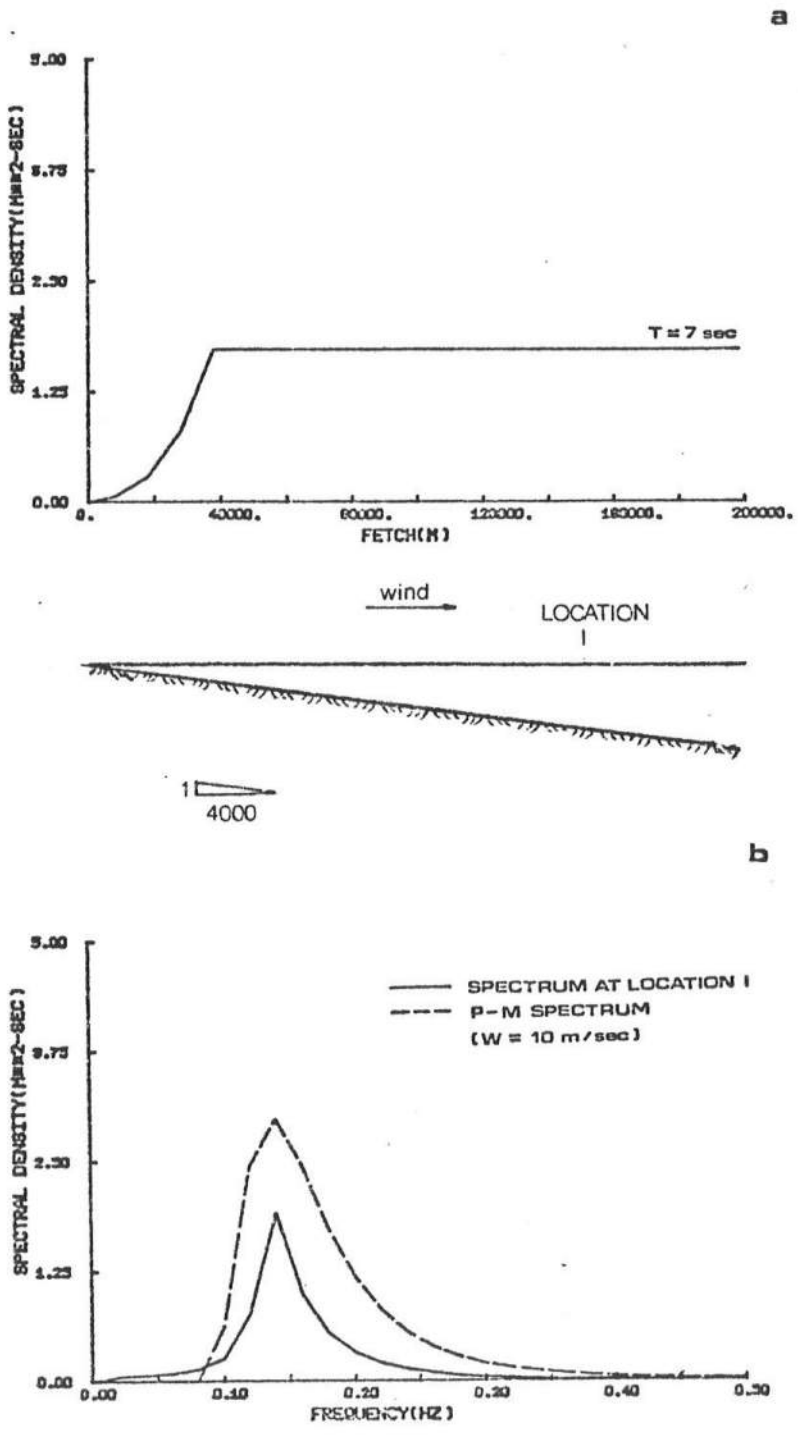

Figure 2.3 Offshore Wind Blows over a Sloping Bottom

other. The total energy, thus the wave height, is apparently lesser for the shallow water case.

3) Wind blows over a deep uniform bottom. The spectrum, following the same pattern as case (2), is shown in Figure 2.4. Although, at present, there is no field verification on the applicability of Phillips' and/or Miles' mechanism in shallow water, the results given above do appear reasonable.

2.4.2 Wave Dissipation

The known wave dissipation mechanisms are bottom friction, wave breaking, percolation, and wave induced bottom motion. The former two are usually considered to be the dominating factors and both are non-linear mechanisms. The latter two proesses are minor and linear mechanisms. In this research, only the two major mechanism: bottom friction and wave breaking, and depth limited wave are considered. The two major mechanisms are the G_3 term in the energy transport equation whereas the last term limits the growth of the total energy under the spectral curve in shallow water.

2.4.2.1 Bottom Friction

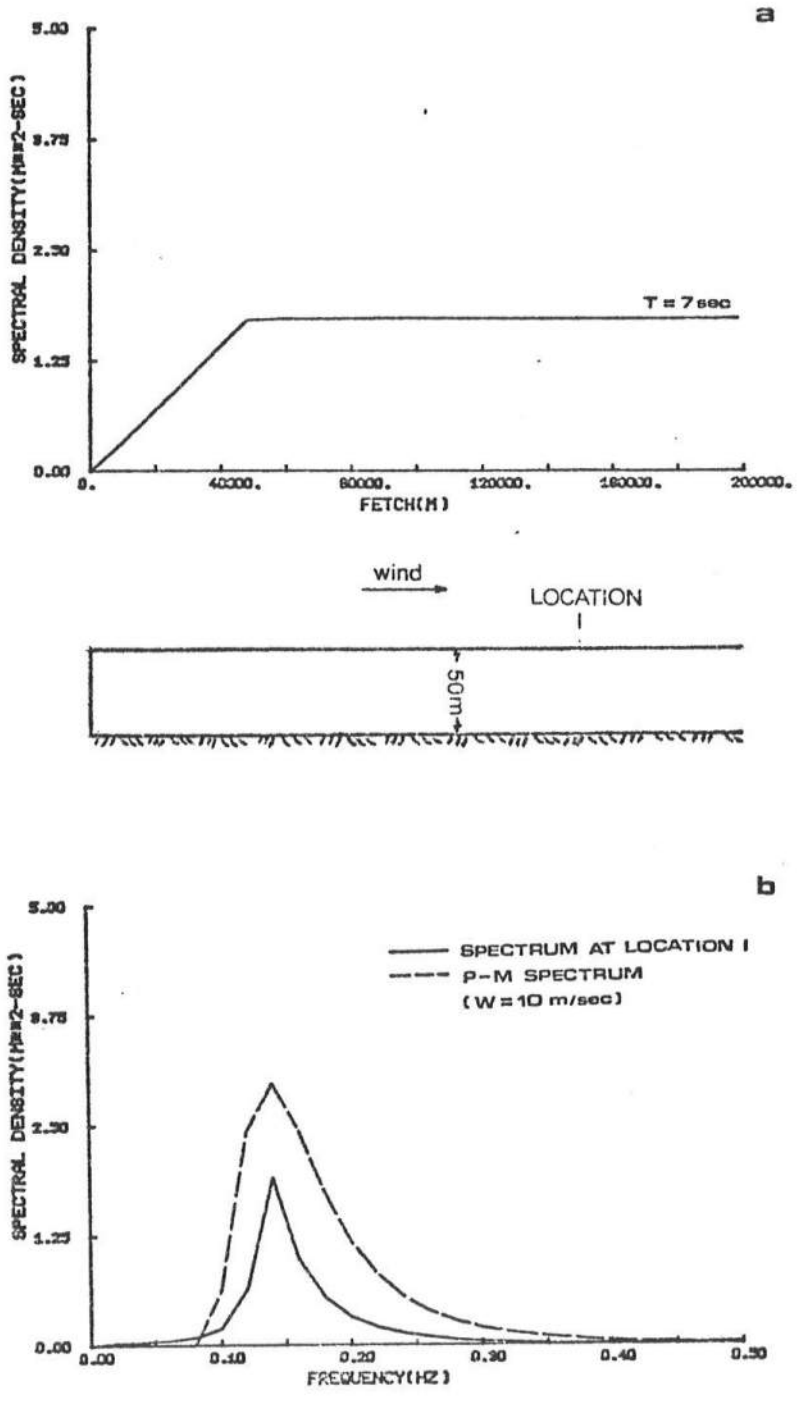

Figure 2.4 Wind Blows over a Deep Uniform Bottom

Energy dissipation due to bottom friction is primarily the result of two physical mechanisms: one involves the dissipative work done against turbulent shear stresses, the so-called turbulent bottom friction, induced by water particle motions near the bottom and the other is responsible for the dissipative work done against the viscous forces induced at the permeable bottom where percolation occurs.

In general, turbulent bottom friction is dominant over other dissipative processes when the sediment is composed of sand with mean diameter in the range of 0.1-0.4 mm for which low permeability prohibits percolation and viscous dissipation is negligible. Putnam and Johnson (1949) investigated this problem first. They used the quadratic friction law to derive the rate of energy dissipation for sinusoidal surface wave. Assuming Gaussian-distributed surface wave field, Hasselmann and Collins (1968) derived the rate of energy dissipation for a random sea. Their derivations are reviewed briefly. The bottom friction can be represented by the quadratic law.

$$\tau_{bi} = -\rho_w c_f u_{bi} |\vec{u_b}| \qquad (2.42)$$

where

u_{bi} (i=1,2) represent the two horizontal components of water particle velocity at the bottom,

c_f is the bottom friction coefficient.

The total dissipation of the wave field is then given by

$$\Phi = -\langle \tau_{bi}\, u_{bi} \rangle = -\rho_w c_f \langle |\vec{u}_b|^3 \rangle \qquad (2.43)$$

< > denotes an ensemble average over all possible wave components in a given wave spectrum. The repeated subscript represents summation over the field i=1,2. After Hasselmann and Collins' result has been changed from wave number space to directional frequency space, Φ becomes

$$\Phi(f,\theta) = -\frac{c_f g k^2}{\alpha^2 \cosh^2 kh} \langle u_b \rangle A(f,\theta)$$

$$= \epsilon A(f,\theta) \qquad (2.44)$$

with

$$\langle u_b \rangle = \left[\sum_f A(f) \frac{g^2 k^2}{\alpha^2 \cosh^2 kh} \Delta f \right]^{1/2} \qquad (2.45)$$

where A(f) is energy spectrum given by Equation (2.17). The above expressions are used in the noncoupled case because the basic assumption of this research is linear process.

As the bottom friction coefficient, Bretschneider and Reid (1954) evaluated the coefficient to be c_f=0.01 for the sandy bottoms of the Gulf of Mexico. Hasselmann and Collins (1968) c_f to be 0.015 using the wave spectra measured offshore of Panama City, Florida. Based on these two studies, c_f values of the order 10^{-2} have been widely used. However, the friction coefficient has been observed to vary significantly above and below this range depending on the sand grain diameter and existence of bottom ripples. Laboratory and semi-theoretical studies by Jonsson (1965) indicate that c_f is a function of Reynold's number and, also, of relative roughness. Dingler (1975) and Nielsen (1977) individually found the criteria for existence of bottom ripples and, also, for predicting the lengths and heights of such ripples. Based on these results, a method, assuming the roughness height being equal to the sediment diameter, was proposed by Hsiao and Shemdin (1978) to estimate the botttom friction coefficient over a broad range of

conditons.

2.4.2.2 Wave Breaking

It is a well observed fact that under sustained wind action, waves will grow to some limiting amplitudes then breakings or whitecaps will limit their growth. This phenomenon can be handled in practice by multiplying the wind generation term $\alpha + \beta A$ by a weighting factor μ where μ is unity during generation and zero at breaking. The condition is stated as

$$G_1 + G_2 = \mu (\alpha + \beta A) \qquad (2.46)$$

where μ is 1 for A unsaturated; μ is 0 for A saturated. Phillips (1958) proposed that in the saturated range of wave spectrum in deep water the expression is

$$A(f, \delta)_{saturated} = B g^2 \alpha^{-5} \text{Ⓗ}(\delta) \qquad (2.47)$$

Barnett (1968) defined Ⓗ as

$$\text{Ⓗ}(\delta) = \frac{8\pi}{3} \cos^4(\delta) \qquad (2.48)$$

The coefficient " B " has been determined experimentally by Burling (1959), Hicks (1960), Kinsman (1960), Pierson et al. (1962), Longuet-Higgins et al. (1963) and others, as a value varying between 0.0080 (Longuet-Higgins et al) to 0.0148 (Burling) with an average value about 0.0123. The value 0.0123 is used herein (Phillips, 1966).

In shallow water, Kitaigorodskii et al. (1975) have extended Phillips arguments to case of finite depth and obtain a modified equaion of the following form:

$$A(f,\delta) = B g^2 \alpha^{-5} \Theta(\delta) \Gamma(\omega_h) \qquad (2.49)$$

where Γ is a non-dimensional function of the quantity $\omega_h = \alpha (\frac{h}{g})^{1/2}$. The function varies from 1 in deep water to 0 in depth h=0. When ω_h is less than 1,

$$\Gamma(\omega_h) \approx \frac{1}{2} \omega_h^2$$

Therefore

$$A(f,\delta) = \frac{1}{2} B g h \alpha^{-3} \Theta(\delta) \qquad (2.50)$$

..Observational evidence for this form has been reported by Thornton (1977), Ou (1980), and the Vincent (1981) in the laboratory and the field.

Finally, when waves reach shallow water they will break because of depth limitation. The energy is supposedly saturated but Eq (2.50) can not account for all of them (the low frequency components) since it opens at low frequency. In the present model, an empirical criteria based upon total wave energy in terms of significant wave height is employed such that (Divoky et al., 1970)

$$\left(\frac{Hs}{L}\right)_b = 0.12 \tanh (kh)_b \qquad (2.51)$$

where $Hs=4\sqrt{E}$ with E the total wave energy under the spectrum.

CHAPTER 3

NUMERICAL SCHEME OF STATIONARY WAVE SPECTRAL TRANSFORMATION

After winds steadily generate waves for quite a long period, stationary wave spectral transformation will be reached. Without knowing the processes, the shallow water wave spectrum, at any specified location, is then simply the contribution resulting from energy associated with different frequency bands of the deep water wave spectrum.

Based on the energy flux conservation, Shiau and Wang (1977) developed numerical model of stationary wave spectrum over irregular bottom. The present study, based on the same numerical scheme as Shiau and Wang, add wave generation and wave dissipation terms in the stationary wave spectral transformation to fit the real phenomenon in the ocean environments.

3.1 Basic Equations for Stationary Wave Spectral Transformation

Under the assumption of steady state, basic equations for wave spectral transformation, i.e., Equations (2.21), (2.25), (2.28) and (2.29) become

i) Wave Conservation Equation:

$$\vec{\nabla}\,\bar{\alpha} = 0$$

or

$$\bar{\alpha} = \text{constant or uniform} \tag{3.1}$$

ii) Wave Number Conservation Equation:

$$(gk\tanh kh)^{1/2} + Uk\cos\theta + Vk\sin\theta = \frac{2\pi}{T} \tag{3.2}$$

iii) Wave Number Irrotational Equation:

$$\frac{\partial(k\cos\theta)}{\partial y} - \frac{\partial(k\sin\theta)}{\partial x} = 0 \tag{3.3}$$

iv) Energy Transport Equation:

$$\frac{\partial}{\partial x}\left(A(U + C_g\cos\theta)\right) + \frac{\partial}{\partial y}\left(A(V + C_g\sin\theta)\right) + S_{xx}\frac{\partial U}{\partial x} + S_{xy}\frac{\partial U}{\partial y} + S_{yx}\frac{\partial V}{\partial x} + S_{yy}\frac{\partial V}{\partial y} = \sum_{i=1}^{3} G_i \tag{3.4}$$

where

$$\sum_{i=1}^{3} G_i = G_1 + G_2 + G_3$$

$$= \mu (\alpha + \beta A) + \Phi \quad .$$

α is Phillips resonant mechanism Eq (2.30)

β is Miles instability mechanism Eq (2.39)

μ is breaking coefficient

Φ is bottom dissipation Eq (2.44)

3.2 Numerical Procedure

Based on Equations (3.1), (3.2), (3.3) and (3.4), Noda, et al.(1974) developed numerical procedures to compute the wave angle and wave height as functions of space variables for beaches with periodic bottom variations in the longshore direction. The advantage of Noda's method is that it predicts the wave angles and wave heights at certain points rather than along a wave ray. This procedure leads itself well to use in the finite difference model because calculations are performed at points which lie in the center of rectangular grid elements which are part of a larger grid mesh. The basic idea to get a steady solution converged by finite difference method is to use the relaxation scheme which will be shown in detail. It is necessary to discuss the error estimates before the numerical scheme to be used.

The acccuracy of the finite difference method is mainly limited by three factors. First there is the truncation error which is the difference between the true solution of the original equations and the approximate solution of the finite difference equation which replaces the differential terms by finite-difference terms. The truncation error can be eliminated as the finite difference mesh size approaches zero. Secondly, there is the round-off error caused by the limited number of digits stored by the computer for each number. As the computer used includes 12 significant digits, no appreciable errors were expected from this source. Thirdly, there is the residual error caused by the difference between the exact solution to the finite difference equations and the actual solution reached when iteration scheme is stopped. Obviously if a large number of iteration cycles were used this error could be reduced virtually to zero but economy insists that the program be stopped as soon as the residual error is reasonably small.

To facilitate numerical computation, the governing equations are, out of necessity, to be transformed into finite difference form. A mixed forward, backward and central difference scheme is used

to minimize the secondary restrictions at the expense of nonuniformity of the order of errors. The reference to the grid schemes is shown in Figure 3.1.

3.2.1 Wave Kinematics and Boundary Conditions

The wave number and wave angle are solved through numerical iterations of wave number conservation equation and wave number irrotational equation. In other words, for given spatial distribution of U, V and h, Equations (3.2) and (3.3) enable us to compute k and θ in the wave region provided the boundary condition is specified. The wave number conservation equation becomes

$$\left[g k_{i,j} \tanh(k_{i,j} h_{i,j})\right]^{1/2} + U_{i,j} k_{i,j} \cos\theta_{i,j} + V_{i,j} k_{i,j} \sin\theta_{i,j} = \frac{2\pi}{T} \qquad (3.5)$$

which is solved through a Newtonian iterative technique defined as

$$k_{new} = k_{old} - \frac{f(k_{old})}{f'(k_{old})} \qquad (3.6)$$

where f'(k) is the first derivative of f(k) which is

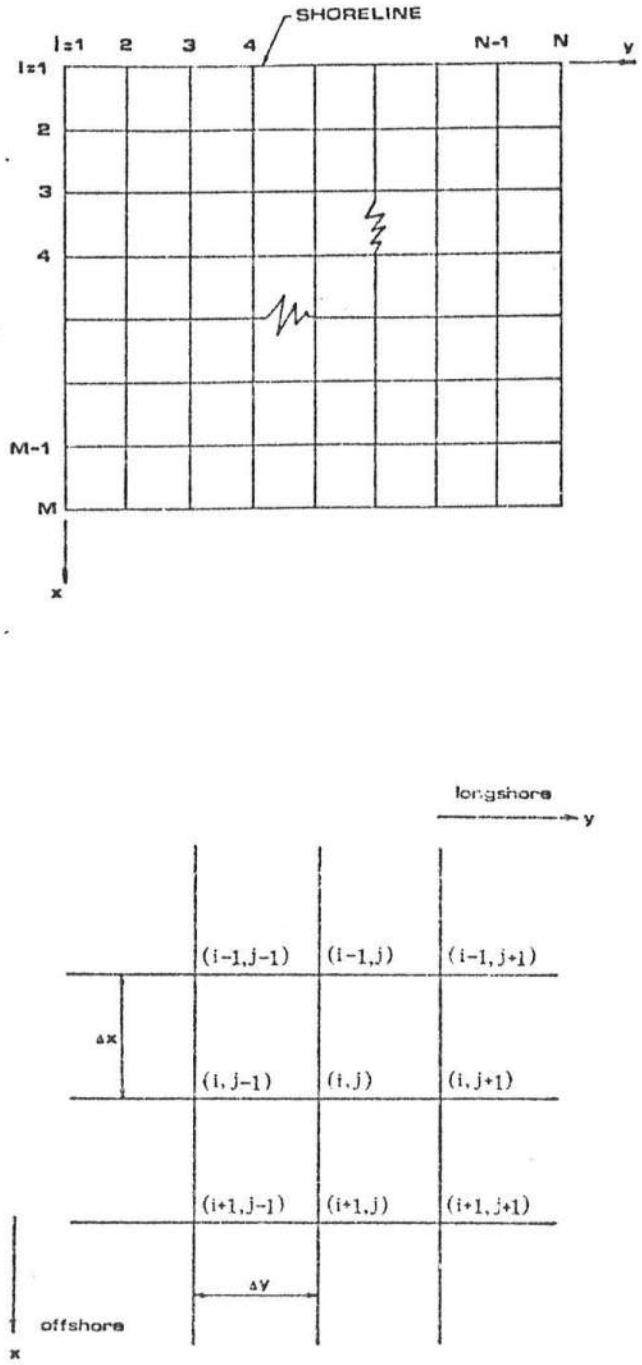

Figure 3.1 Full Grid and Local Grid Description

defined

$$f(k) = gk\tanh kh - \left[\frac{2\pi}{T} - Uk\cos\theta - Vk\sin\theta\right]^2 \qquad (3.7)$$

The iteration is considered to satisfy the relaxation criteria

$$|k_{new} - k_{old}| \leq 0.001\,|k_{new}| \qquad (3.8)$$

The value k is then fed into the wave number irrotational equation to solve the wave angle. Expanding Equation (3.3) yields

$$\cos\theta\left[\frac{\partial\theta}{\partial x} - \frac{1}{k}\frac{\partial k}{\partial y}\right] + \sin\theta\left[\frac{\partial\theta}{\partial y} + \frac{1}{k}\frac{\partial k}{\partial x}\right] = 0 \qquad (3.9)$$

From Equation (3.2), $\frac{\partial k}{\partial x}$, $\frac{\partial k}{\partial y}$ can be derived as

$$\frac{\partial k}{\partial x} = \left\{k\frac{\partial\theta}{\partial x}(U\sin\theta - V\cos\theta) - k\left(\cos\theta\frac{\partial U}{\partial x} + \sin\theta\frac{\partial V}{\partial x}\right) - \frac{gk^2\operatorname{sech}^2 kh}{2(gk\tanh kh)^{1/2}}\frac{\partial h}{\partial x}\right\} \div \left\{U\cos\theta + V\sin\theta + \frac{g(\tanh kh + kh\operatorname{sech}^2 kh)}{2(gk\tanh kh)^{1/2}}\right\} \qquad (3.10)$$

$$\frac{\partial k}{\partial y} = \left\{k\frac{\partial\theta}{\partial y}(U\sin\theta - V\cos\theta) - k\left(\cos\theta\frac{\partial U}{\partial y} + \sin\theta\frac{\partial V}{\partial y}\right) - \frac{gk^2\operatorname{sech}^2 kh}{2(gk\tanh kh)^{1/2}}\frac{\partial h}{\partial y}\right\} \div \left\{U\cos\theta + V\sin\theta + \frac{g(\tanh kh + kh\operatorname{sech}^2 kh)}{2(gk\tanh kh)^{1/2}}\right\} \qquad (3.11)$$

However, Equation (3.9) really needs $\frac{1}{K}\frac{\partial K}{\partial x}$, $\frac{1}{K}\frac{\partial K}{\partial y}$ which can be represented as follows:

$$\frac{1}{K}\frac{\partial K}{\partial X} = \frac{\partial \theta}{\partial x}\left(\frac{U\sin\theta - V\cos\theta}{AA}\right) + \overline{\frac{1}{K}\frac{\partial K}{\partial x}} \tag{3.12}$$

$$\frac{1}{K}\frac{\partial K}{\partial y} = \frac{\partial \theta}{\partial y}\left(\frac{U\sin\theta - V\cos\theta}{AA}\right) + \overline{\frac{1}{K}\frac{\partial K}{\partial y}} \tag{3.13}$$

with

$$AA = U\cos\theta + V\sin\theta + \frac{1}{2}\left(1 + \frac{2kh}{\sinh 2kh}\right)\left(\frac{\sigma}{K} - U\cos\theta - V\sin\theta\right) \tag{3.14}$$

and

$$\overline{\frac{1}{K}\frac{\partial K}{\partial X}} = \frac{-\left(\frac{\partial U}{\partial x}\cos\theta + \frac{\partial V}{\partial x}\sin\theta\right) - \frac{(\sigma - UK\cos\theta - VK\sin\theta)}{\sinh(2Kh)}\frac{\partial h}{\partial x}}{AA} \tag{3.15}$$

$$\overline{\frac{1}{K}\frac{\partial K}{\partial y}} = \frac{-\left(\frac{\partial U}{\partial y}\cos\theta + \frac{\partial V}{\partial y}\sin\theta\right) - \frac{(\sigma - UK\cos\theta - VK\sin\theta)}{\sinh(2Kh)}\frac{\partial h}{\partial y}}{AA} \tag{3.16}$$

Substituting (3.12) and (3.13) into (3.9), the following final equation is arrived at

$$\frac{\partial\theta}{\partial x}\left[\cos\theta + \frac{\sin\theta\,(U\sin\theta - V\cos\theta)}{AA}\right] + \frac{\partial\theta}{\partial y}\left[\sin\theta - \frac{\cos\theta\,(U\sin\theta - V\cos\theta)}{AA}\right]$$

$$+ \overline{\frac{1}{K}\frac{\partial K}{\partial x}}\sin\theta - \overline{\frac{1}{K}\frac{\partial K}{\partial y}}\cos\theta = 0 \qquad (3.17)$$

Finite differencing the above equation by using a forward difference in x and a backward difference in y, and solving for $\theta_{i,j}$

$$\theta_{i,j} = \frac{1}{B_{i,j}}\left\{\overline{\frac{1}{K}\frac{\partial K}{\partial y}}\cos\theta_{i,j} - \overline{\frac{1}{K}\frac{\partial K}{\partial x}}\sin\theta_{i,j} + \right.$$

$$\frac{\theta_{i,j-1}}{\Delta y}\left[\sin\theta_{i,j} - \frac{\cos\theta_{i,j}}{AA_{i,j}}\left(U\sin\theta_{i,j} - V\cos\theta_{i,j}\right)\right] -$$

$$\left.\frac{\theta_{i+1,j}}{\Delta x}\left[\cos\theta_{i,j} + \frac{\sin\theta_{i,j}}{AA_{i,j}}\left(U\sin\theta_{i,j} - V\cos\theta_{i,j}\right)\right]\right\} \qquad (3.18)$$

where

$$B_{i,j} = \frac{\sin\theta_{i,j}}{\Delta y} - \frac{\cos\theta_{i,j}}{\Delta x} - \frac{1}{AA_{i,j}}\left(U\sin\theta_{i,j} - V\cos\theta_{i,j}\right)$$

$$\left(\frac{\cos\theta_{i,j}}{\Delta y} + \frac{\sin\theta_{i,j}}{\Delta x}\right) \qquad (3.19)$$

$AA_{i,j}$ is defined in equation (3.14).

$\overline{\frac{1}{K}\frac{\partial K}{\partial x}}$ and $\overline{\frac{1}{K}\frac{\partial K}{\partial y}}$ are defined in Equations (3.15) and (3.16). The computation is carried out to satisfy the relaxation criteria

$$\left| \theta_{new} - \theta_{old} \right| \leq 0.001 \left| \theta_{new} \right| \qquad (3.20)$$

The boundary condition of θ is specified at the offshore boundary at the x-axis. The offshore boundary value is the input. The condition of the x-axis could be specified in such a manner that $\theta_{i,1} = \theta_{i,2}$ without introducing significant error if the longshore bottom variation in the vicinity of the x-axis is slow.

$\theta_{i,j}$ will not converge when $B_{i,j}$ approaches zero. Using the null-current condition as a guide, one arrives at the following condition:

$$\frac{\Delta y}{\Delta x} > \tan \theta_m \qquad (3.21)$$

where θ_m is the expected maximum wave angle. For example, if the maximum wave angle is expected to be less than 60°, the ratio of $\frac{\Delta y}{\Delta x}$ should be larger than 1.7.

The current and depth gradients required in the computation are determined by central difference, i.e.,

$$\frac{\partial \xi_{i,j}}{\partial x_\kappa} = \frac{\xi_{i+1,j} - \xi_{i-1,j}}{2\Delta x_\kappa} \tag{3.22}$$

where ξ represents U, V or h and x_κ is either x or y.

3.2.2 Wave Dynamics and Boundary Condition

The energy transport Equation (3.4) can be derived as the following form.

$$(U + C_g \cos\theta)\frac{\partial A}{\partial x} + (V + C_g \sin\theta)\frac{\partial A}{\partial y} +$$
$$A\left(\frac{\partial}{\partial x}(U + C_g \cos\theta) + \frac{\partial}{\partial y}(V + C_g \sin\theta) +\right.$$
$$\sigma_{xx}\frac{\partial U}{\partial x} + \sigma_{xy}\frac{\partial U}{\partial y} + \sigma_{yx}\frac{\partial V}{\partial x} + \sigma_{yy}\frac{\partial V}{\partial y} -$$
$$\left.\mu\beta - \epsilon\right) - \mu\alpha = 0 \tag{3.23}$$

or

$$(U + C_g \cos\theta)\frac{\partial A}{\partial x} + (V + C_g \sin\theta)\frac{\partial A}{\partial y} +$$
$$A(-Q - \mu\beta - \epsilon) - \mu\alpha = 0 \tag{3.23a}$$

where
$$Q = -\left(\frac{\partial U}{\partial x} + \frac{\partial V}{\partial y}\right) + C_g \sin\theta \frac{\partial \theta}{\partial x} - \cos\theta \frac{\partial C_g}{\partial x}$$
$$- C_g \cos\theta \frac{\partial \theta}{\partial y} - \sin\theta \frac{\partial C_g}{\partial y} - J$$

$$J = \alpha_{xx} \frac{\partial U}{\partial x} + \alpha_{xy} \frac{\partial U}{\partial y} + \alpha_{yx} \frac{\partial V}{\partial x} + \alpha_{yy} \frac{\partial V}{\partial y}$$

Finite differencing the above equation by using a forward difference in x and a backward difference in y, it becomes

$$(U + C_g \cos\theta) \frac{A_{i+1,j} - A_{i,j}}{\Delta x} + (V + C_g \sin\theta) \frac{A_{i,j} - A_{i,j-1}}{\Delta y}$$

$$+ A_{i,j} (- Q_{i,j} - \mu \beta_{i,j} - \epsilon_{i,j}) - \mu \alpha_{i,j} = 0 \qquad (3.24)$$

Rearranging Equation (3.24), $A_{i,j}$ can be represneted as

$$A_{i,j} = \frac{\frac{(V + C_g \sin\theta)}{\Delta y} A_{i,j-1} - \frac{(U + C_g \cos\theta)}{\Delta x} A_{i+1,j} + \mu \alpha_{i,j}}{\frac{(V + C_g \sin\theta)}{\Delta y} - \frac{(U + C_g \cos\theta)}{\Delta x} - Q_{i,j} - \mu \beta_{i,j} - \epsilon_{i,j}} \qquad (3.25)$$

Here all the values of U, V, and θ are evaluated at (i,j).

Again, Equation (3.25) is solved through a row by row relaxation until

$$| \text{Anew} - \text{Aold} | \leq 0.001 \, | \text{Anew} | \qquad (3.26)$$

The boundary condition is also defined in a similar manner in that the shoreward boundary is specified as the input and the values on the x-axis is taken the same as the next column ($A_{j,1} = A_{j,2}$).

On the shoreward direction, the wave will eventually break. Under such conditions, the wave breaking dissipation is more important than bottom friction dissipation. In the present model, Equation (2.51) will be chosen as the criterion.

3.3 Examples

A plane beach of parallel bottom contours, with the distance of 25,000 m between the offshore boundary and the shoreline, is shown in Figure 3.2. The coordinates are chosen as x-axis toward offshore, y-axis alongshore, and z-axis upward. To apply the numerical scheme, along the positive x-axis, the domain is divided into five sections, with Δx=5000 m, denoted as location 1 to 6, and along the positive y-axis, it is divided into two sections, with Δy=5000 m, denoted as location I to III. Three pressure gauges are installed at location 6II (boundary), location 5II, and location 2II of which the water depth are 25 m, 20 m, and 2 m, respectively.

There are three examples to be discussed: i) energy flux conservation case, ii) bottom dissipation case, iii) local wind generation case.

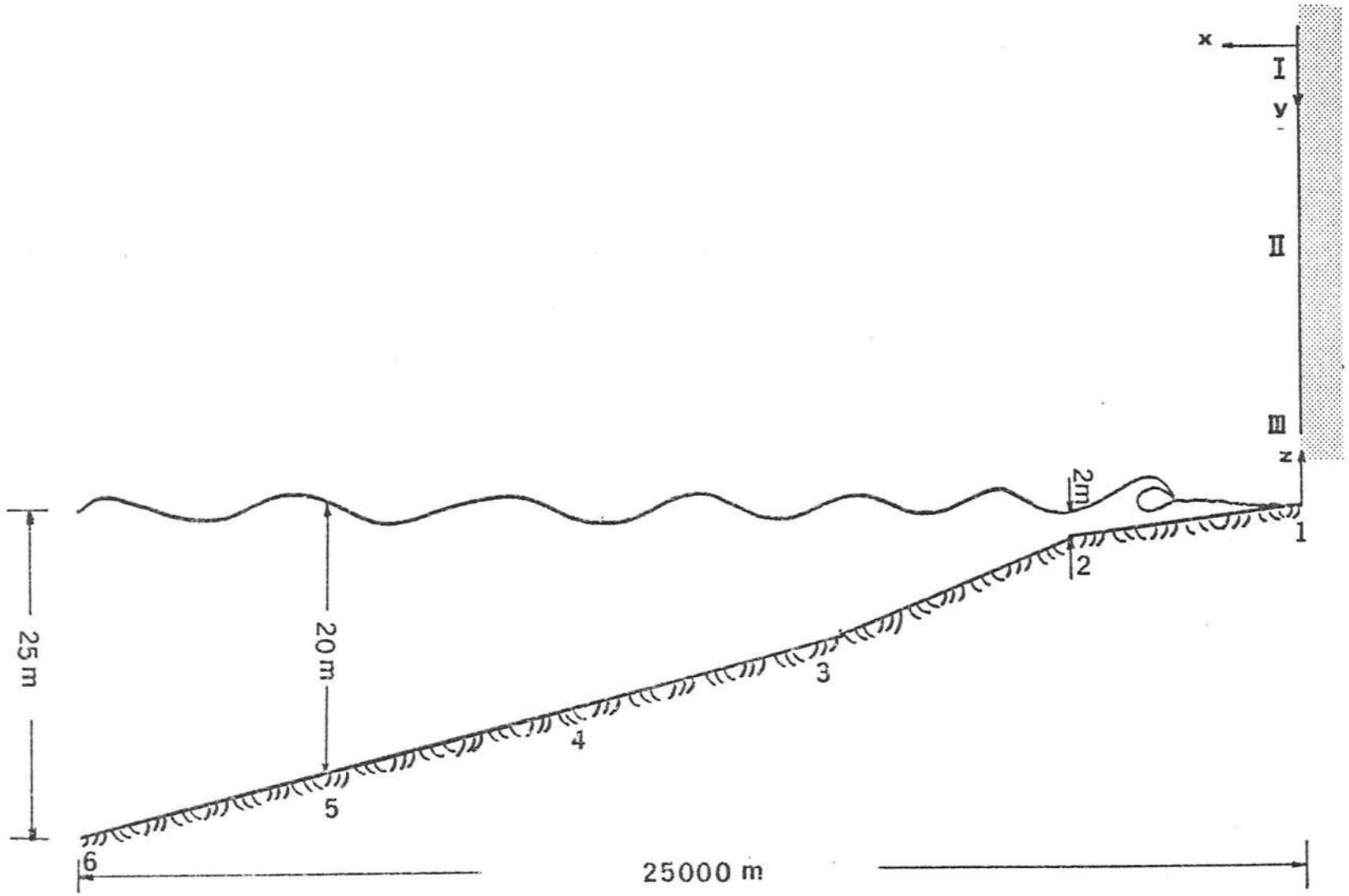

Figure 3.2 Schematic View of Ocean Environment

3.3.1 Energy Flux Conservation Case

The energy flux conservation case considers no energy generation or dissipation, i.e., $\sum_{i=1}^{3} G_i = 0$, in the process of the wave spectral transformation. The wave spectra at different locations are shown in Figures 3.3 and 3.4. Since the shoaling coefficient K_{sh}, (unaffected by refraction),

$$K_{sh} = \frac{\text{wave height in shallow water}}{\text{wave height in deep water}}$$

is less than 1 when $0.06 < \frac{h}{L_o} < 0.5$ and larger than 1 when $\frac{h}{L_o} < 0.06$, (L_o is the wave length in deep water), the wave height will increase or decrease in shoaling water depending on the range of $\frac{h}{L_o}$. In the example given in Figure 3.3, the energy spectrum at location 5II is lower than the input spectrum (location 6II), because the value of $\frac{h}{L_o}$ of all the frequency components fall between 0.06 and 0.5. On the other hand, the components of energy spectrum at location 2II are lower than the inputs at low frequency but higher than the inputs at high frequency. Figure 3.4 shows the refraction effects in shoaling water. The directional sensitivity is further examined in Figure

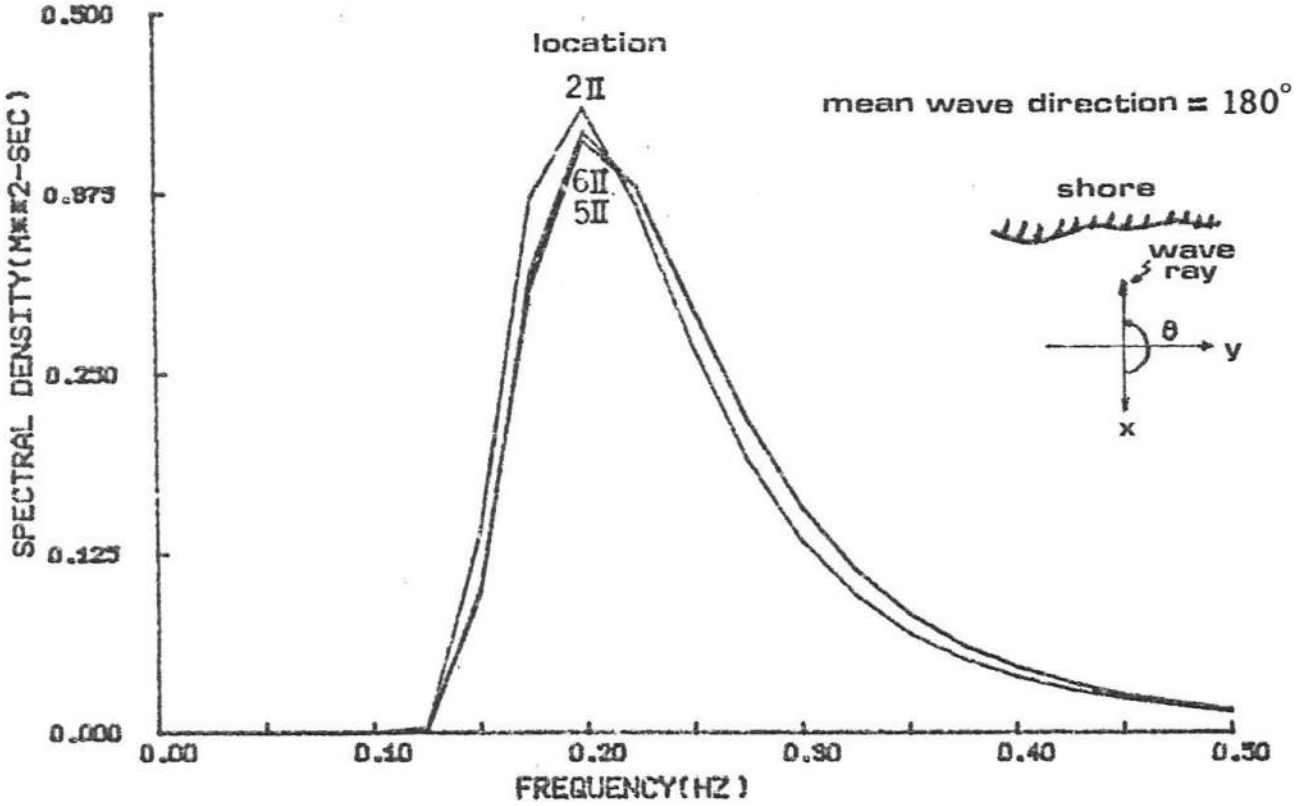

Figure 3.3 Variation of Energy Spectrum in Energy Flux Conservation Case at Boundary, Location 5II and Location 2II

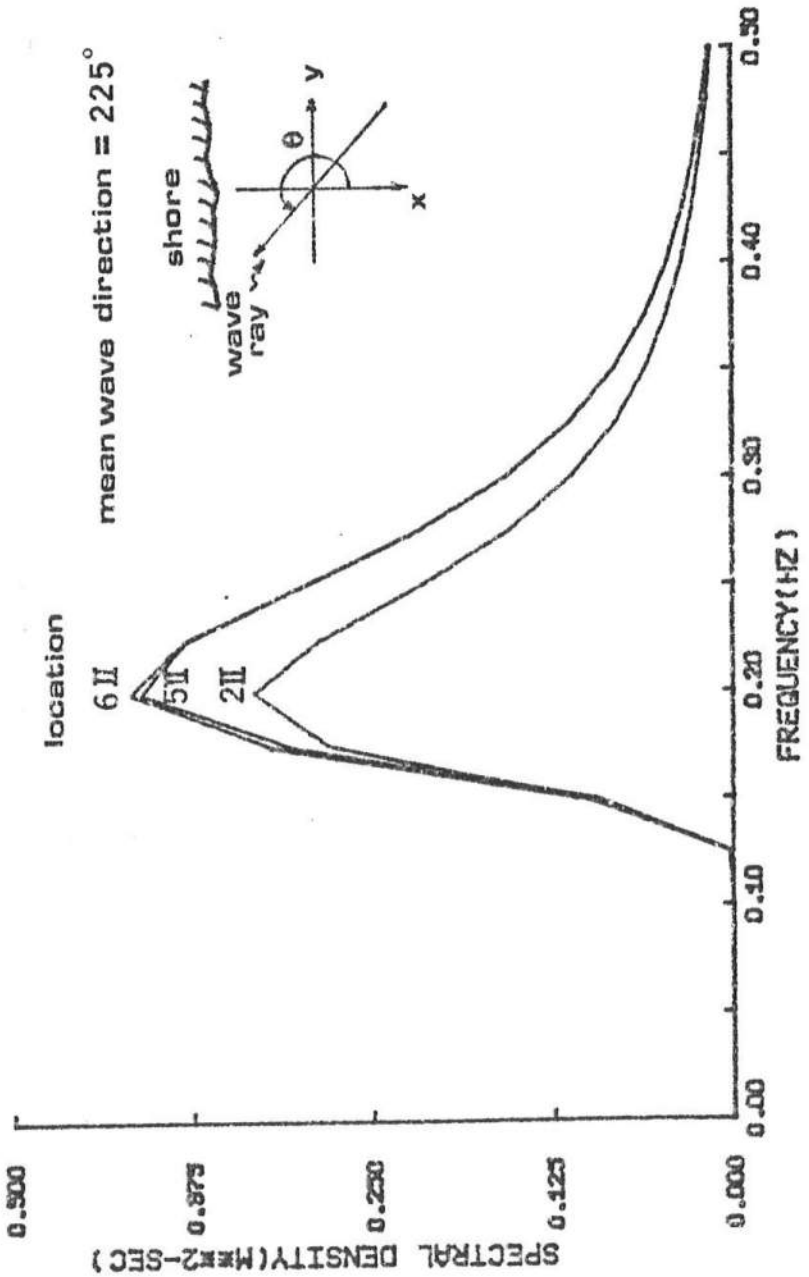

Figure 3.4 Variation of Energy Spectrum in Energy Flux Conservation Case at Boundary, Location 5II and Location 2II.

3.5. It plots the percentage error of spectral density of each frequency component for various approaching angles that deviate from a designated mean wave angle. It can be seen that error increases with increasing wave period. More importantly, the approaching angle plays a significant role in directional sensitivity. For waves with small approaching angle (perpendicular to the shoreline), the wave transformation is far less sensitive to the wave angle variations than for waves with large approaching angle (parallel to the shoreline). Therefore, the energy spectrum is dominated by frequency variations for small approaching angle but by wave angle variations for large approaching angle.

3.3.2 Bottom Dissipation Case

The bottom dissipation case concerns the energy loss due to the bottom friction in the process of wave spectral transformation. As shown in Figure 3.6, the influence of bottom friction is quite limited at location 5II because few wave components are affected by the bottom. The difference between the wave spectrum with bottom friction and the wave spectrum without bottom friction is only a few percent for the

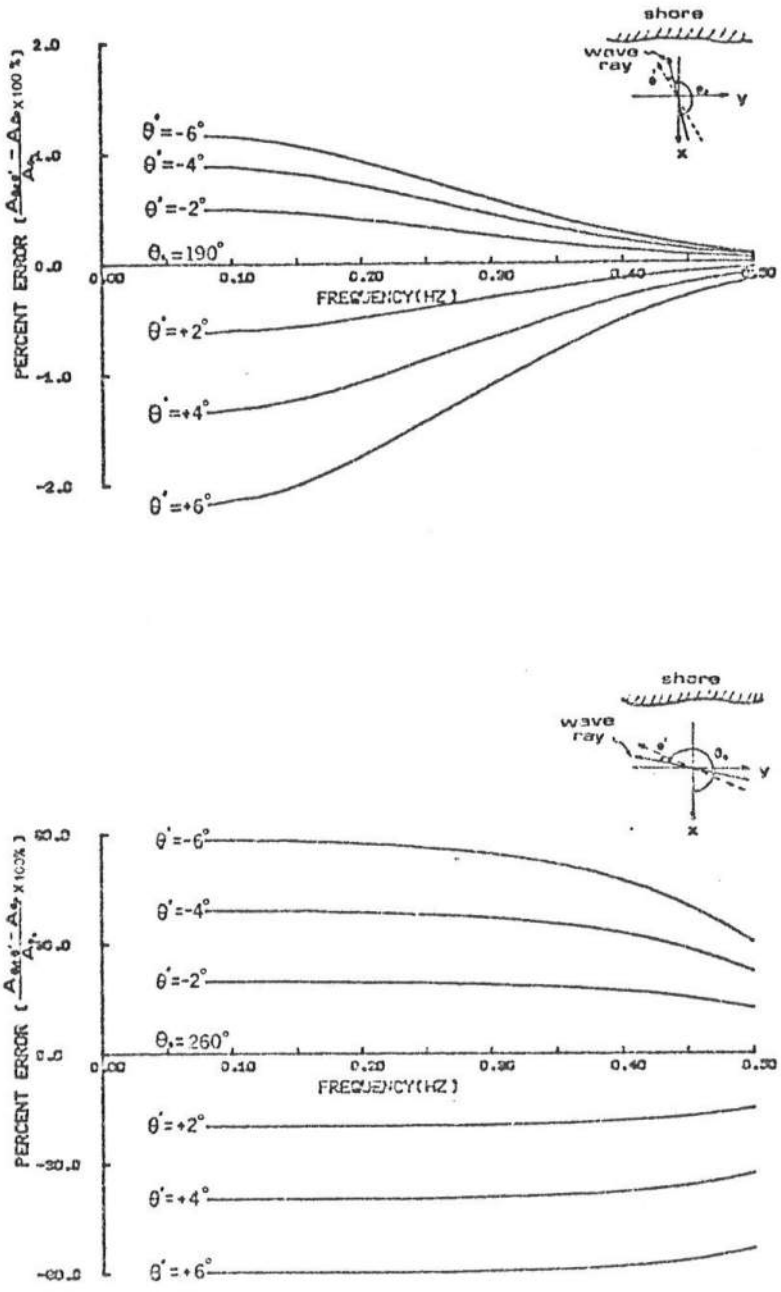

Figure 3.5 Percentage Error of Spectral Density vs. Deviations of Wave Directions

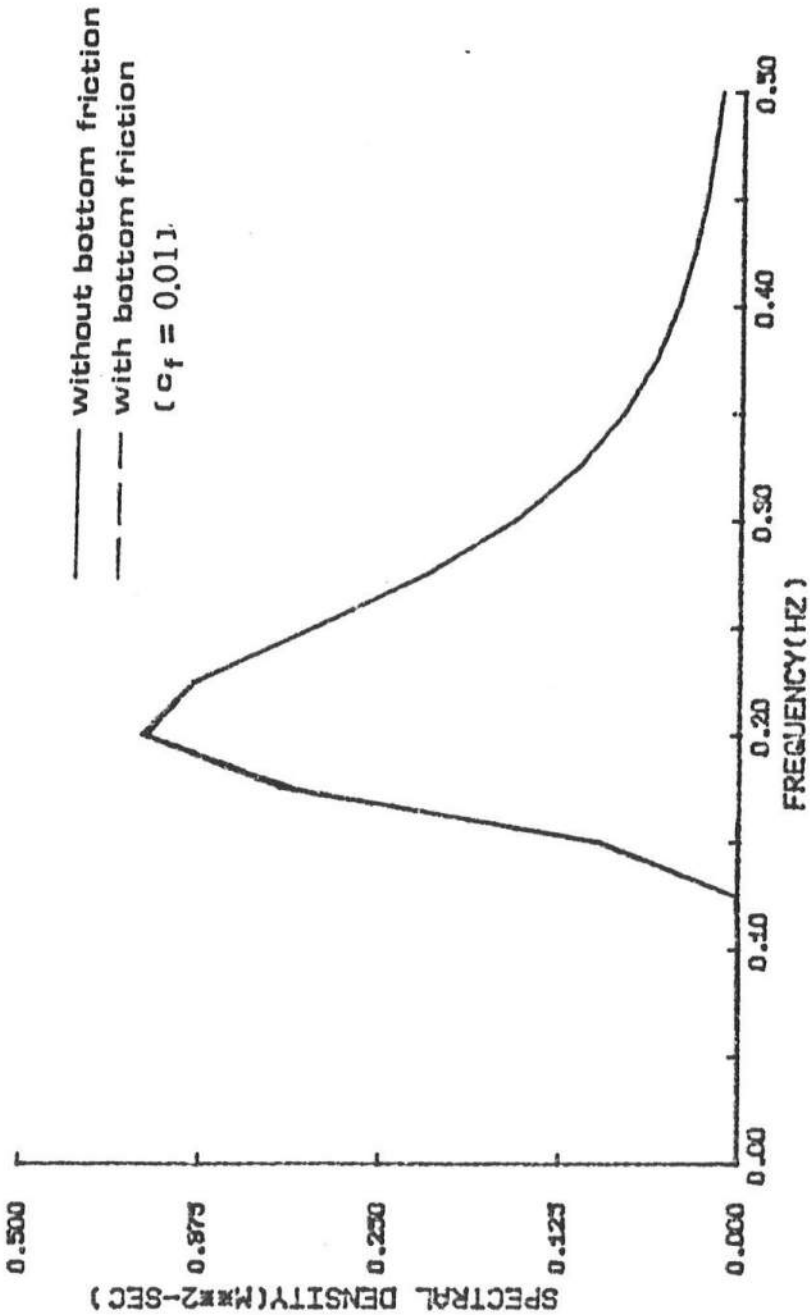

Figure 3.6 Comparison between Energy Spectrum with and without Bottom Friction at Location 5II

low frequencies under consideration and these two spectra practically overlap. However, in Figure 3.7, the influence of the bottom friction is quite significant at location 2II because most of the wave components have already felt the bottom. It is reasonable that the bottom dissipation effect for long wave is more significant than that for short wave in shallow water because long wave feels the bottom earlier than short wave.

3.3.3 Local Wind Generation Case

The local wind generation case deals with the energy generation in the process of wave spectral transformation. Considering no energy input at the boundary, the steady local wind generates waves in a closed region. As shown in Figure 3.8, the local wind wave spectrum at location 5II still stays at high frequency, whereas, with increasing fetch, not only the local wind wave spectrum at location 2II increases singificantly but its spectral peak shifts toward the lower frequency. Hasselmann et al. (1973) in the JONSWAP measurements which traced the development of the wave spectrum with increasing fetch under conditions of steady offshore winds illustrate this

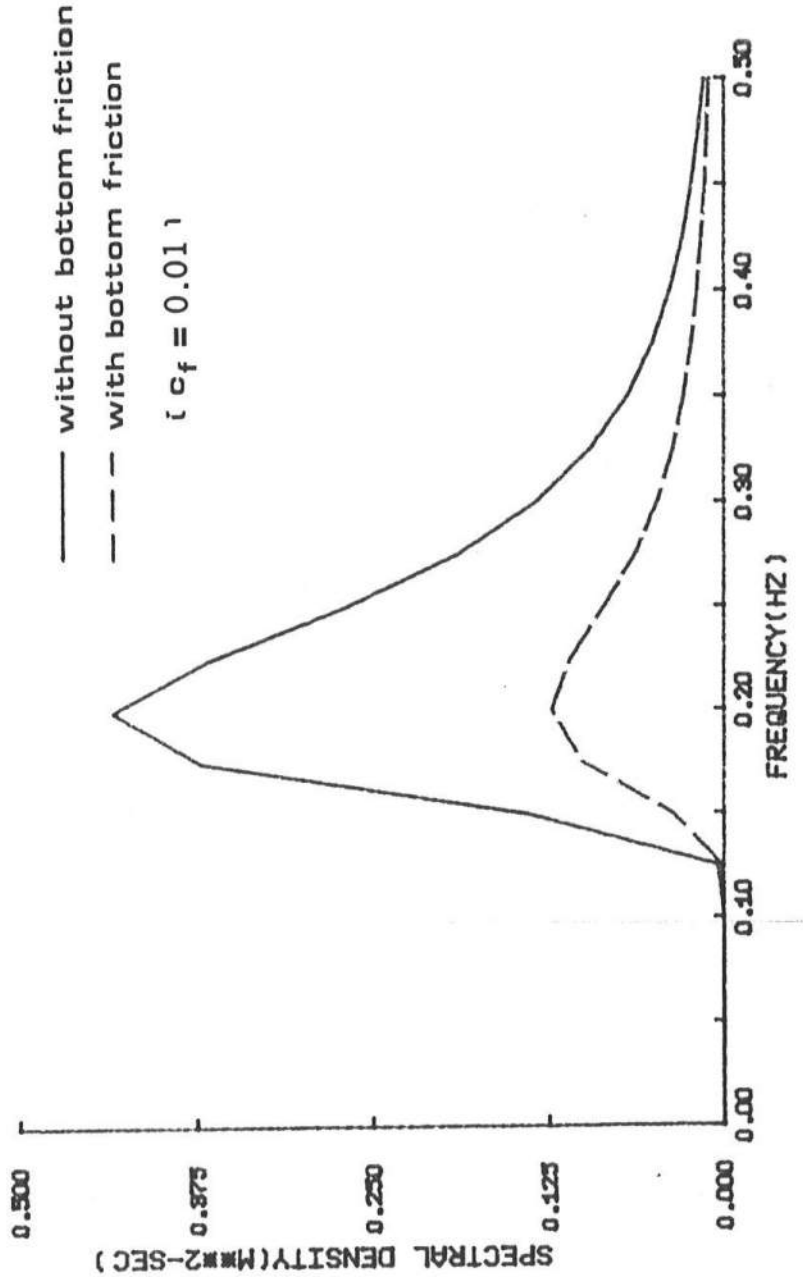

Figure 3.7 Comparison between Energy Spectrum with and without Bottom Friction at Location 2II

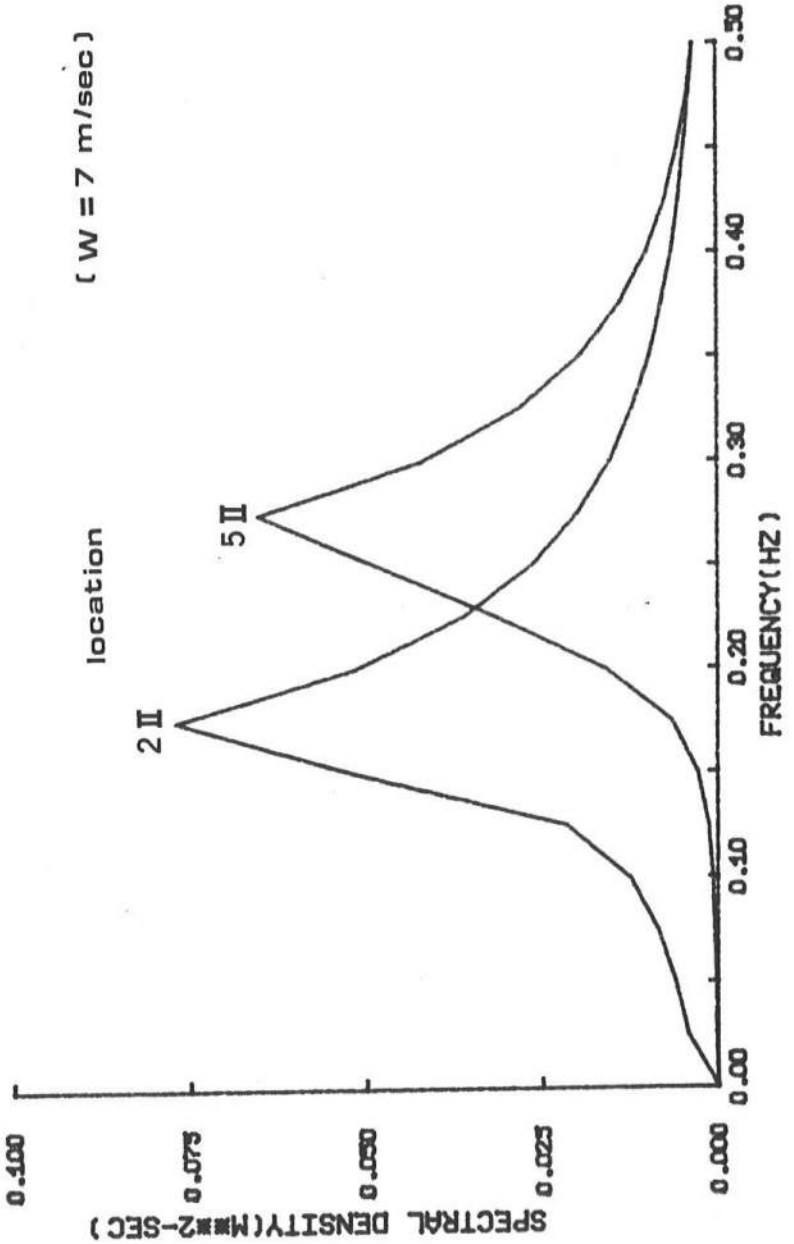

Figure 3.8 Energy Spectrum of Local Wind at Location 5II and Location 2II

phenomenon. Since the Kitaigorodskii's shallow water equilibrium energy criteria ,open at one end, can only handle the wave breaking for a specific range, the criteria for the breaking of the long wave components needs to be restricted by the depth-limited wave condition. The comparison of the local wind wave spectrum at location 5II and location 2II with P-M spectrum is shown in Figure 3.9. The result at location 5II is fair because the energy spectrum of that particular location hasn't been fully developed yet. The result at location 2II is also fair because the P-M spectrum is only valid in deep water.

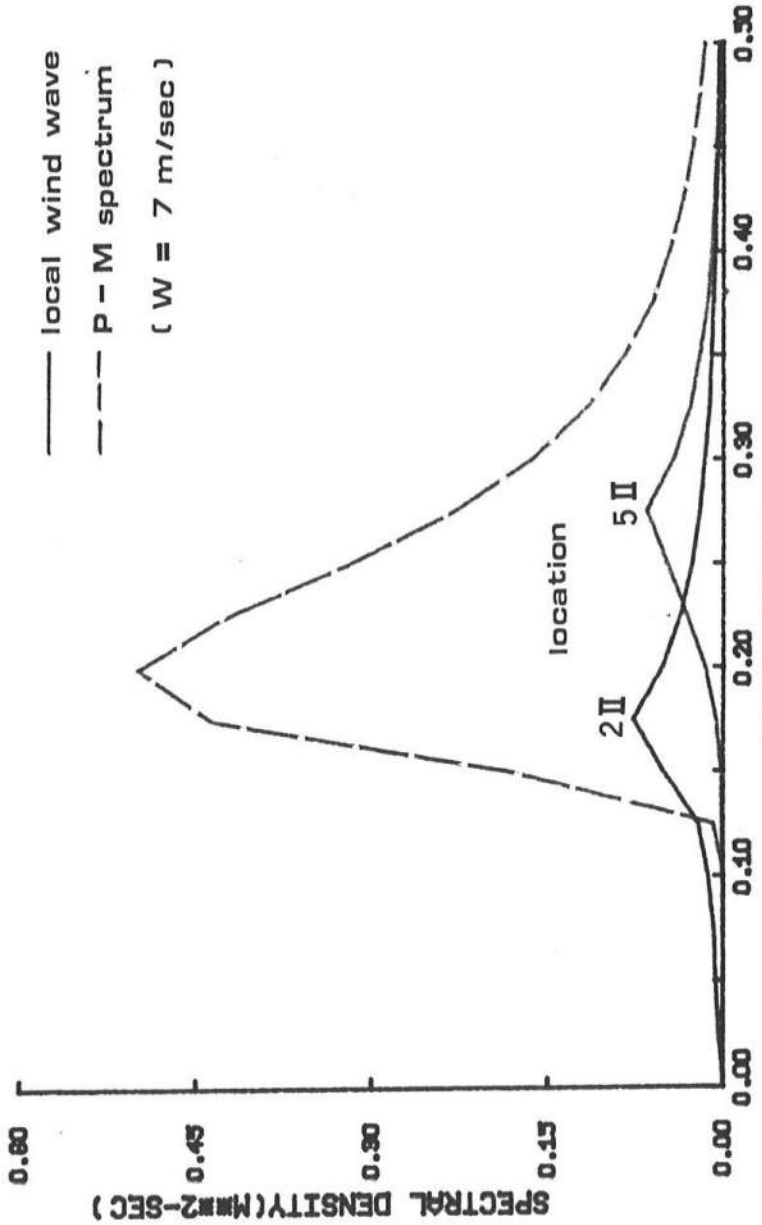

Figure 3.9 Comparison of Energy Spectrum of Local Wind at Location 5II and 2II with Pierson-Moskowitz Spectrum

CHAPTER 4

NUMERICAL SCHEME OF NON-STATIONARY WAVE SPECTRAL TRANSFORMATION

In the previous chapter, the numerical scheme for the stationary wave spectral transformation was developed. For the case of non-stationary wave spectral transformation, the problem is more complicated because the kinematic and dynamic characteristics change with time. This chapter extends the model to unsteady state case when the offshore boundary condition and the local wind effect in the domain of consideration are no longer stationary. This is a common situation when a hurricane or storm sweeps through offshore of a coastal region.

4.1 Basic Equations for Non-Stationary Wave Spectral Transformation

Basic equations for non-stationary wave spectral transformation have been developed in chapter 2. They are repeated here:

i) Wave Conservation Equation:

$$\frac{\partial \vec{k}}{\partial t} + \vec{\nabla} \bar{\alpha} = 0 \qquad (4.1)$$

ii) Wave Number Conservation Equation:

$$(gk \tanh kh)^{1/2} + Uk\cos\theta + Vk\sin\theta = \frac{2\pi}{T} \qquad (4.2)$$

iii) Wave Number Irrotational Equation:

$$\frac{\partial (k\cos\theta)}{\partial y} - \frac{\partial (k\sin\theta)}{\partial x} = 0 \qquad (4.3)$$

iv) Energy Transport Equation:

$$\frac{\partial A}{\partial t} + \frac{\partial}{\partial x}\left[A(U + C_g\cos\theta)\right] + \frac{\partial}{\partial y}\left[A(V + C_g\sin\theta\right]$$

$$+ S_{xx}\frac{\partial U}{\partial x} + S_{xy}\frac{\partial U}{\partial y} + S_{yx}\frac{\partial V}{\partial x} + S_{yy}\frac{\partial V}{\partial y}$$

$$= \sum_{i=1}^{3} G_i \qquad (4.4)$$

where

$$\sum_{i=1}^{3} G_i = G_1 + G_2 + G_3$$

$$= \mu(\alpha + \beta A) + \bar{\Phi}$$

α is Phillips resonant mechanism Eq. (2.30)

β is Miles instability mechanism Eq. (2.39)

μ is breaking coefficient

Φ is bottom dissipation Eq. (2.44)

4.2 Method of Solution

The numerical scheme described in the previous chapter can not be easily extended to the non-statioary case because the nature of the differential equations changed significiantly with the addition of the unsteady term $\frac{\partial(\ )}{\partial t}$. An entirely new numerical scheme has to be developed.

4.2.1 Two-Step Lax-Wendroff Scheme

The finite difference scheme for initial-boundary value problems can be classified into two categories: one is implicit method and the other is explicit method. Although the implicit method ensures unconditional stability criteria, it usually involves lengthy computations due to matrix inverse. Therefore, an explicit method is explored here. The two-step Lax-Wendroff scheme, i.e., the first half step is Lax-Friedrichs scheme and the second half step is leap-frog scheme, was used. The reasons for selecting this scheme are that (1) it is second order accurate, and relatively low in dissipation; (2) it is

single-leveled and easy to apply; and (3) it is widely used by fluid dynamicists and hence it would be desirable to understand fully.

Before applying the actual problem posed above, the numerical scheme is explained first with the application to an initial-boundary value problem which has the similar characteristics as the actual problems but with exact solution. In this way, the validity of the numerical scheme can be established. The stability criteria was then examined.

The example, with a non-constant coefficient and non-homogeneous term, is shown as follows.

Governing Equation (G.E.):

$$\frac{\partial U}{\partial t} + \left(\frac{2x - x^2}{69162 + t}\right)\frac{\partial U}{\partial x} = -\left(\frac{x - 1}{69162 + t}\right)U \qquad (4.5)$$

Initial Condition (I.C.):

$$U(x,0) = x / 69162$$

Boundary Conditions (B.C):

$$U(0,t) = 0$$

$$U(35,t) = 35 / (69162 + t)$$

Then the exact solution is

$$U(x,t) = x / (69162 + t) \qquad (4.6)$$

Let's define the coefficients as

$$a_1(x,t) = \frac{2x - x^2}{69162 + t}$$

$$a_2(x,t) = \frac{x - 1}{69162 + t}$$

Equation (4.5) becomes

$$\frac{\partial U}{\partial t} + a_1(x,t)\frac{\partial U}{\partial x} = -a_2(x,t)U \qquad (4.7)$$

According to the two-step Lax-Wendroff scheme, the difference equation of Equation (4.7) becomes

i) Lax-Friedrichs' Scheme: modified forward difference.

$$\frac{U_i^n - \frac{1}{2}(U_{i+1}^{n-1} + U_{i-1}^{n-1})}{\Delta t} + a_1(x,t)_i^{n-1}\frac{(U_{i+1}^{n-1} - U_{i-1}^{n-1})}{2\Delta x}$$

$$= -a_2(x,t)_i^{n-1} U_i^{n-1} \qquad (4.8)$$

ii) Leap-Frog Scheme: three time level.

$$\frac{U_i^{n+1} - U_i^{n-1}}{2\Delta t} + a_1(x,t)_i^n \frac{(U_{i+1}^n - U_{i-1}^n)}{2\Delta x} = -a_2(x,t)_i^n U_i^n \qquad (4.9)$$

where

the subscript i, j represent the discritization of x-axis and y-axis,

the superscript n represents the discritization in time axis.

Using a time step $\Delta t/2$ instead of Δt in the first two half steps, the accuracy of the first calculation has been improved. The computation procedures are illustrated schematically in Figure 4.1 and 4.2.

4.2.2 Stability Analysis

Richtmyer and Morton (1967) showed that the well-known Lax Equivalence Theorem is

"For a well-posed initial-value problem for linear differential equations, and for a consistent difference approximation, stability is necessary and sufficient for convergence."

In other words, to show stability analysis is to show convergence.

4.2.2.1 Homogeneous Equation

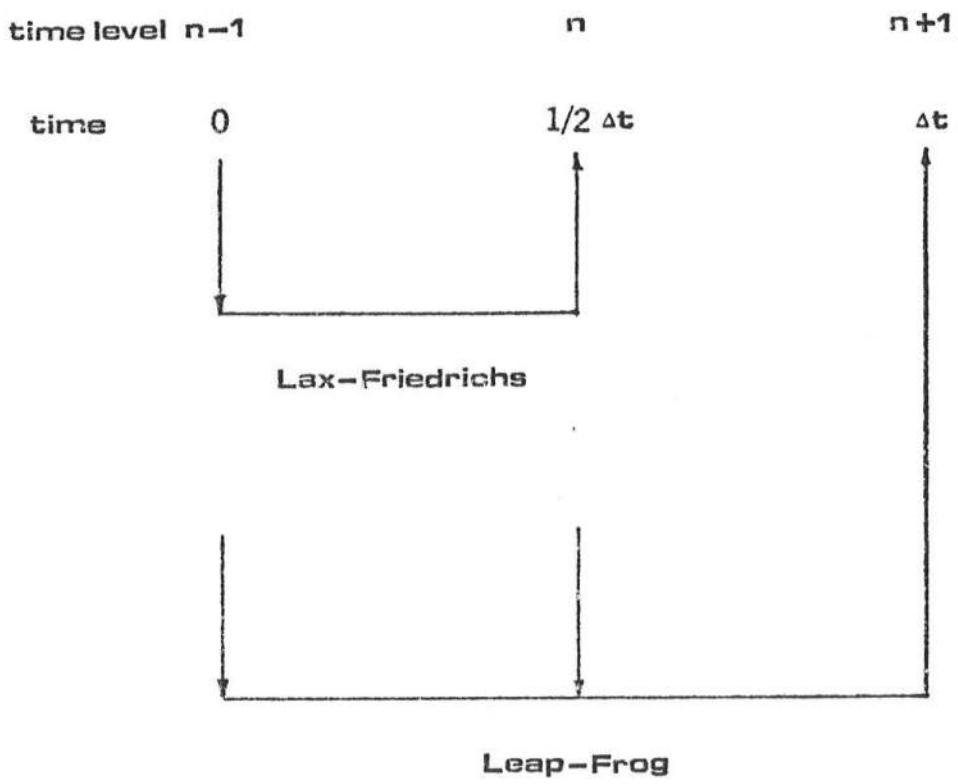

Figure 4.1 Initial Lax-Friedrichs and the First Leap-Frog Scheme Solution Steps

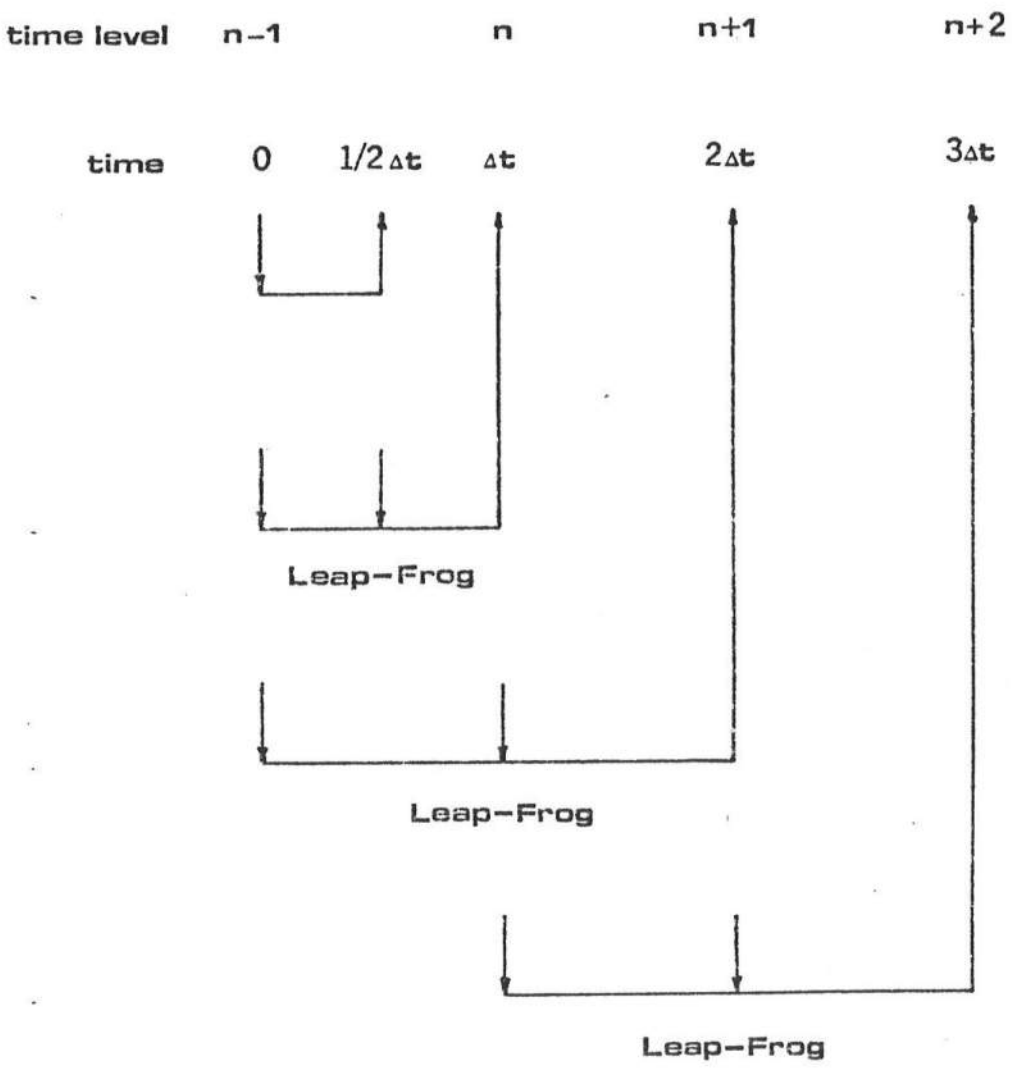

Figure 4.2 General Leap-Frog Solution Scheme

The homogeneous equation for Equation (4.7) is

$$\frac{\partial U}{\partial t} + a_1(x,t)\frac{\partial U}{\partial x} = 0 \qquad (4.10)$$

The stability criteria can be found as

$$\left| a_1(x,t)\frac{\Delta t}{\Delta x} \right| \leq 1$$

or

$$\Delta t \leq \left| \frac{\Delta x}{a_1(x,t)} \right| \qquad (4.11)$$

If $a_1(x,t)$ is constant, the stability criteria will vary with Δx only and follow the Equation (4.11). Whereas, $a_1(x,t)$ is not a constant, the time step Δt actually used is much less than that given by the above criteria.

4.2.2.2 Non-Homogeneous Equation

The stability criteria for the non-homogeneous equation has to meet the following condition, one condition is the same as that of homogeneous equation, i.e.,

$$\Delta t \leq \left| \frac{\Delta x}{a_1(x,t)} \right|$$

the other condition is

$$|a_2(x,t)\Delta t| < 1 \qquad (4.12)$$

The domain of the problem, with distance of 35 along the x-axis, is divided into five sections, denoted as location 1 to 6. By using Δt equal to 84 and Δx equal to 7, the comparison between the exact and the approximate solution from location 2 to 5 are shown in Figure 4.3. It seems that the approximate solution becomes unstable after a few time steps. The reason is due to the time level of the non-homogeneous term in Leap-Frog Scheme. By using (n-1)th time level instead of nth time level for the non-homogeneous term, the problem will be handled. Equation (4.9) is rewritten as follows:

$$\frac{U_i^{n+1} - U_i^{n-1}}{2\Delta t} + a_1(x,t)_i^n \frac{(U_{i+1}^n - U_{i-1}^n)}{2\Delta x} = -a_2(x,t)_i^{n-1} U_i^{n-1} \qquad (4.13)$$

The new results are shown in Figure 4.4 and agree reasonably well. Thus the effectiveness of the numerical scheme for solving a transient problem is demonstrated.

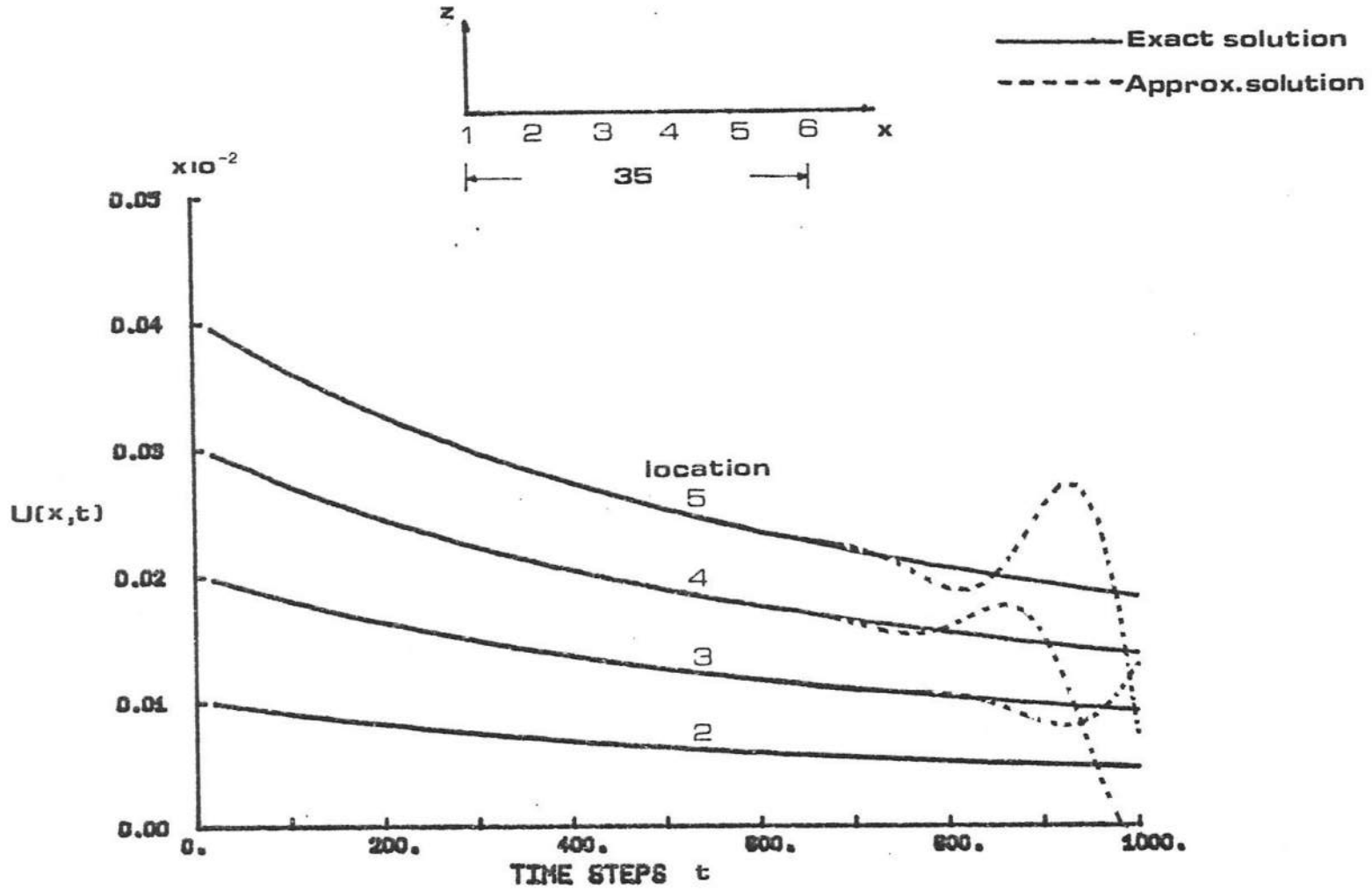

Figure 4.3 Comparison between Exact and Approximate Solutions with Non-Homogeneous Term in nth Time Level in Leap-Frog Scheme

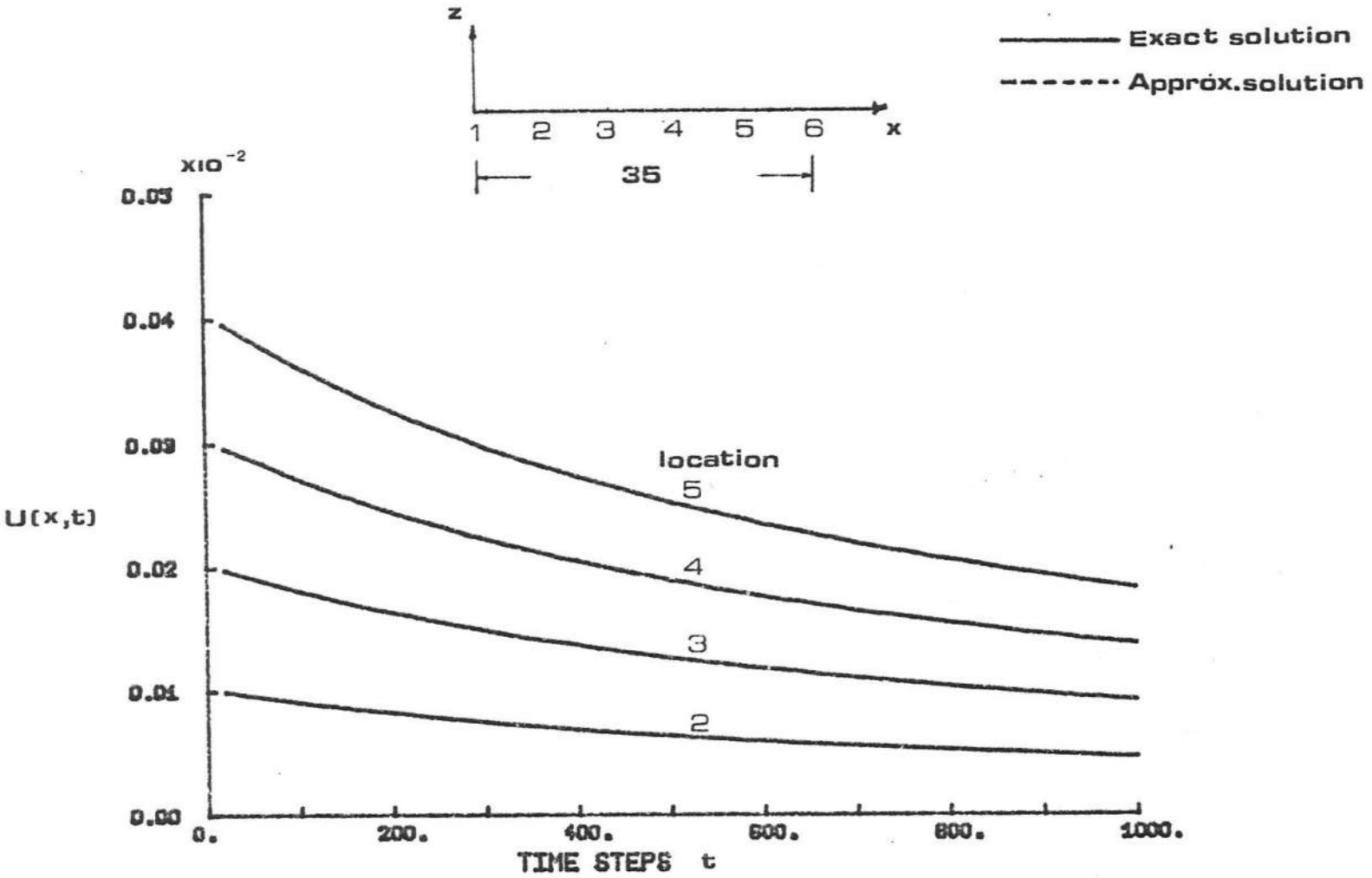

Figure 4.4 Comparison between Exact and Approximate Solutions with Non-Homogeneous Term in (n-1)th Time Level in Leap-Frog Scheme

4.2.3 Numerical Dissipation and Dispersion Analysis

It is well known that numerical schemes introduce numerical dissipation and dispersion, in roughly the same way as physical dissipation and dispersion occur in phenomena of fluid flow. Dissipation means the damping of Fourier components or plane waves. Dispersion means the propagation of plane waves of different components at different speeds c.

For the case of one dimensional shallow water wave in uniform depth and zero current, the wave conservation equation and the energy transport eqution can be written as

$$\frac{\partial k}{\partial t} + C \frac{\partial k}{\partial x} = 0 \qquad (4.14)$$

$$\frac{\partial A}{\partial t} + C \frac{\partial A}{\partial x} = 0 \qquad (4.15)$$

Both equations are wave equations representing a wave of form k or A propagating without change of shape at speed c in the positive x direction. To illustrate the effect of numerical dissipation and dispersion, an example, with a function f representing k and A in

Equations (4.14) and (4.15), is shown as follows:.

Governing Equations (G.E.):

$$\frac{\partial f}{\partial t} + c \frac{\partial f}{\partial x} = 0 \qquad (4.16)$$

Initial Condition (I.C.):

$$f(x,0) = 0$$

Boundary Condition (B.C.):

$$f(0,t) = \begin{cases} 0 & t<0 \\ 2t & 0 \le t < 2 \\ 4-t & 2 \le t < 4 \\ 0 & t \ge 4 \end{cases}$$

The exact solution is

$$f(x-ct) \qquad (4.17)$$

which is recognized as having the wave character noted. According to the two-step Lax-Wendroff scheme, the difference equation of Equation (4.16) becomes

i) Lax-Friedrichs' Scheme:

$$\frac{f_i^n - \frac{1}{2}(f_{i+1}^{n-1} - f_{i-1}^{n-1})}{\Delta t} + c \frac{f_{i+1}^{n-1} - f_{i-1}^{n-1}}{2\Delta x} = 0 \qquad (4.18)$$

ii) Leap-Frog Scheme:

$$\frac{f_i^{n+1} - f_i^{n-1}}{2\Delta t} + C\,\frac{f_{i+1}^{n} - f_{i-1}^{n}}{2\Delta x} = 0 \qquad (4.19)$$

The comparison of exact and numerical solution for $r(=C\frac{\Delta t}{\Delta x})=1/2$ is shown in Figure 4.5. It can be seen that both the dissipation and dispersion effects are more significant for $\Delta t=1/2$ than for $\Delta t=1/4$. A large number of spurious oscillations near sharp transition is due to the conservative scheme which will be discussed later.

To illustrate the dissipation and dispersion effects of the Lax-Friedrichs scheme and the Leap-Frog scheme, the amplification factors for the two schemes need to be found. By using the Von Neumann method, a funtion can be represented by a finite Fouries series.

$$f_i^n = \sum_{l=-\infty}^{l=\infty} F^n(l)\, e^{i^* \frac{2\pi l}{L}(i\Delta x)} \qquad (4.20)$$

where

l represents the wave component,

L is wave length,

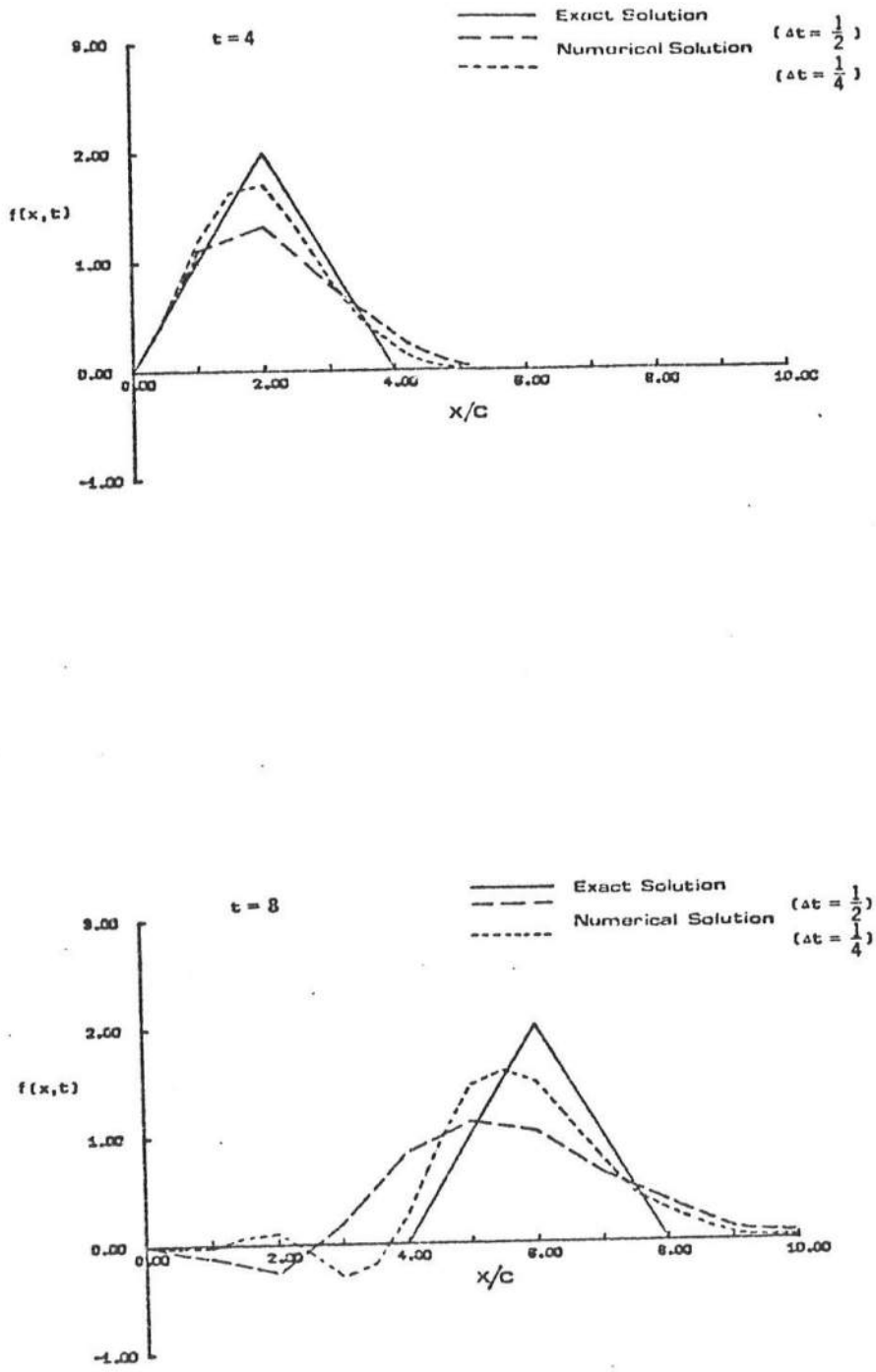

Figure 4.5 Comparison of Exact and Numerical Solution for r=1/2

$$i^* = \sqrt{-1}$$

Substuting Equation (4.20) into Equation (4.18), respectively, one can obtain

$$f_i^n = \sum_{\ell=-\infty}^{\ell=\infty} F^{n-1}(\ell)\, e^{i^* \frac{2\pi\ell}{L}(i\Delta x)} \left\{ \cos \frac{2\pi\ell}{L}\Delta x - i^* r \sin \frac{2\pi\ell}{L}\Delta x \right\} \tag{4.21}$$

and

$$\begin{pmatrix} F^{n+1} \\ F^n \end{pmatrix} = \begin{pmatrix} -i^* 2r \sin \frac{2\pi\ell}{L}\Delta x & 1 \\ 1 & 0 \end{pmatrix} \begin{pmatrix} F^n \\ F^{n-1} \end{pmatrix} \tag{4.22}$$

where $r = C\frac{\Delta t}{\Delta x}$. The amplification factors for Lax-Friedrichs' scheme and leap-frog scheme become

$$RA = \cos \frac{2\pi\ell}{L}\Delta x - i^* r \sin \frac{2\pi\ell}{L}\Delta x \tag{4.23}$$

and

$$RA = -i^* r \sin \frac{2\pi\ell}{L}\Delta x \pm \left(1 - r^2 \sin^2 \frac{2\pi\ell}{L}\Delta x\right)^{1/2} \tag{4.24}$$

Then the amplitudes |RA| for the two schemes are given respectively by

$$|RA| = \left(1 - (1-r^2) \sin^2 \frac{2\pi\ell}{L} \Delta x \right)^{1/2} \qquad (4.25)$$

and

$$|RA| = 1 \qquad (4.26)$$

The phase angles φ_N for the two schemes can be shown respectively as:

$$\varphi_N = \tan^{-1} \left(r \tan \frac{2\pi\ell}{L} \Delta x \right) \qquad (4.27)$$

and

$$\varphi_N = \tan^{-1} \frac{r \sin \frac{2\pi\ell}{L} \Delta x}{\left(1 - r^2 \sin^2 \frac{2\pi\ell}{L} \Delta x \right)^{1/2}} \qquad (4.28)$$

Then the dispersion effect can be shown as

$$\frac{C_{Num}}{C_{exa}} = \frac{\varphi_N}{\frac{2\pi}{m} r} \qquad (4.29)$$

where $m = \frac{(\frac{L}{g})}{\Delta x}$ represents the number of samples per wave length.

The dissipation and dispersion for the Lax-Friedrichs scheme and leap-frog scheme are shown in Figures 4.6 and 4.7, respectively. It can be seen that both dissipation and dispersion effects are more significant for short wave than long wave. The Lax-Friedrichs scheme is dissipative and dispersive, while the leap-frog scheme is non-dissipative, or conservative and dispersive.

4.3 Numerical Analysis for Wave Conservation Equation

Wave conservation equation is a homogeneous equation which can use the two-step Lax-Wendroff scheme. However, it can't be solved singly because it contains angular frequency σ, wave number k, and wave direction θ. The wave kinematic equation including wave conservation equation, wave number conservation equation, and wave number irrotational equation have to be solved simultaneously.

4.3.1 Numerical Procedures

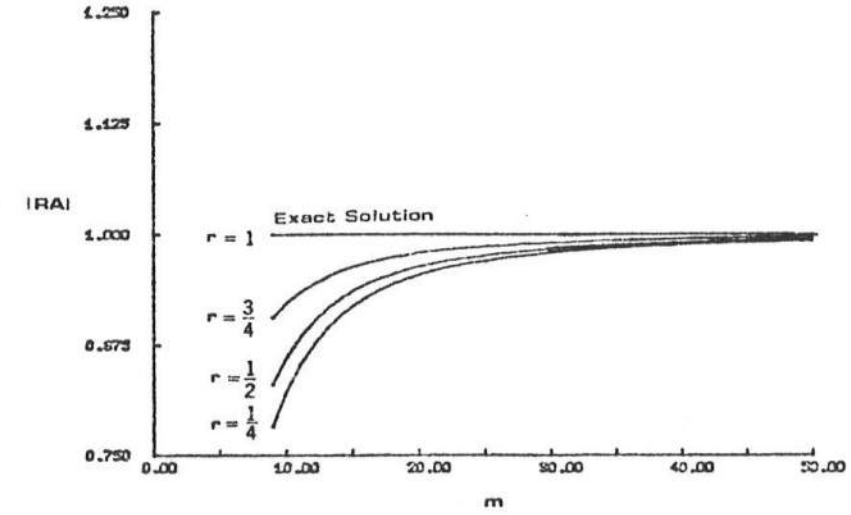

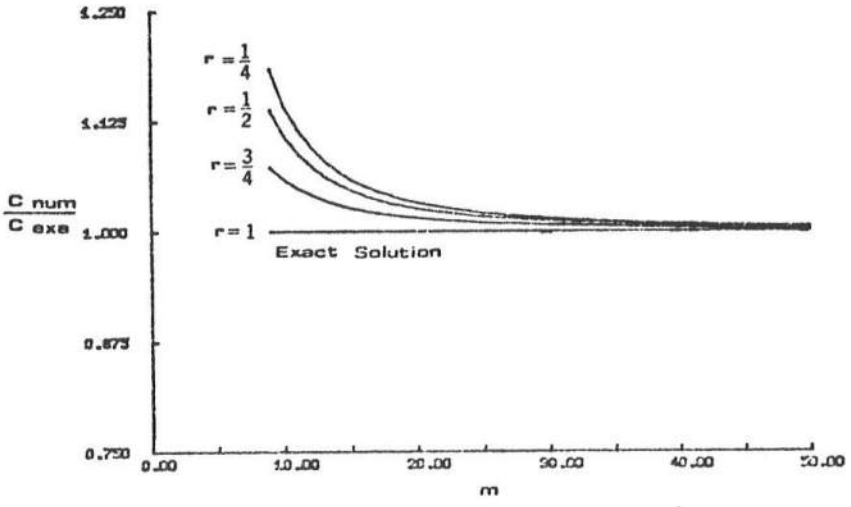

Figure 4.6 Dissipation and Dispersion for the Lax-Friedrichs Scheme

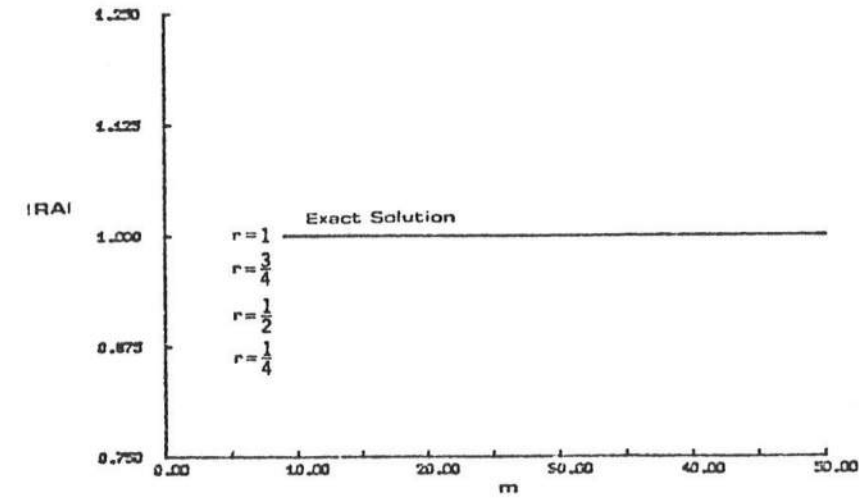

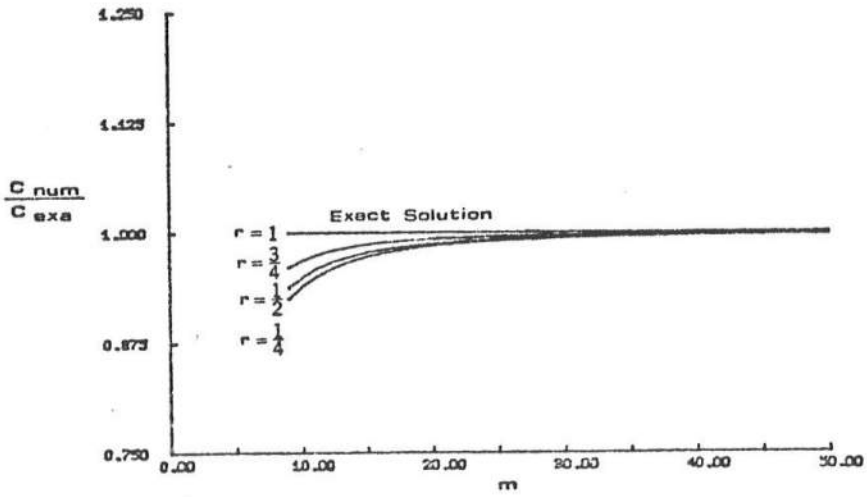

Figure 4.7 Dissipation and Dispersion for the Leap-Frog Scheme

To solve it algebraically, the vector form of wave conservation equation has to be decomposed into two scalar forms, one in x-direction and the other in y-direction. If the wave direction θ measured from the positive x-axis in a counterclockwise direction, Equation (4.1) becomes

x-direction $$\frac{\partial(k\cos\theta)}{\partial t} + \frac{\partial\sigma}{\partial x} = 0 \qquad (4.30)$$

y-direction $$\frac{\partial(k\sin\theta)}{\partial t} + \frac{\partial\sigma}{\partial y} = 0 \qquad (4.31)$$

The other two wave kinematic equations remain to be:

$$(gk\tanh kh)^{1/2} + Uk\cos\theta + Vk\sin\theta = \frac{2\pi}{T} \qquad (4.2)$$

and

$$\frac{\partial(k\cos\theta)}{\partial y} - \frac{\partial(k\sin\theta)}{\partial x} = 0 \qquad (4.3)$$

For given spatial distribution of U, V, and h; σ, k, and θ can be obtained by solving Equations (4.30), (4.31), (4.2) and (4.3) simultaneously with specified initial and boundary conditions. Using the two-step Lax-Wendroff scheme.

i) Lax-Friedrichs' Scheme

$$\frac{(K\cos\theta)^{n}_{i,j} - \frac{1}{2}\left[(K\cos\theta)^{n-1}_{i+1,j} + (K\cos\theta)^{n-1}_{i-1,j}\right]}{\Delta t} + \frac{\alpha^{n-1}_{i+1,j} - \alpha^{n-1}_{i-1,j}}{2\Delta x} = 0 \qquad (4.32)$$

$$\frac{(K\sin\theta)^{n}_{i,j} - \frac{1}{2}\left[(K\sin\theta)^{n-1}_{i,j+1} + (K\sin\theta)^{n-1}_{i,j-1}\right]}{\Delta t} + \frac{\alpha^{n-1}_{i,j+1} - \alpha^{n-1}_{i,j-1}}{2\Delta y} = 0 \qquad (4.33)$$

ii) Leap-Frog Scheme

$$\frac{(K\cos\theta)^{n+1}_{i,j} - (K\cos\theta)^{n-1}_{i,j}}{2\Delta t} + \frac{\alpha^{n}_{i+1,j} - \alpha^{n}_{i-1,j}}{2\Delta x} = 0 \qquad (4.34)$$

$$\frac{(K\sin\theta)^{n+1}_{i,j} - (K\sin\theta)^{n-1}_{i,j}}{2\Delta t} + \frac{\alpha^{n}_{i,j+1} - \alpha^{n}_{i,j-1}}{2\Delta y} = 0 \qquad (4.35)$$

4.3.2 Stability Analysis

According to the stability analysis for homogeneous equation, the stability criteria for the present difference equation is

$$\frac{\Delta t}{\Delta x} + \frac{\Delta t}{\Delta y} \leq 1$$

or

$$\Delta t \leq \Delta x + \Delta y \qquad (4.36)$$

Because the coefficient is a constant, the time step Δt obeys the stability criterion as given by Eq. (4.20).

4.3.3 Initial Condition and Boundary Conditions

To solve the wave conservation equation, it is necessary to choose suitable initial condition in the domain and boundary conditions at boundaries. The initial condition can be decided by either angular frequency or wave number and wave angle. Based on the steady state assumption, the angular frequency does not change with space. It is constant even as the water depth changes. Hence, the initial condition is determined more conveniently by constant angular frequency, which is invariant with space, than by the wave number and wave angle, which varies with space.

As for the boundary conditions, the variation of the wave energy has an effect on the offshore boundary condition. In other words, the kinematic condition will vary if the dynamic condition changes. The rest of the boundary conditions, shore boundary and side boundaries, need to be specified to carry out the numerical scheme. At shore, no flow of water occurs across the shoreline, thus the shore boundary doesn't

vary with the changing dynamic condition. The side boundaries require that the longshore bottom variation in the vincinty of both sides is slow.

4.4 Numerical Analysis for Energy Transport Equation

The energy transport equation is a non-homogeneous equation which is the same type as Equation (4.7) except it is a two dimemsional equation.

4.4.1 Numerical Procedures

After expanding and rearranging, Equation (4.4) arrives at

$$\frac{\partial A}{\partial t} + (U + C_g \cos\theta)\frac{\partial A}{\partial x} + (V + C_g \sin\theta)\frac{\partial A}{\partial y} +$$

$$A\left[\frac{\partial}{\partial x}(U + C_g \cos\theta) + \frac{\partial}{\partial y}(V + C_g \sin\theta) + \alpha_{xx}\frac{\partial U}{\partial x} + \right.$$

$$\left.\alpha_{xx}\frac{\partial U}{\partial y} + \alpha_{yx}\frac{\partial V}{\partial x} + \alpha_{yy}\frac{\partial V}{\partial y} - \mu\beta - \epsilon\right] - \mu\alpha = 0 \quad (4.37)$$

or

$$\frac{\partial A}{\partial t} + (U + C_g \cos\theta)\frac{\partial A}{\partial x} + (V + C_g \sin\theta)\frac{\partial A}{\partial y} = (Q + \mu\beta + \epsilon)A + \mu\alpha \quad (4.38)$$

where

$$Q = -\left(\frac{\partial U}{\partial x} + \frac{\partial V}{\partial y}\right) + C_g \sin\theta \frac{\partial \theta}{\partial x} - \cos\theta \frac{\partial C_g}{\partial x}$$

$$- C_g \cos\theta \frac{\partial \theta}{\partial y} - \sin\theta \frac{\partial C_g}{\partial y} - J$$

$$J = \alpha_{xx}\frac{\partial U}{\partial x} + \alpha_{xy}\frac{\partial U}{\partial y} + \alpha_{yx}\frac{\partial V}{\partial x} + \alpha_{yy}\frac{\partial V}{\partial y}$$

Applying the two-step Lax-Wendroff scheme, the finite difference form of Equation (4.38) is

i) Lax-Friedrichs' Scheme

$$\frac{A_{i,j}^{n} - \frac{1}{4}\left(A_{i,j+1}^{n-1} + A_{i,j-1}^{n-1} + A_{i+1,j}^{n-1} + A_{i-1,j}^{n-1}\right)}{\Delta t} +$$

$$(U + C_g \cos\theta)_{i,j}^{n-1} \quad \frac{(A_{i+1,j}^{n-1} - A_{i-1,j}^{n-1})}{2\Delta x} +$$

$$(V + C_g \sin\theta)_{i,j}^{n-1} \quad \frac{(A_{i,j+1}^{n-1} - A_{i,j-1}^{n-1})}{2\Delta y}$$

$$= (Q_{i,j}^{n-1} + \mu\beta_{i,j}^{n-1} + \epsilon_{i,j}^{n-1})\, A_{i,j}^{n-1} + \mu\alpha_{i,j}^{n-1} \qquad (4.39)$$

ii) Leap-Frog Scheme

$$\frac{A_{i,j}^{n+1} - A_{i,j}^{n-1}}{2\Delta t} + (U + C_g \cos\theta)_{i,j}^{n} \quad \frac{(A_{i+1,j}^{n} - A_{i-1,j}^{n})}{2\Delta x}$$

$$+ (V + C_g \sin\theta)_{i,j}^{n} \quad \frac{(A_{i,j+1}^{n} - A_{i,j-1}^{n})}{2\Delta y}$$

$$= (Q_{i,j}^{n-1} + \mu\beta_{i,j}^{n-1} + \epsilon_{i,j}^{n-1})\, A_{i,j}^{n-1} + \mu\alpha_{i,j}^{n-1}$$

(4.40)

To avoid instabilities,, the non-homogeneous term has to be put in (n-1) time level as shown in Equation (4.40).

4.4.2 Stability Analysis

According to the stability analysis for non-homogeneous equation, the stability criteria for the present difference equation has to meet the following two conditions:

i)

$$|U + C_g \cos\theta| \frac{\Delta t}{\Delta x} + |V + C_g \sin\theta| \frac{\Delta t}{\Delta y} \leq 1$$

or

$$\Delta t \leq \frac{\Delta x}{|U + C_g \cos\theta|} + \frac{\Delta y}{|V + C_g \sin\theta|} \qquad (4.41)$$

and

ii)

$$|(Q + \mu\beta + \epsilon)\Delta t| < 1$$

or

$$\Delta t < \frac{1}{|Q + \mu\beta + \epsilon|} \qquad (4.42)$$

In general, the first condition can be stated in the following manner: the speed of propagation of any

disturbance in the model must be less than or equal to the speed it takes the disturbance to cross one computational grid block in one computational time step. The disturbance speed is in general the speed of gravity wave plus the time-independent mean current. Therefore, in shallow water, Equation (4.41) can be expressed approximately as

$$\Delta t \leqq \frac{\sqrt{(\Delta x)^2+(\Delta y)^2}}{|U| + C} \qquad (4.43)$$

In general, the maximum magnitude of the wave speed far exeeds the current speed, the stability criteria can be expressed as

$$\Delta t \leqq \frac{\sqrt{(\Delta x)^2+(\Delta y)^2}}{C_{max}} \qquad (4.44)$$

which is a type of two dimensional Courant number.

As stated before, the time step actually used in the numerical model is much less than that given by the criteria above due to the fact that the coefficient is not a constant in Equation (4.41).

4.4.3 Initial Condition and Boundary Conditions

It is necessary to specify the initial and boundary conditions to solve energy transport equation. Commonly, the initial condition falls in one of the two types: one is for calm sea where the wave energy is equal to zero and the other is the fully developed sea where the wave energy is saturated.

There are also two types of offshore boundary conditions. The first type is an open boundary. It is a time varying boundary condition which is affected by the offshore wave condition. In general, it can be prescribed by a continuous variation of wave spectrum at the offshore boundary. The second type is a closed boundary which is not affected by the offshore wave condition but self-adjusting. In order to apply the numerical scheme, the shore boundary condition and the side boundary conditions also need to be specified. At the shoreline, the wave numbers are to be perpendicular to the shoreline and the bottom slope to be finite. The side boundaries are such that the bottom contours are parallel outside the region of computation.

4.5 Application in Monochromatic Wave

To examine the micro-mechanism of wave spectral transformation, the cases of a one-dimensional and two-dimensional monochromatic wave are illustrated here. The random wave model and the field data comparison are dealt with in the next chapter.

In computing wave kinematics, the initial condition is set at constant angular frequency over the entire region of computation. Therefore, the boundary conditions should also be specified in terms of angular frequency. The offshore boundary condition can be determined from a continous variation of wave spectrum at the offshore boundary. The shore boundary doesn't vary with changing the dynamic condition. In order to proceed with the numerical scheme, the boundary conditions at both sides will be specified as follows:

$$\frac{\partial \sigma}{\partial t} \pm C_g \frac{\partial a}{\partial y} = 0 \qquad (4.45)$$

In the energy transport equation, the steady state wave spectral transformation is chosen as the initial condition. Since only swell condition is considered in this section, an open offshore boundary

condition is used. The boundary condition at the shoreline is assumed to be both no energy flux into the shoreline and no reflection from the shoreline. The boundary conditions at both sides need to be specified because of the numerical procedure. They can be expressed as follows:

$$\frac{\partial A}{\partial t} \pm C_g \frac{\partial A}{\partial y} = 0 \qquad (4.46)$$

A schematic view of a two-dimensional case, with horizontal dimensions 60 m by 150 m and water depth 1 m, is shown in Figure 4.8. The coordinates are chosen as x-axis toward the offshore, y-axis alongshore, and z-axis upward. To apply the numerical scheme, the region is divided into five sections along the positive x-axis, with Δx=20 m, denoted as location 1 to 6, and it is divided into four sections along the positive y-axis, with Δy=15 m, denoted as location I to V. The time step Δt=1 sec is used in all cases.

4.5.1 One-Dimensional Case

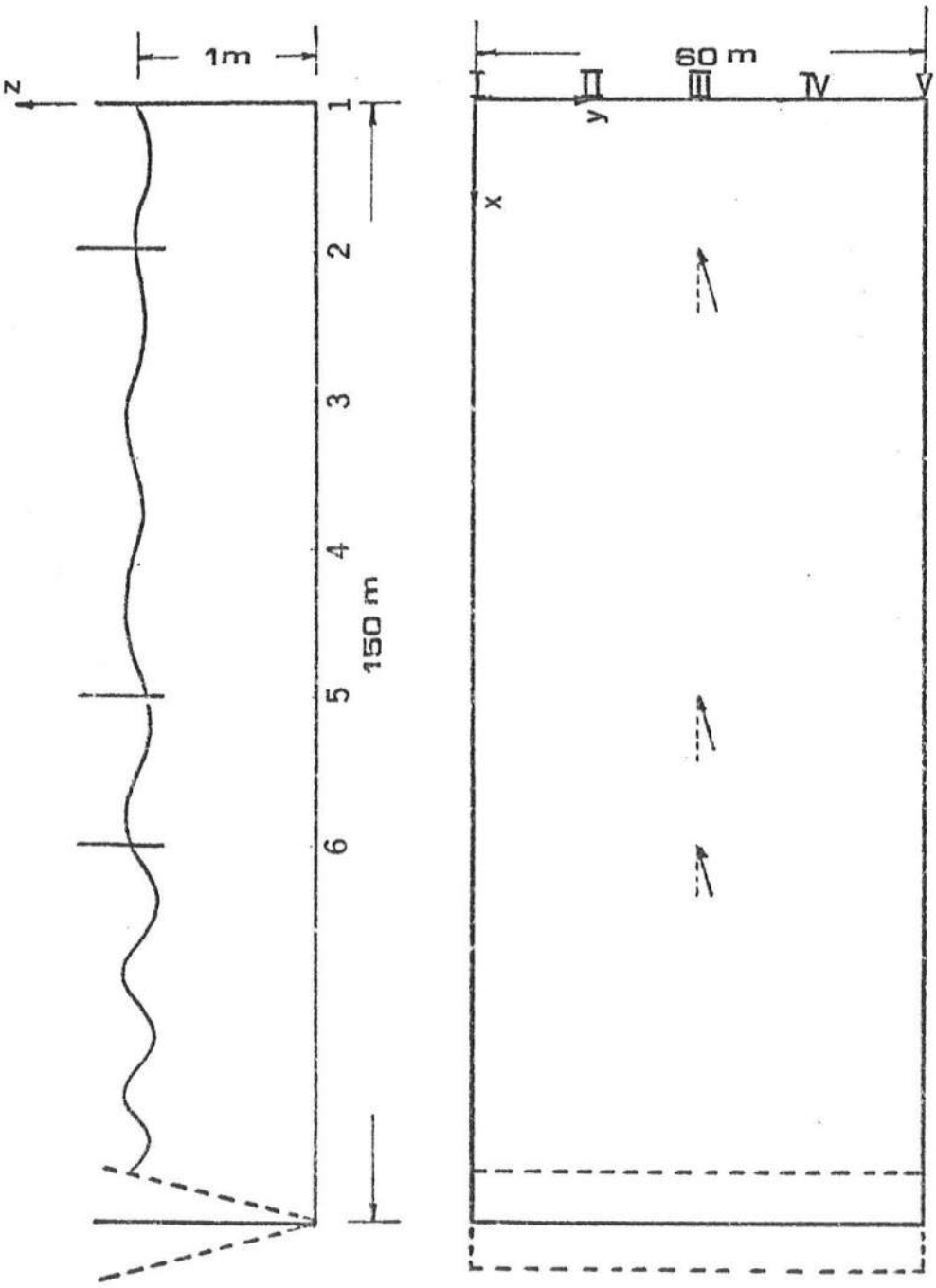

Figure 4.8 Schematic View of a Two Dimensional Case

In this section, three different conditions will be considered. The first case examines the wave transformation process when the wave at the offshore boundary becomes increasingly shorter (a case of diminishing wind). A monochromatic wave, with T=10 sec and H=0.1m, propagates along the negative x-axis. On reaching the steady state, the frequency of the wave component stays at 0.1 HZ no matter where the location is. As shown in Figure 4.9, the three plots represent the wave spectrum at location 6III (boundary), location 5III and location 2III, respectively; the wave spectrum of each plot denoted by t=0 sec is at steady state. The wave at offshore boundary is then gradually adjusted to generate a higher frequency wave component, which increases frequency from f=0.10 HZ to f=0.15 HZ, within 60 seconds. When t=20 sec, the frequency of the wave component at location 6III is higher than that of the wave component at location 5III. However, the wave component at location 2III is still at steady state. It is due to the fact that the component at the boundary has not arrived at location 5III and location 2III yet. As time elapses, this phenomenon occurs also at both location 5III and location 2III. If the wave component at the boundary becomes steady again, the

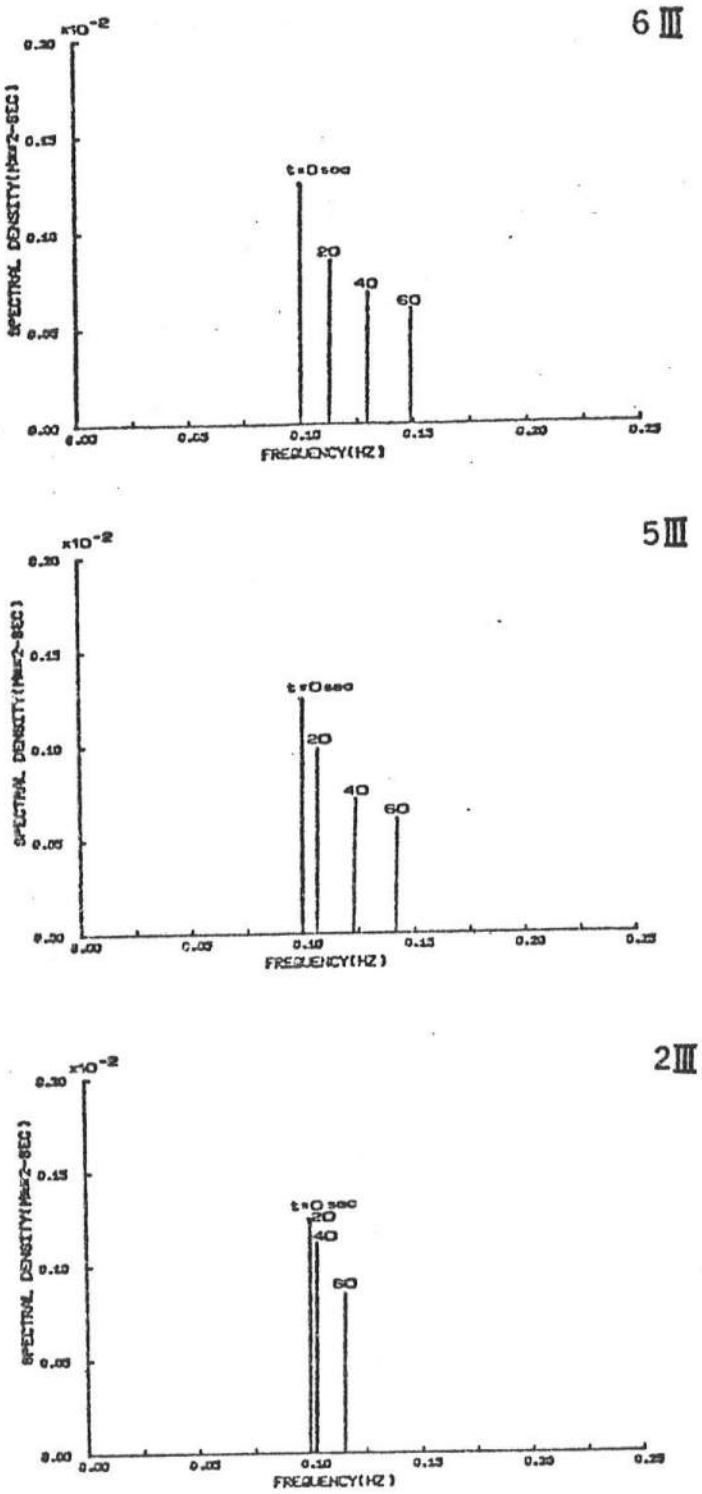

Figure 4.9 Variation of Wave Energy Decreasing with T=10sec, $\theta=0^{\circ}$ at Boundary, Location 5III and Location 2III

wave component at other locations continues to change until it reaches the new steady state.

The second case, shown in Figure 4.10, investigates the wave transformation for a shorter wave with T=2.5 sec and H=0.08 m. Under the same condition as in the first case, all the short wave components will follow the same pattern as that of long wave component except that the short wave component travels slower than the long wave component within the same time period. It is owing to the fact that the group velocity of a short wave is smaller than that of a long wave. The short wave component lags behind as the long wave component moves ahead.

In contrast to the first two cases, the third case investigates the wave transformation when the wave at offshore boundary becomes longer with the short wave component as the initial steady state condition. As soon as the monochromatic wave, T=10 sec and H=0.1 m, propagating along the negative x-axis, reaches steady state, the offshore wave is adjusted to lower frequency, from f=0.10 HZ to f=0.05 HZ within 60 seconds. This phenomenon is shown in Figure 4.11.

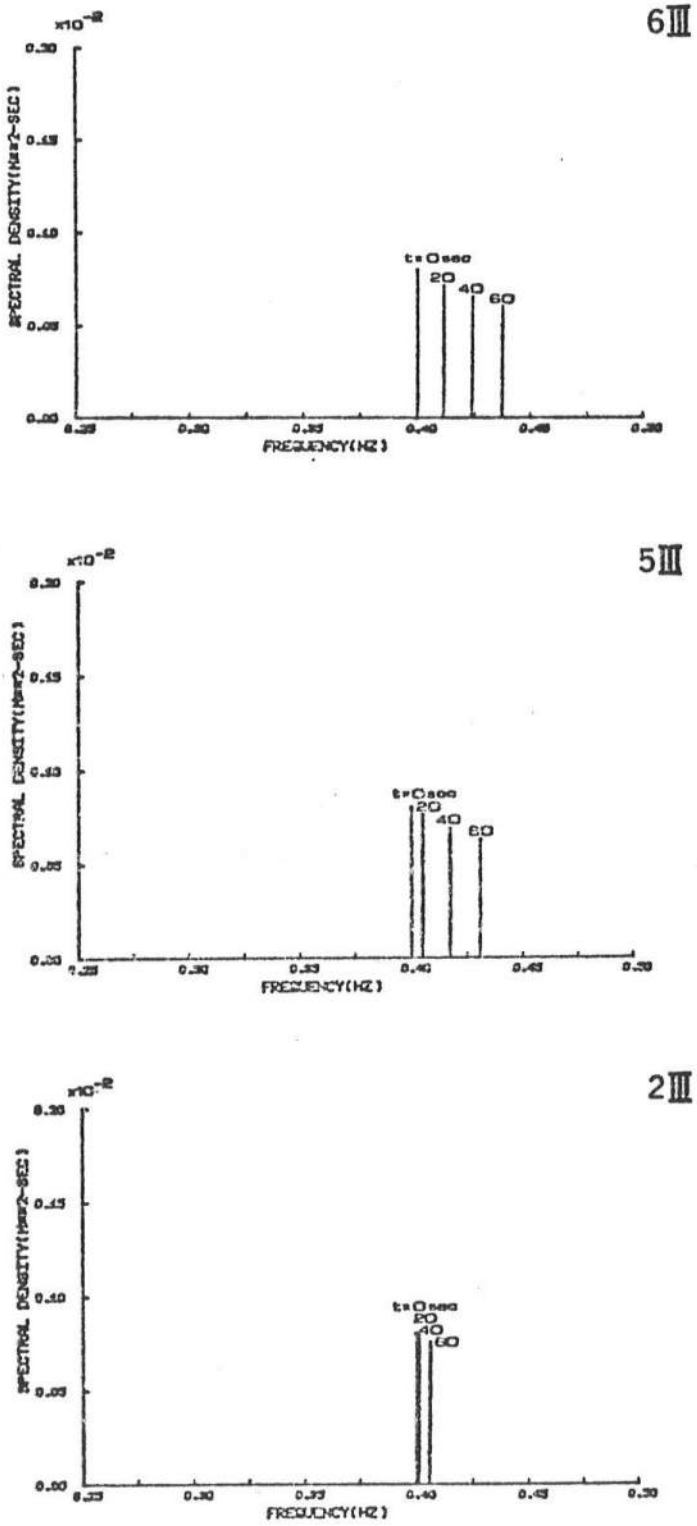

Figure 4.10 Variation of Wave Energy Decreasing with T=2.5sec, θ=0° at Boundary, Location 5III and Location 2III

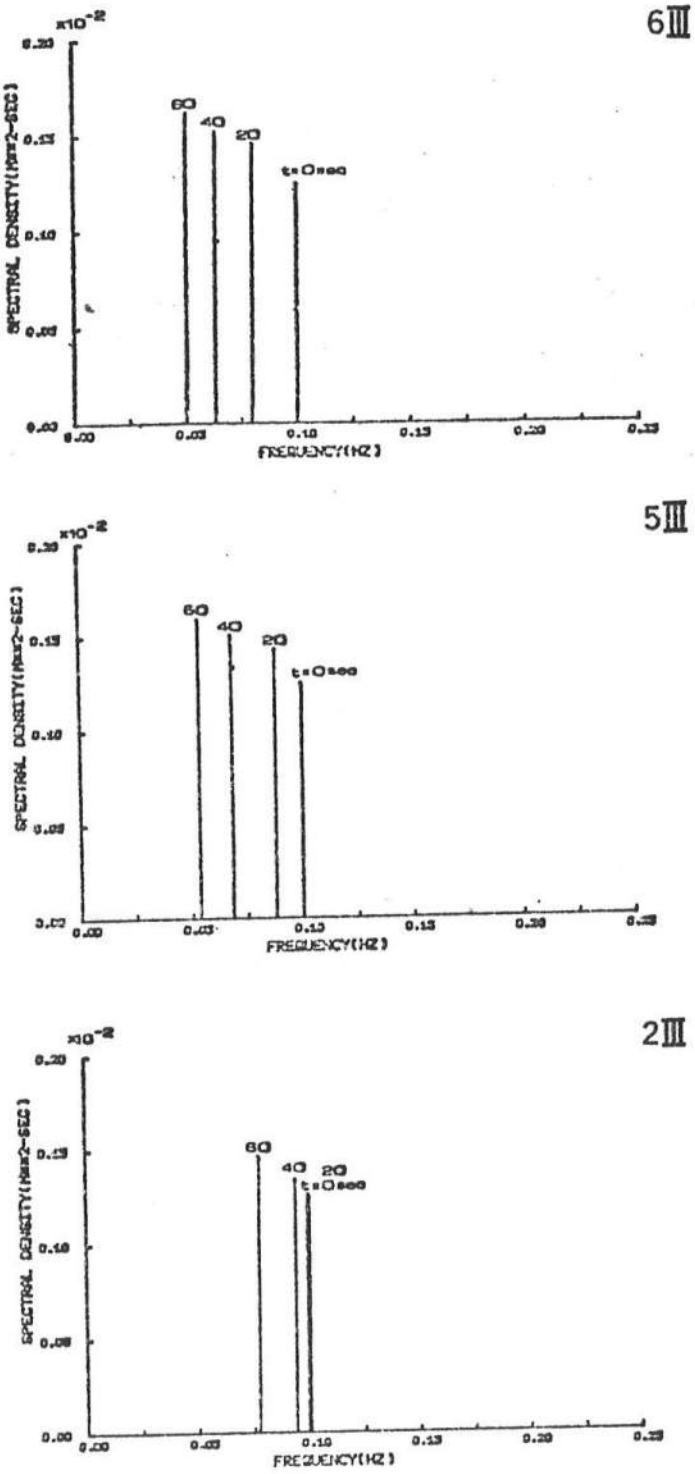

Figure 4.11 Variation of Wave Energy Increasing with T=10sec, $\theta=0^{\circ}$ at Boundary, Location 5III and Location 2III

4.5.2 Two-Dimensional Case

Three different cases are discussed in this section. The first case illustrates when a monochromatic wave, with T=10 sec and H=0.1 m, propagates in the direction of $\theta=20^{\circ}$ with respect to negative x-axis. After the wave transformation reaches its steady state, the wave at offshore boundary is then adjusted to generate higher frequency component from f=0.10 HZ to f=0.15 HZ and smaller wave angle within 60 seconds. The variation of energy spectrum in two-dimensions, as shown in Figure 4.12, is similar to that in one-dimension. As time elapses, as shown in Figure 4.13, the wave component approaching the center line, i.e., $\theta=0^{\circ}$, from right to left, occurs first at boundary, then at location 5III and finally at location 2III. It is because the wave frequency, wave number and wave angle are correlated during the non-stationary process. The wave angle will change as the wave frequency varies with time.

Figure 4.14 provides the second case with the same condition as the first case except propagating in the direction of $\theta=-20^{\circ}$ with respect to the negative x-axis. As time elapses, the wave component

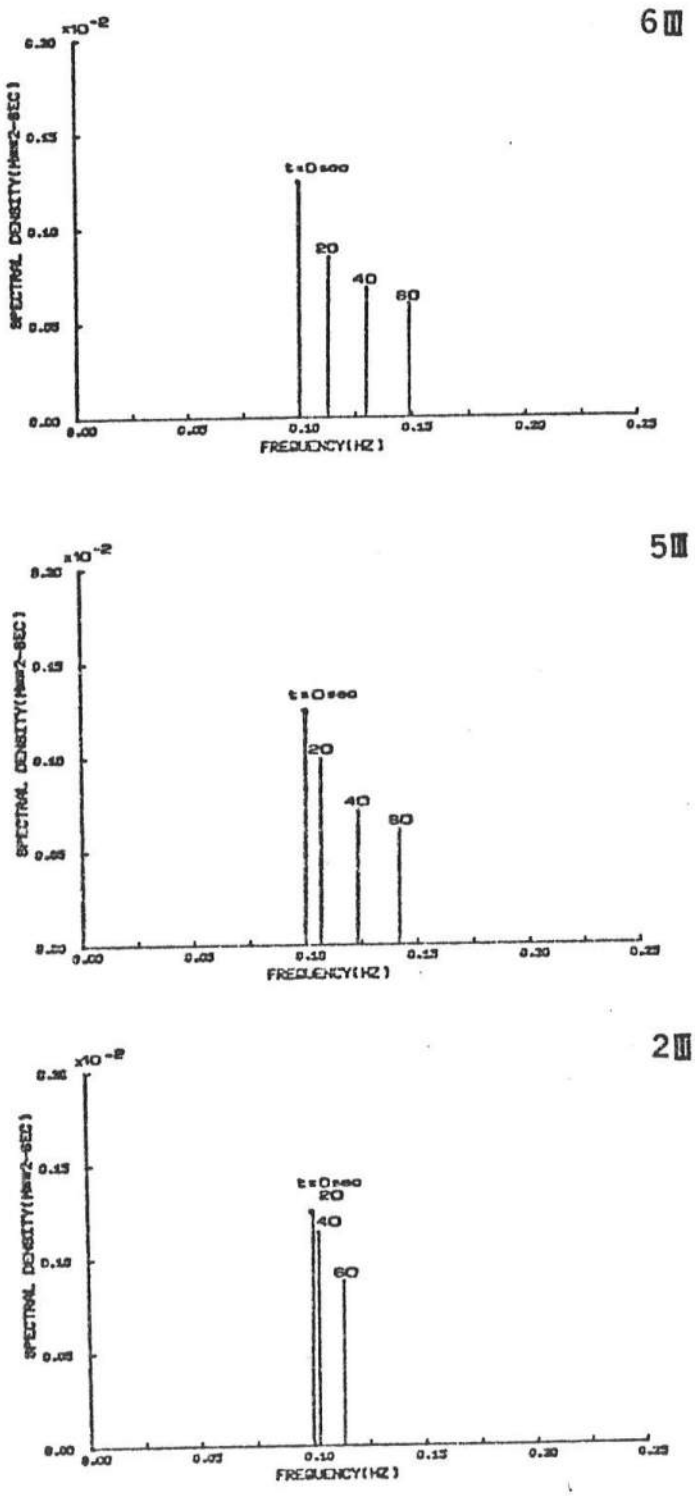

Figure 4.12 Variation of Wave Energy Decreasing with T=10sec, θ=20° at Boundary, Location 5III and Location 2III

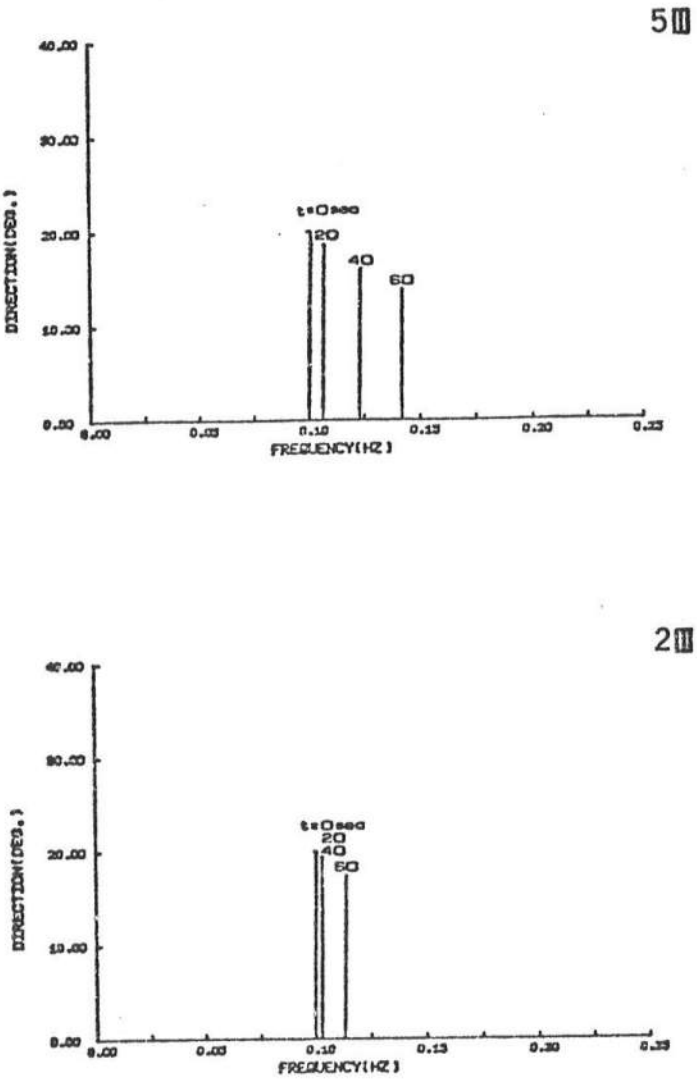

Figure 4.13 Variation of Wave Angle Decreasing with T=10sec, θ=20° at Location 5III and Location 2III

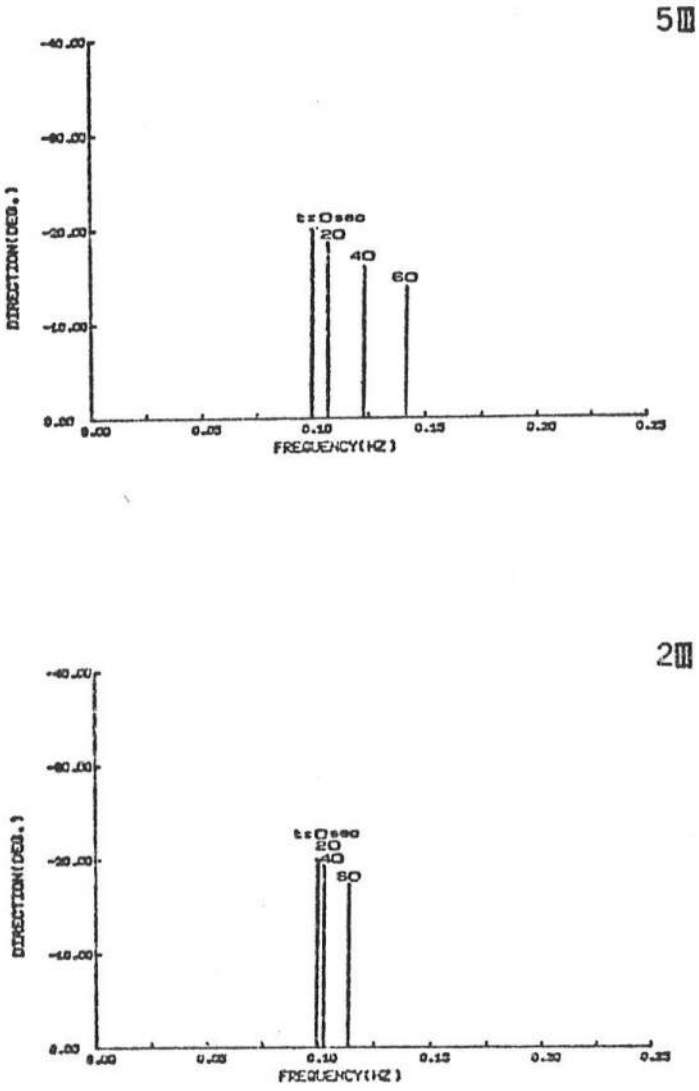

Figure 4.14 Variation of Wave Angle Decreasing with T=10sec, θ=-20° at Location 5III and Location 2III

approaching the center line, from left to right, is opposite to the first case.

The third case with a situation just opposite to the first case in that the wave at offshore boundary is adjusted to generate lower frequency component from f=0.10 HZ to f=0.05 HZ and larger wave angle within 60 seconds after the monochromatic wave has reached the steady state. As shown in Figure 4.15, the evolution of the energy spectrum in two-dimension is similar to that in one-dimension. The variation of the wave direction, moving away from the center line instead of approaching it, is shown in Figure 4.16.

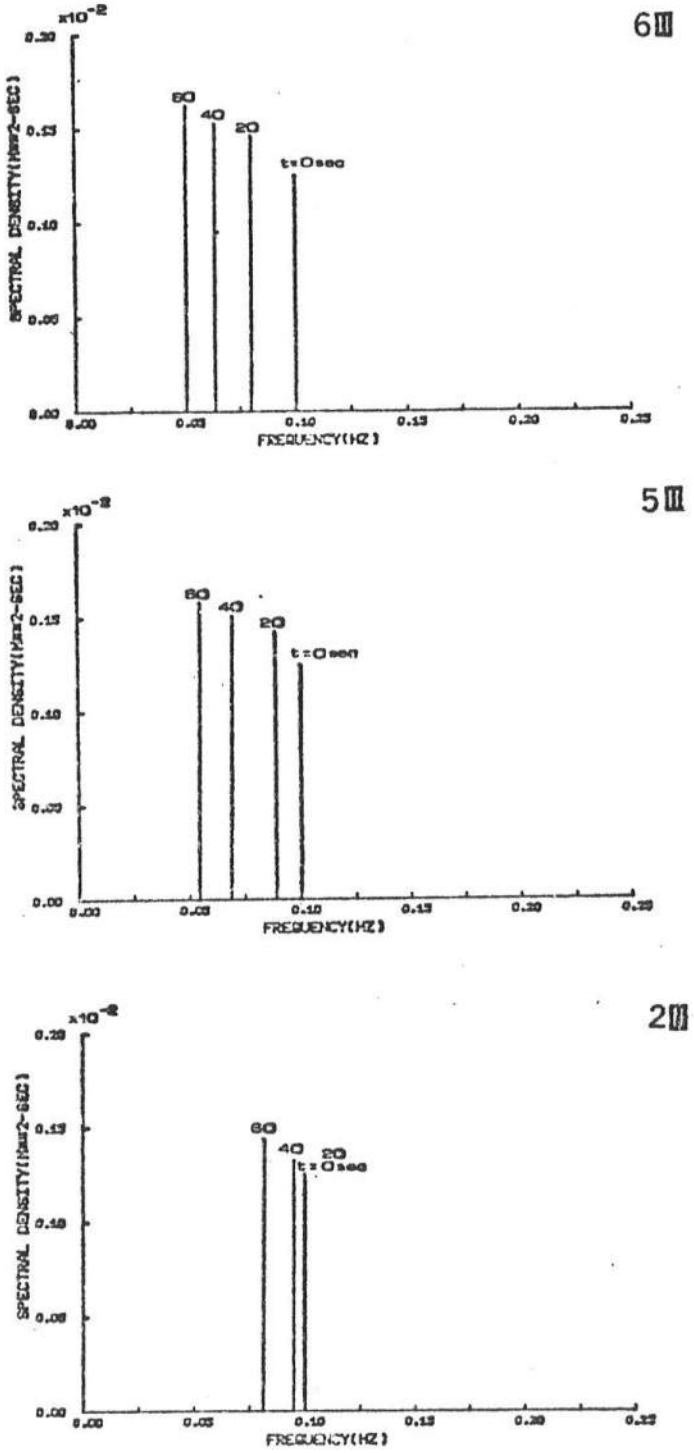

Figure 4.15 Variation of Wave Energy Increasing with T=10sec, θ=20° at Boundary, Location 5III and location 2III

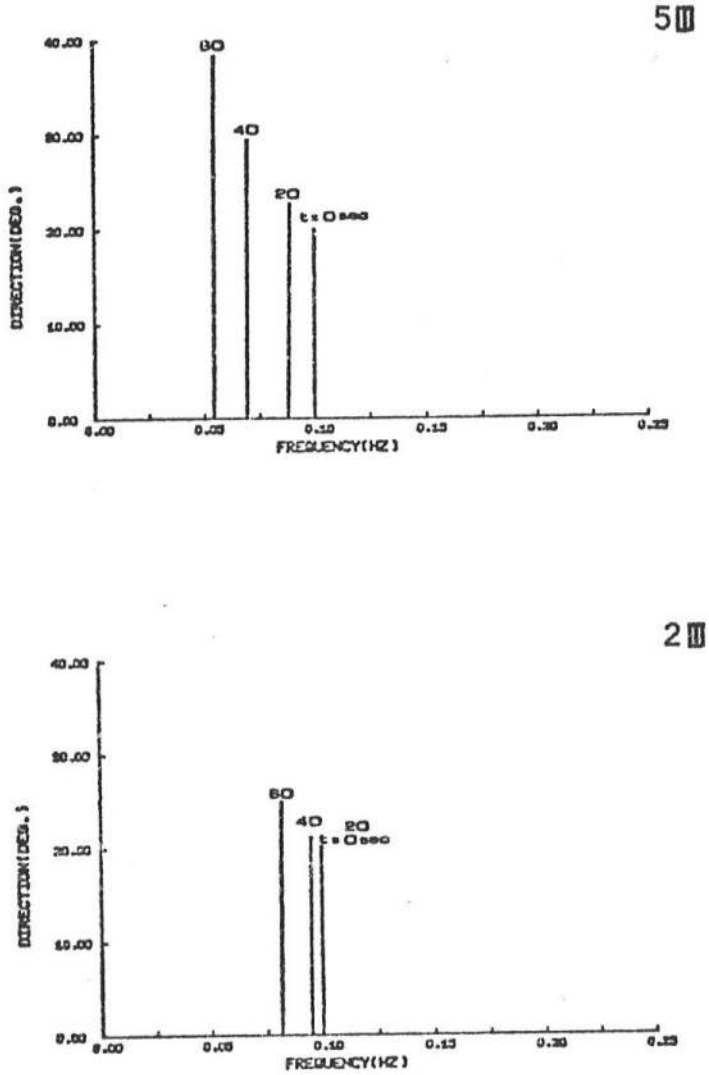

Figure 4.16 Variation of Wave Angle Increasing with T=10sec, θ=20° at Location 5III and Location 2III

CHAPTER 5

RANDOM WAVE MODEL FOR NON-STATIONARY WAVE SPECTRAL TRANSFORMATION

In this chapter, discussion is focused on the random wave model which consists of three sub-models : 1) swell wave model, 2) wind wave model, 3) hybrid wave model. The field data comparison is also included. A schematic view of ocean environment which is the same as Figure 3.3 is illustrated in Figure 5.1. To apply the numerical scheme, Δx=5000m, Δy=5000m and Δt=60 seconds are used in the three sub-models.

5.1 Swell Wave Model

The swell wave model, without the consideration of local wind generation, computes wave transfromation when the offshore boundary condition is unsteady. In the example given here, Pierson - Moskowitz (P-M) spectrum, a fully developed sea of the form,

$$A(\omega) = \frac{\beta' g^2}{\omega^5} e^{-\alpha' \left\{ \frac{\omega_0}{\omega} \right\}^4} \qquad (5.1)$$

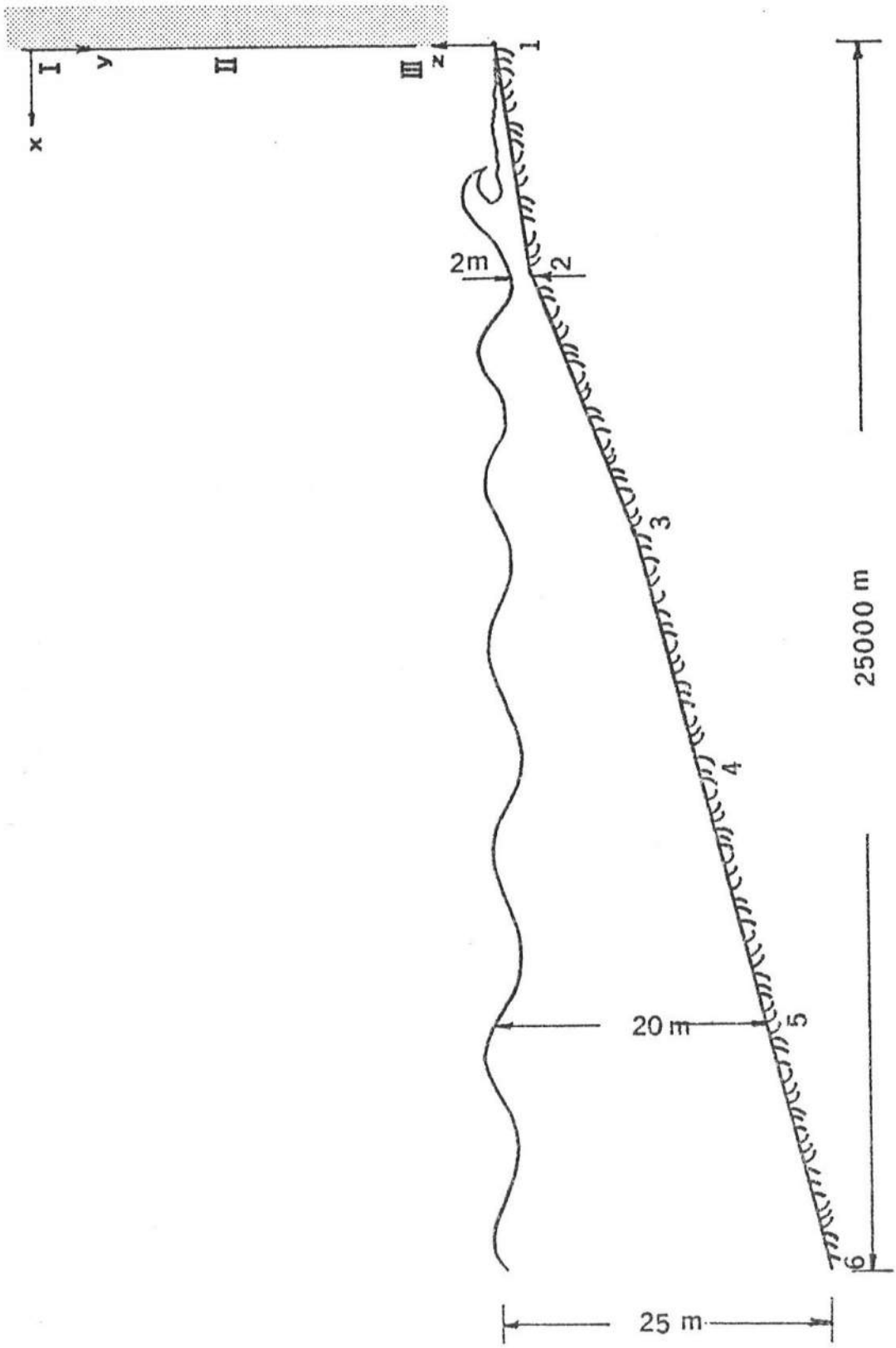

Figure 5.1 Schematic View of Ocean Environment

where

$$\alpha_0 = \frac{g}{w}$$

is chosen as the initial condition. The offshore boundary is treated as open boundary which is affected by the offshore wind variation.

Two different offshore open boundary conditions are illustrated: one for increasing wind speed, hence, growing spectrum and the other for decreasing wind. First, the decreasing wind case is examined. The initial condition is established by inputting a wave spectrum at offshore boundary (location 6II). This spectrum corresponds to a fully developed sea of 7 m/sec wind and a main direction 20 degree normal to the shore. The steady state spectra at boundary (location 6II), location 5II and location 2II are denoted as t=0 min curves in Figure 5.2. The wave condition at the offshore is then allowed to vary by diminishing the wind speed from 7 m/sec to 4 m/sec in one hour at constant rate with the spectral curves marked successively as 20,40,60 (min) from time 0. The corresponding wave conditions at location 5II and location 2II for the successive times are as

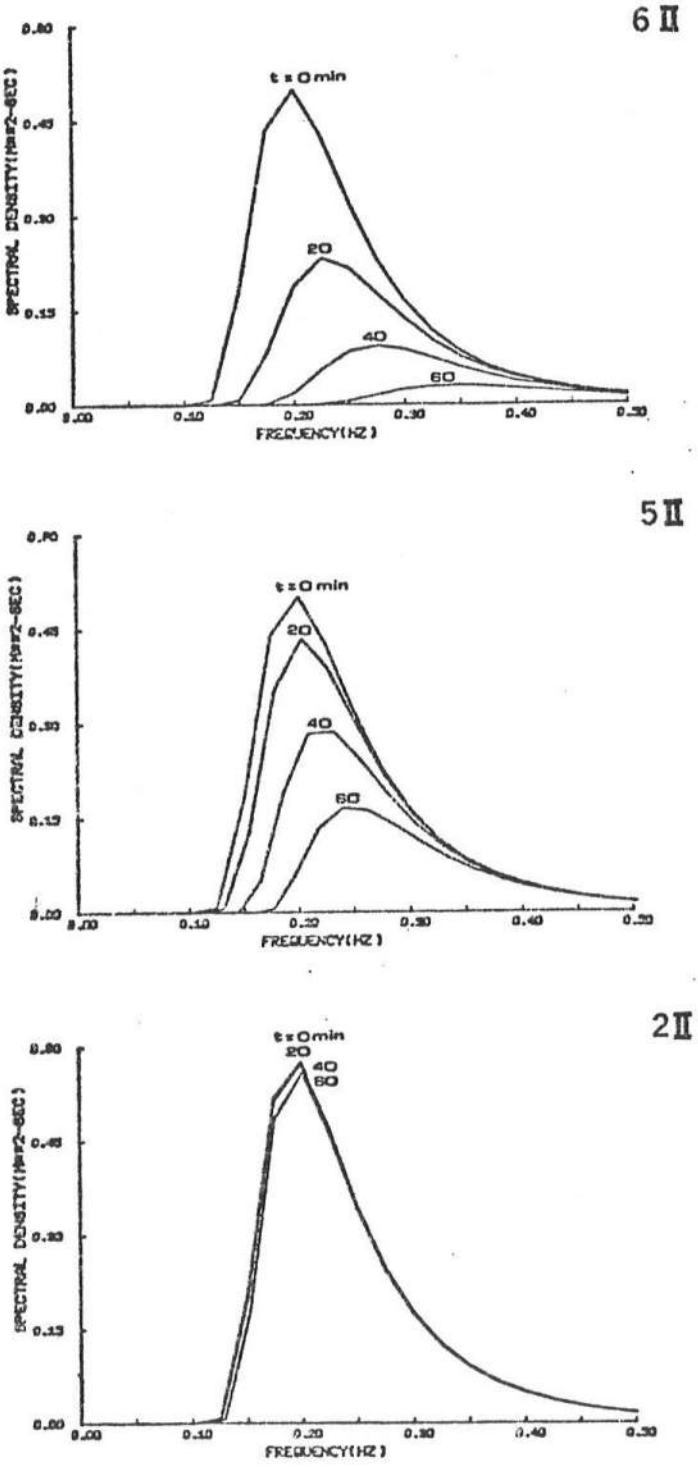

Figure 5.2 Variation of Energy Spectrum Decreasing due to Swell at Boundary, Location 5II and Location 2II

illustrated. The effect of non-stationary wave transformation is clearly revealed here. By comparing spectra at boundary (location 6II) and at location 2II, it can be seen that although the wave conditions changed drastically at offshore within one hour, the waves in nearshore region were hardly affected during this time period.

Figure 5.3 provides another example with a situation just opposite to the previous one in that the initial wind condition is 4 m/sec and begins to pick up in an hour at steady rate to a final speed of 7 m/sec.

Field data measured by Ijima (1958) is shown in Figure 5.4 which illustrates the time change of wave spectrum during a decreasing period of typhoon-generated swell. The effect that the wave components disappear as wind speed decreases is observed.

5.2 Wind Wave Model

The wind wave model is concerned with the effect of local wind generation. A calm sea is chosen as the initial condition with an open offshore boundary.

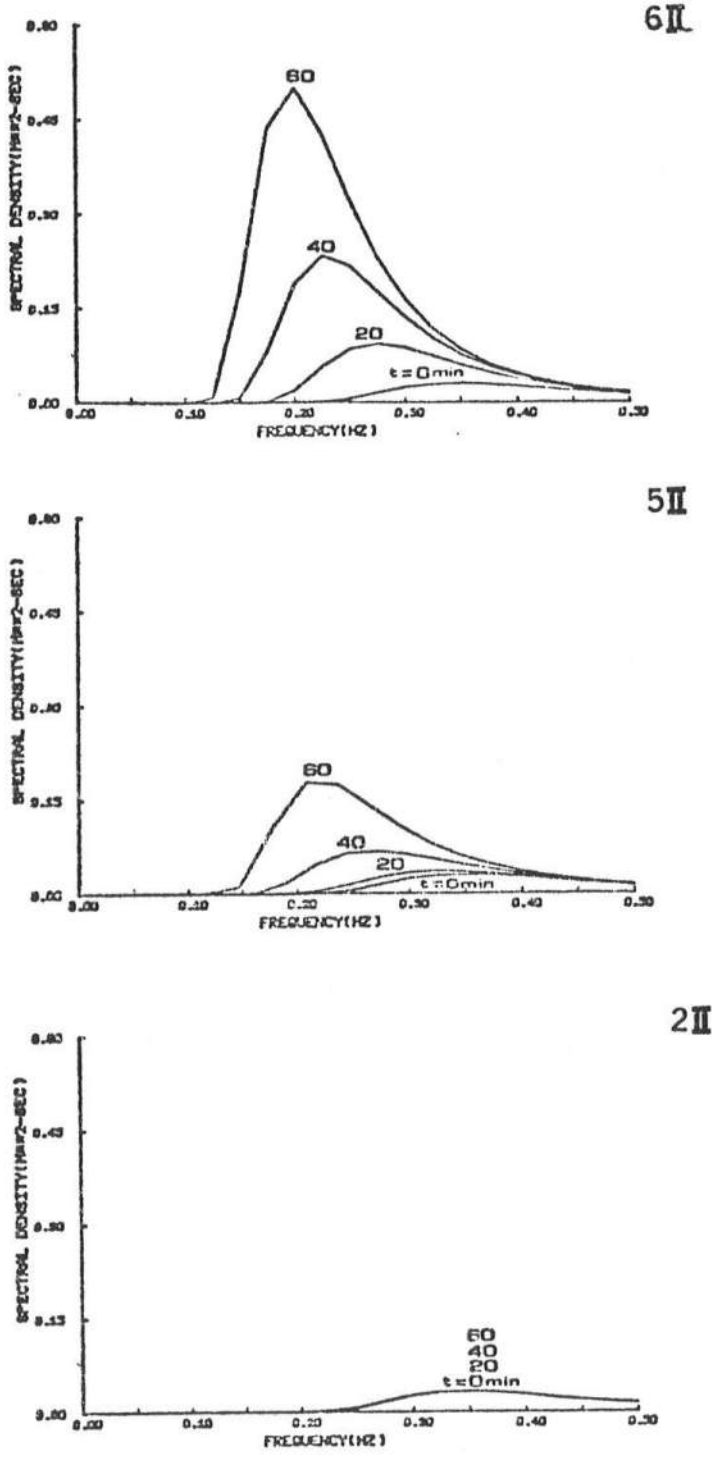

Figure 5.3 Variation of Energy Spectrum Increasing due to Swell at Boundary, Location 5II and location 2II

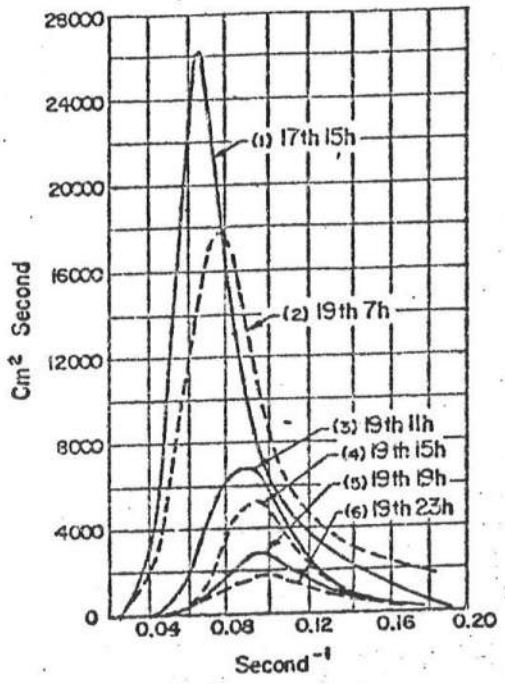

Figure 5.4 Time Changes of Wave Energy Spectrum in the Decrease of Swell of a Typhoon (After Ijima, 1957)

The wind beginning to build up from 0 to 7 m/sec in the first half hour and then maintaining 7 m/sec for the second half hour, blows over a calm sea in the direction perpendicular to the shoreline. As shown in Figure 5.5, the spectral peak shifts toward lower frequency with increasing time. This phenomenon is consistent with the field observation in the ocean.

5.3 Hybrid Wave Model

Based on linear superposition, the swell wave model and the wind wave model can be combined into a hybrid wave model to predict the real ocean waves.

Here, the offshore wave condition is the same as given in the first case of the swell wave model, i.e.,waves at outer boundary diminish from a spectrum corresponding to 7 m/sec wind to that of a 4 m/sec wind in one hour. In the region of consideration, a local wind of the same nature as given in the wind wave model, i.e., wind begins to build up from 0 to 7 m/sec in the first half hour and then maintains at 7 m/sec for the second half hour, is also occurring concurrently. The corresponding wave conditions at location 5II and location 2II are shown in Figure 5.6.

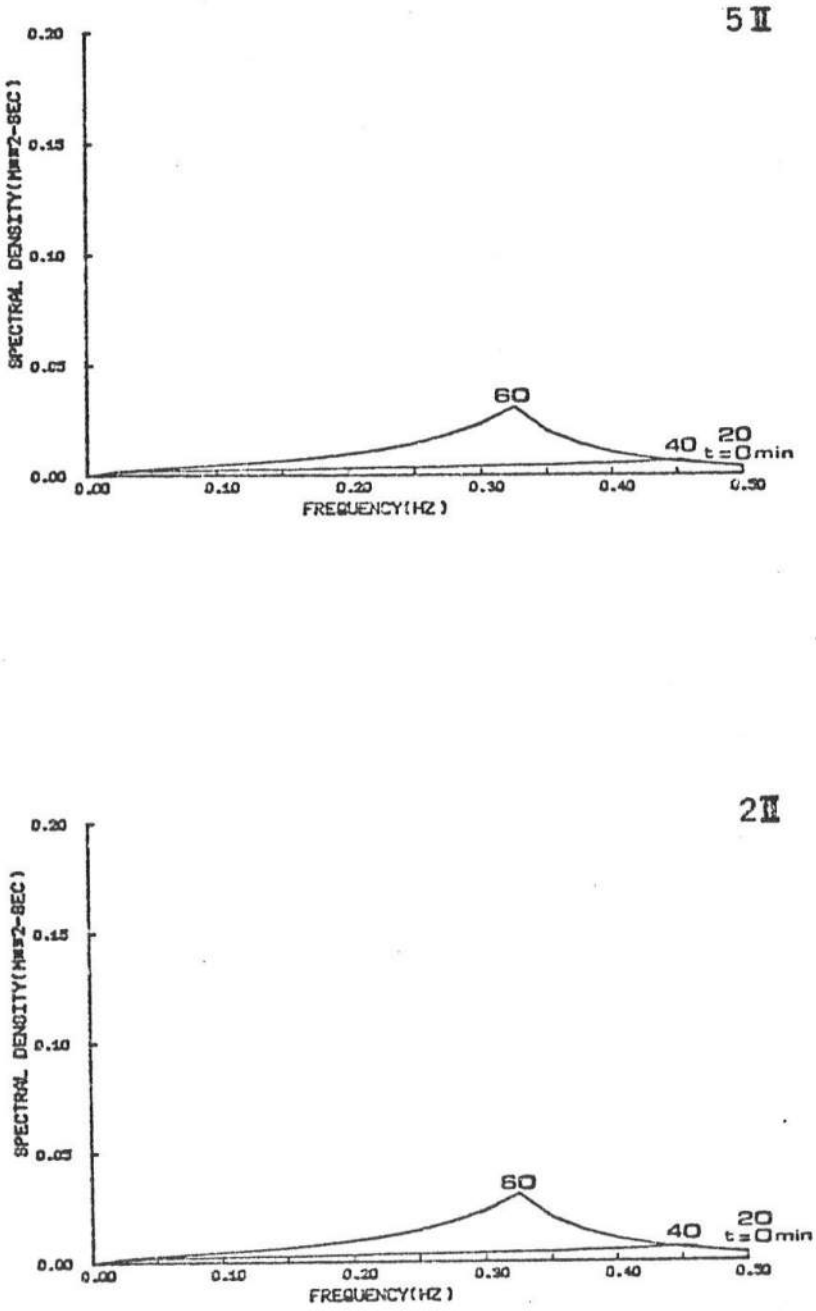

Figure 5.5 Variation of Energy Spectrum Increasing due to Wind Generation at Location 5II and Location 2II

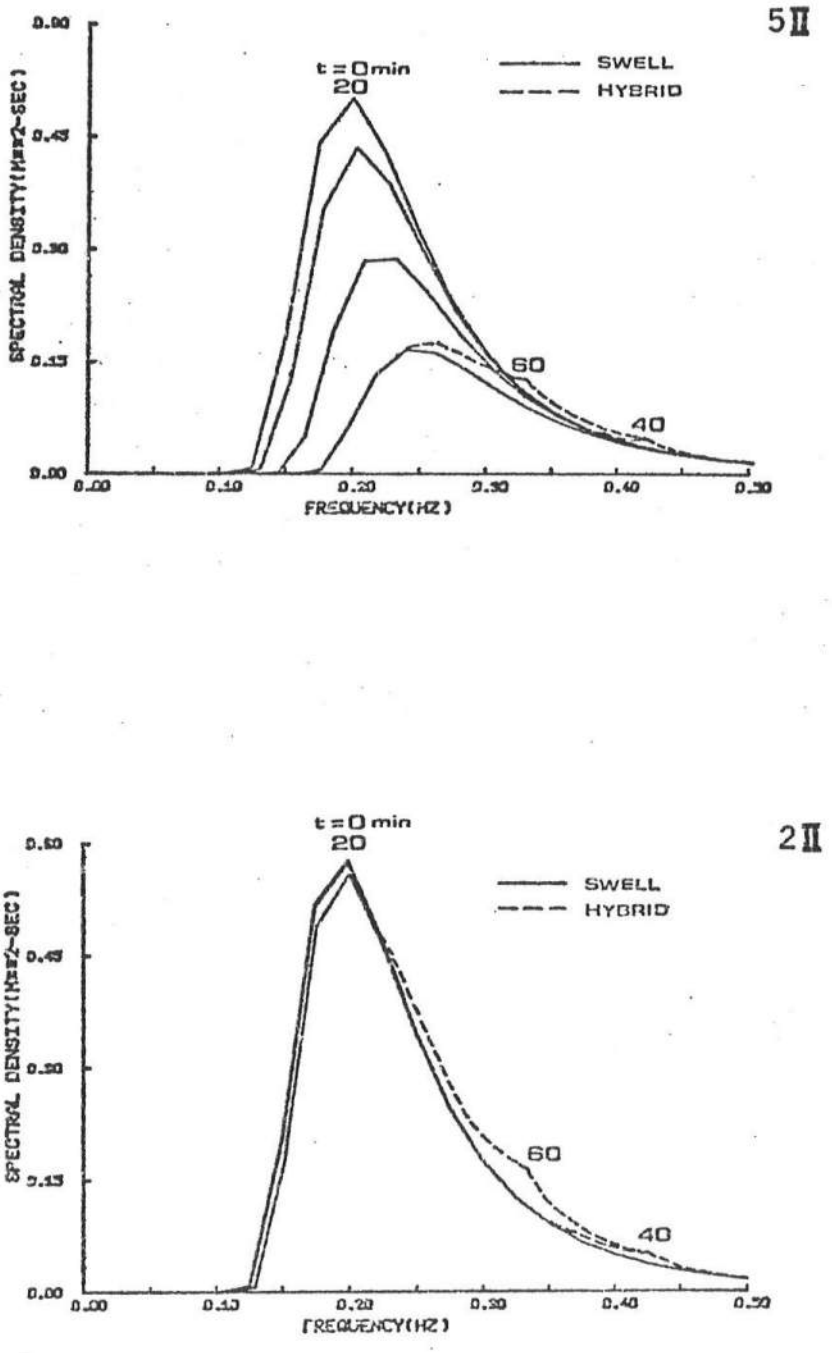

Figure 5.6 Variation of Energy Spectrum due to Decrease of Swell and Increase of Wind Wave at Location 5II and Location 2II

The spectra are now dual-peaked; the peak due to swell shifts toward higher frequencies as the offshore wave diminishes in strength whereas the peak corresponding to local wind wave shifts towards the lower frequencies as the local wind picks up. Eventually, the wave spectrum of the local wind wave will dominate the whole wave spectrum. This phenomenon is very clearly shown in Figure 5.7 from Long and Hasselmann (1979).

5.4 Comparison with the North Sea Field Data

Documented field data with sufficient information for the purpose of comparing with the present numerical model is scarce. The recent MARSEN I experiment was conducted during the months of September and October 1979. Waves were measured in shallow water by a series of wave gages as well as in deep water by a number of pitch-and-roll buoys. It is an attempt to understand the characteristics of wave spectral transformation from deep to shallow water.

The experiments were performed in the German Bight around the Island of Helgoland and Sylt. Figure 5.8 shows the locations of the nearshore site and deepwater measurements in the MARSEN test region.

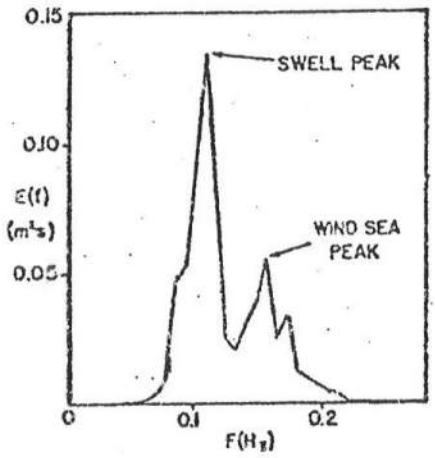

Figure 5.7 Frequency Spectrum Indicating Wind Sea and Swell Peaks (After Long and Hasselmann, 1979)

Buoys and stations in the German Bight

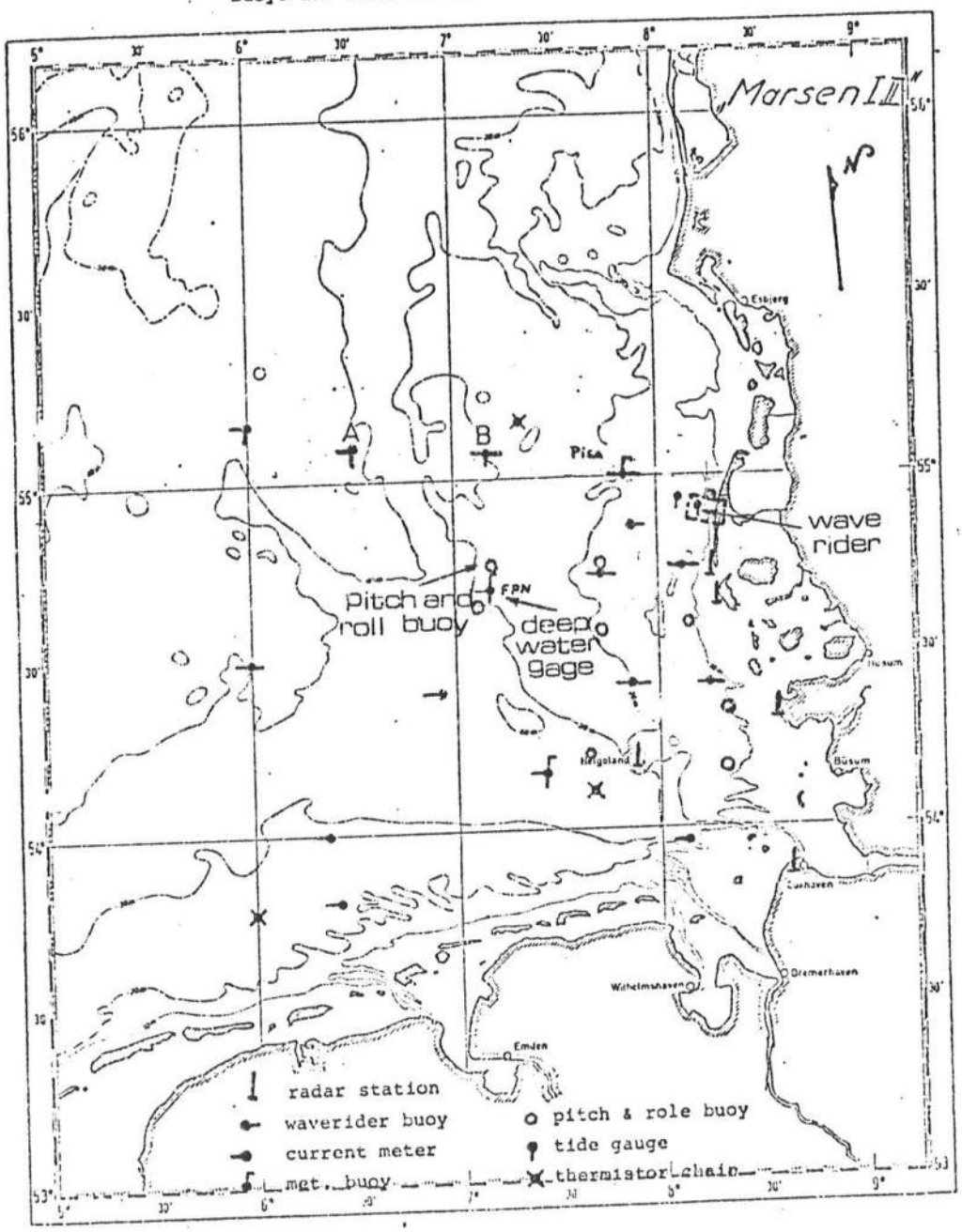

Figure 5.8 MARSEN Wave Measurement Stations

Deepwater wave information was obtained from the pitch-and-roll buoy maintained by Deutsches Hydrographisches Institute of Germany. The shallow water measurements by Wang et al. (1980) with emphasis on surf zone characteristics were carried out at the Island of Sylt. The distance between the pitch-and-roll buoy and the nearshore site is approximately 70 km.

Figure 5.9 shows the instrument arrangement in the nearshore zone. The wave gauges at locations 1225 m (approximately 1100 m from shoreline , 1225 m denotes the distance in meter from a base line which is approximate 100 m inland from shoreline), 940 m, and 225 m are bottom mounted echo-transceivers as developed by Fuhrentholz Laboratory. These echo sounders are capable of measureing water surface variation to $\pm$ 0.5 cm for water depths up to 90 m. The shallow water gauges are staff-mounted pressure transducers of type MDS 76 as manufactured by H. Maihak AG, Hamburg with a pressure range of 0 - 1 kg/cm^2. The current meters are COMEX electromagnetic two component type.

Data were taken with recording length of approximately 20 minutes. Spectral analysis was

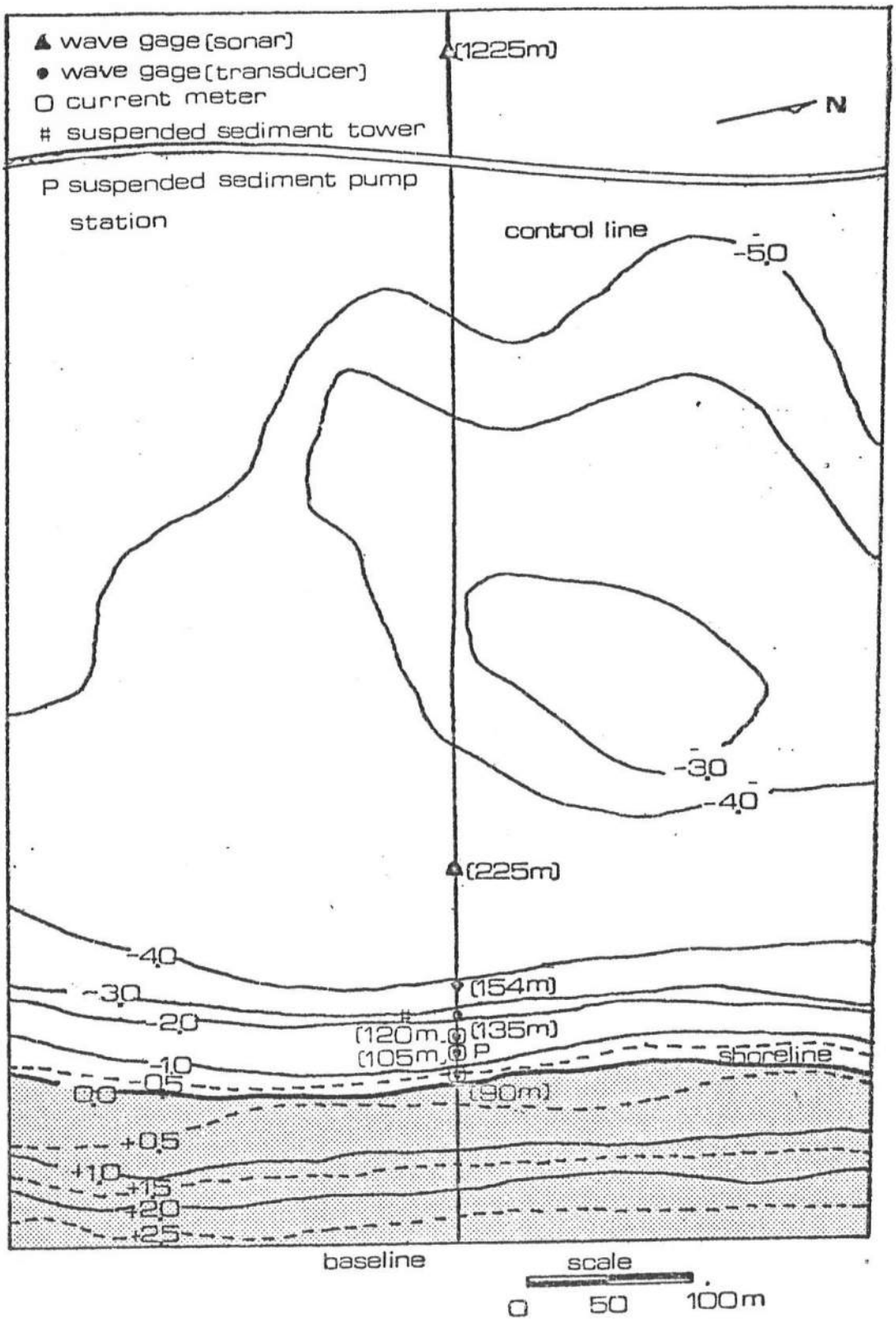

Figure 5.9 Nearshore Field Instrument Arrangement

performed using the FFT technique developed by Cooley and Tukey (1965) with Hanning Window (Blackman and Tukey, 1958) for data smoothing. All the data sets were sampled uniformly at a time interval $\Delta t=0.5$ sec to a total data point N=2048 or 1024. In order to maintain good resolution, a degree of freedom DF=40 for N=2048 and DF=20 for N=1024 was selected as the optimum.

The mean water depth at location of pitch-and-roll buoy and at location 1225 m are 28 m and 8 m, respectively. The wave data were still being analyzed and sorted out. So far, we have indentified only one set of data that marginally suitable for the present purpose (simultaneous wave recordings with all the necessary input information documented). The results of this data set which was taken on Sept. 24, 1979 are reported here. First of all, the wind condition of this particular day is shown in Figure 5.10. The wind speed variation was rather moderate for the whole day somewhere around 8 -10 m/sec for the bulk part of the day; the wind direction was from SWS during 0 to 8 o'clock local time and then suddenly shifted to N from 8 o'clock till midnight. Since the wind direction changes drastically at 8 o'clock, wind

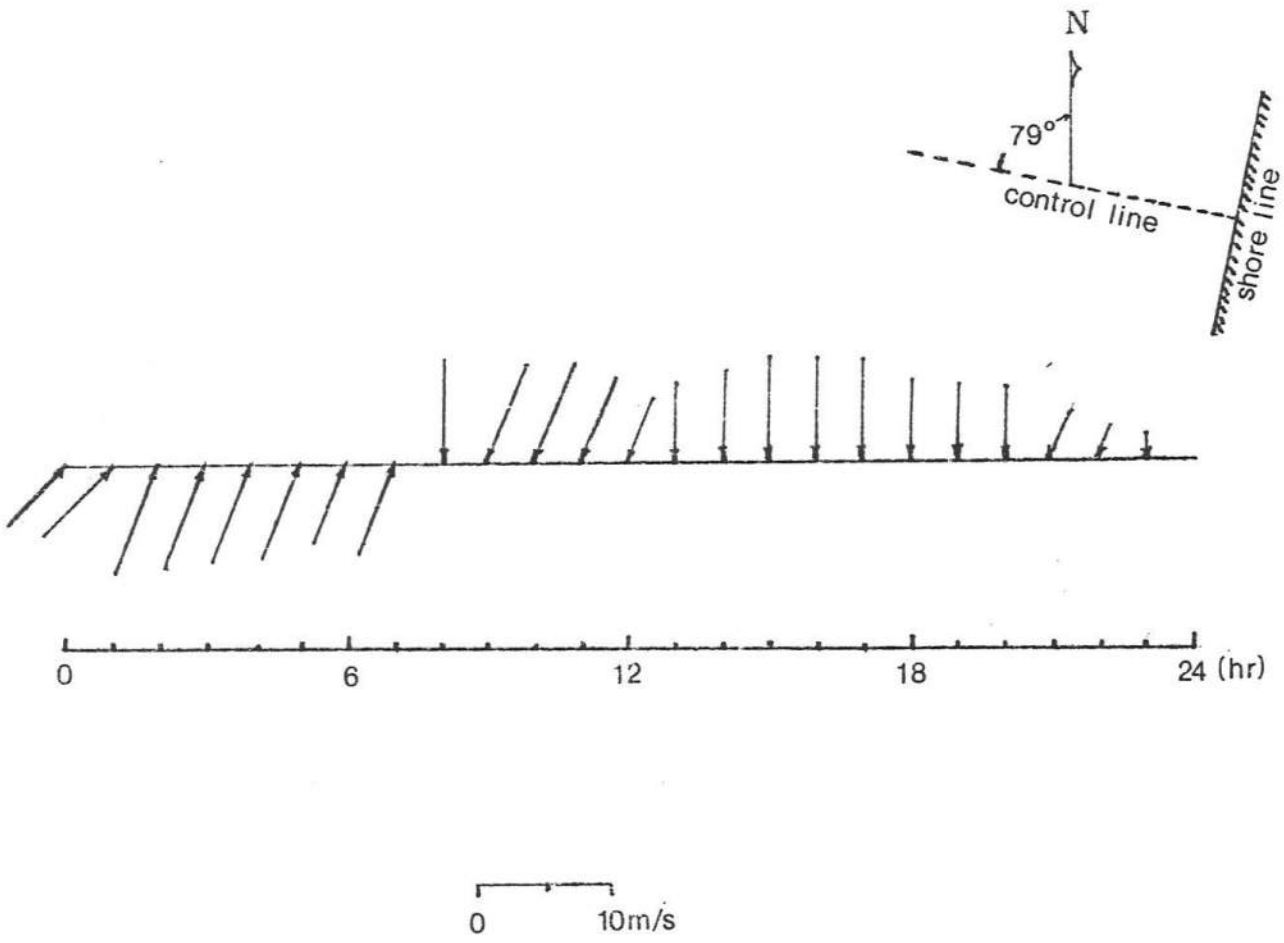

Figure 5.10 Wind Speed and Direction on september 24, 1979

wave generated from that time meets the criteria of the local wind model described above.

Wave data were collected at offshore location from 8 o'clock at approximatly 2 hour interval. The energy spectra and their corresponding directional information are given in Figure 5.11. Shallow water waves were recorded at location 1225 m, during the same period. A rough calculation indicated that the dominant wave component ($\backsim$ 0.16HZ) would take approximately 2 hours to travel from the offshore site to the nearshore zone. Thus, to predict wave condition at the nearshore site, the input at offshore location should be chosen about 2 hours in advance. Based upon this approximation, deepwater waves at 12:14 pm were used as input to compute the condition at location 1225 m at 14:00 pm. The bottom friction coefficient is chosen as 0.01 because of the sandy bottom. The grid system, with Δx=5000 m, Δy=5000 m and Δt=60 seconds which used in the computation is shown in Figure 5.12.

The comparison of numerical results and field data is shown in Figure 5.13 and Figure 5.14. The contributions to the total energy spectrum from local wind generation and swell transformation are indicated

MARSEN VO 7909241214

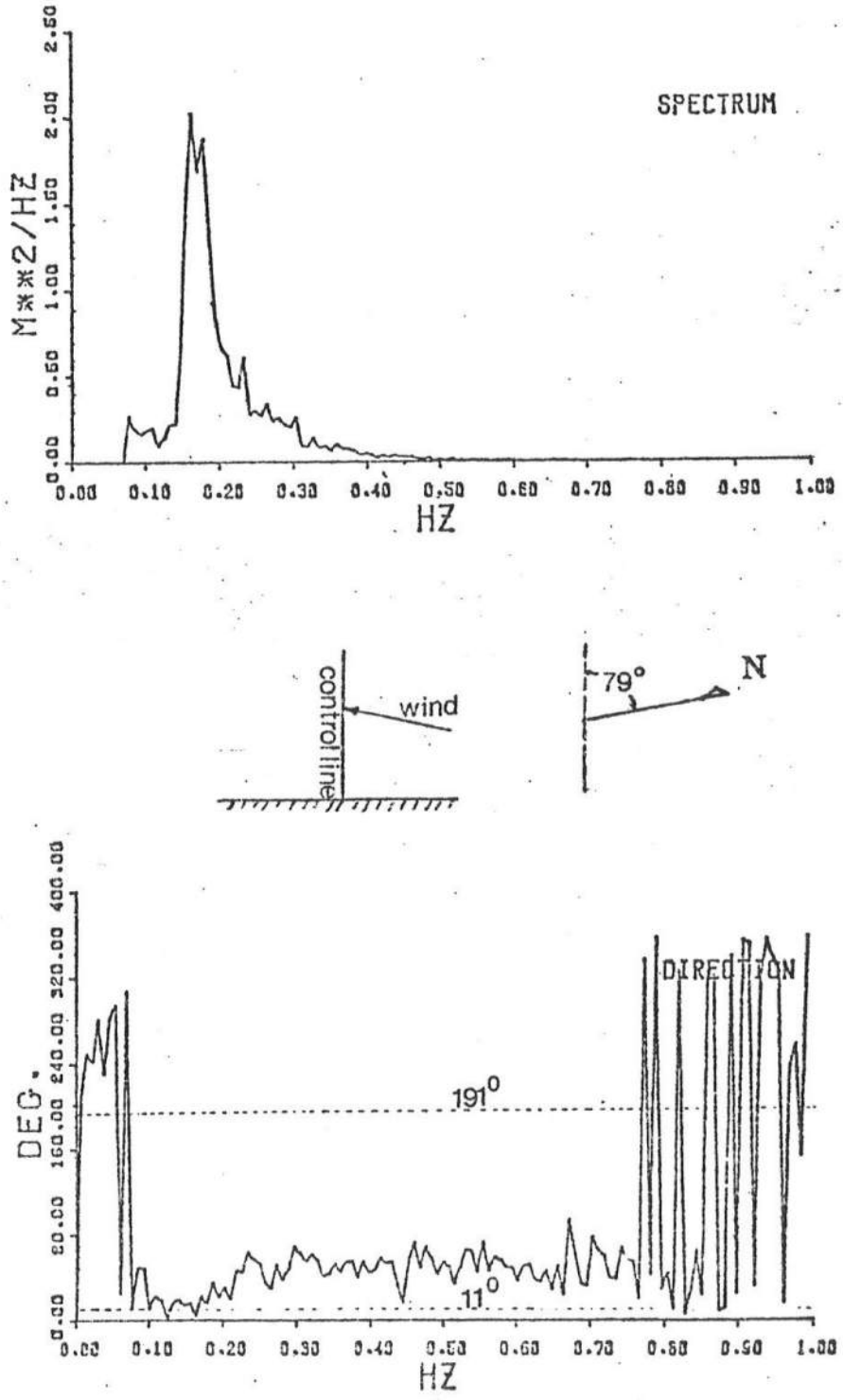

Figure 5.11 Energy Spectrum and Mean Wave Direction at Deep Water at 12:14, September 24, 1979

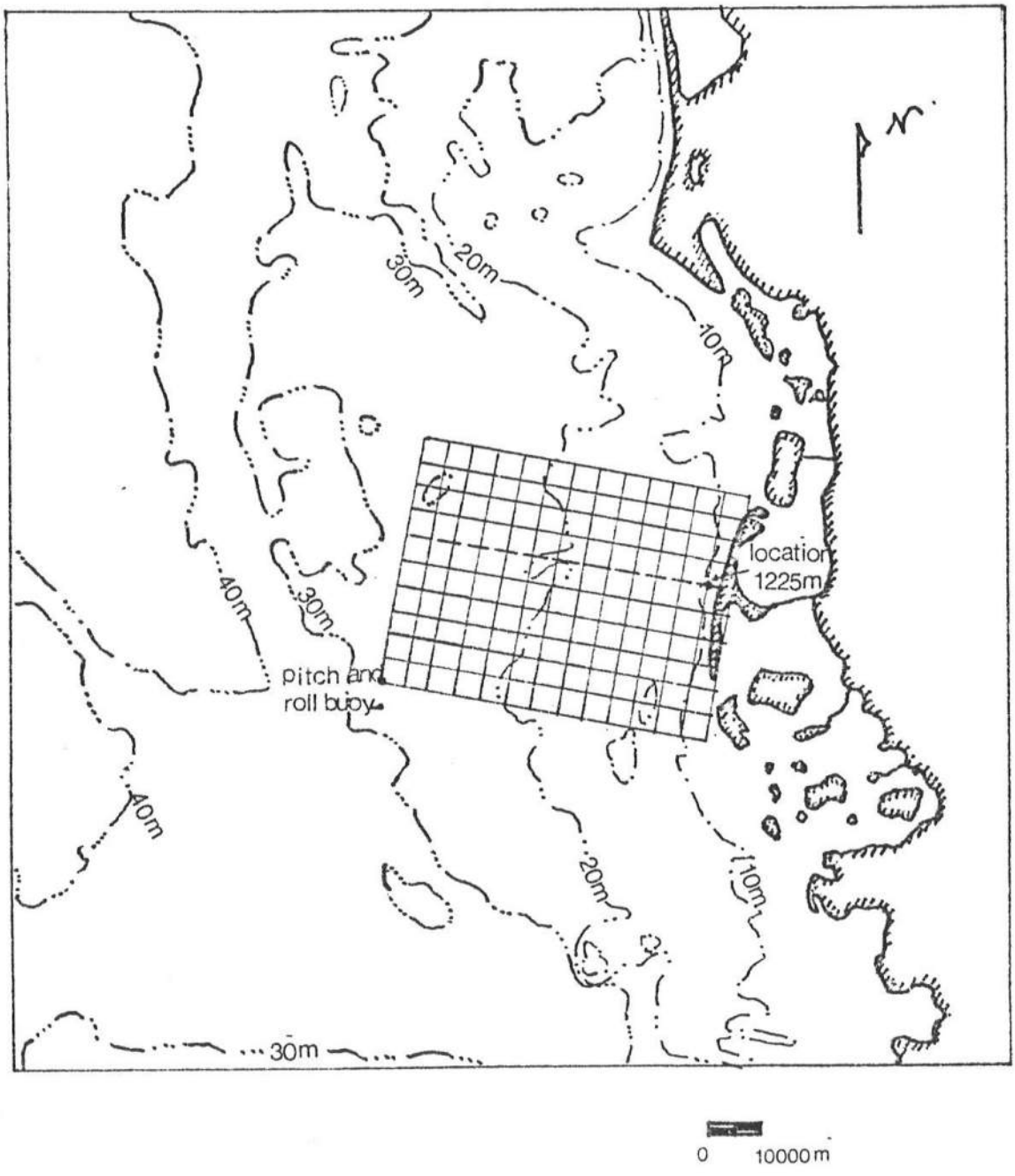

Figure 5.12 Grid System used in the Computation

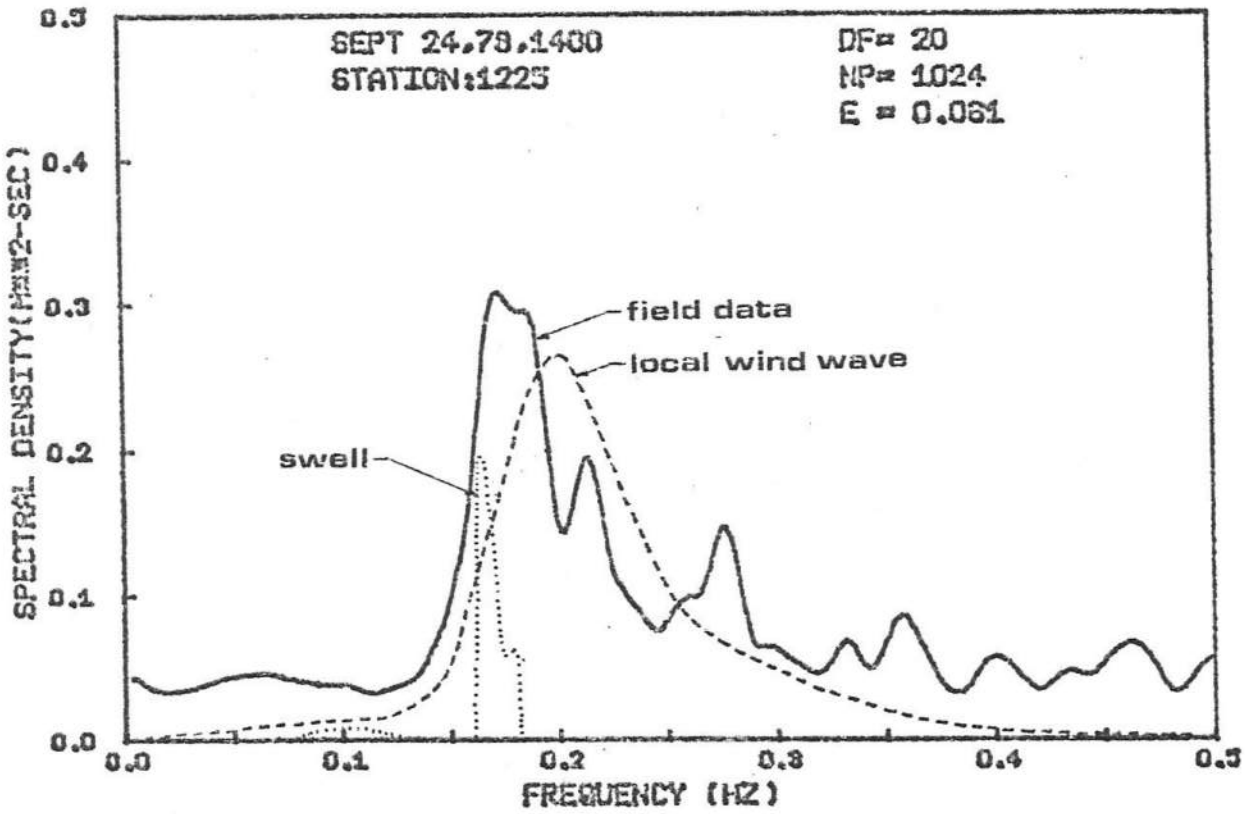

Figure 5.13 Comparison between Swell Wave Model from 12:14, Wind Wave Model from 8:00 and Field Data at 14:00 at Location 1225m

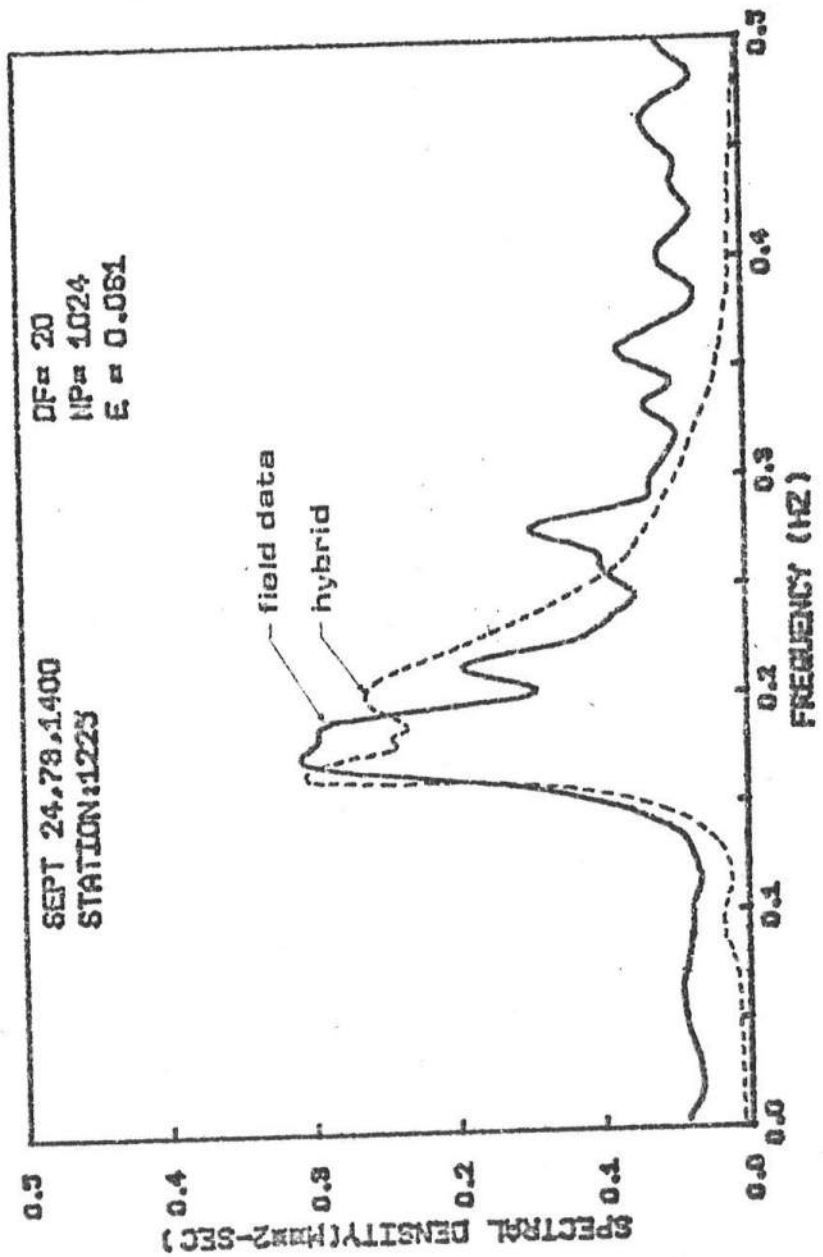

Figure 5.14 Comparison between Hybrid Wave Model and Field Data at 14:00 at Location 1225m

in Figure 5.13. As can be seen, for the specific case, local wind waves were the major contributor. The swell component while important to the peak energy was minor as a whole. A majority of the wave components present in the offshore region actually never arrived at the nearshore zone. As we have stated earlier, this set of data is really marginal for verification purpose because of this minor contribution due to swell components.

CHAPTER 6

SUMMARY AND CONCLUSIONS

A mathematical model which can predict the stationary and non-stationary wave spectral transformation in shallow water of irregular bottom has been developed. The model contains the physical dynamic processes which are conserved, such as wave refraction and shoaling, as well as those which are not conserved, such as wave energy generation and dissipation. The numerical results can be used to guide further research in wave phenomenon of which very little is known.

The theory of wave spectral transformation is presented in Chapter 2. Instead of using the parametrical method which was developed by Hasselmann (1976), the theory is based on the physical method. Both methods, physical and parametric, have their relative advantages and limitations. The problem becomes much more complicated when the shallow water effect is to be considered. Several additional

effects, such as wave shoaling, refraction and bottom dissipation must be taken into account. Furthermore, the non-linear wave-wave interactions become increasingly important in shallow water. The physical method includes the former effects but excludes the latter effect, whereas, the parametrical method can only handle the local wind fields which are characterized by extremely large spatial and temporal gradients. Based on the reasons specified above, the physical method which can handle the time varying wind condition in shallow water is chosen as the basis of wave spectral transformation. The results are found to be reasonable.

The theory consists of three kinematic conditions, which handle the wave refraction , and one dynamic condition, which controls the wave shoaling, wave generation and wave dissipation. In the wave generation, two mechanisms are considered: one is Phillips' resonant mechanism which causes the initial wave growth and the other is Miles' instability mechanism which controls the major wave growth. In the wave dissipation, there are also two mechanisms. The bottom friction and wave breaking are chosen from Hasselmann and Collins' derivation and Kitaigorodskii's

shallow water equilibrium energy spectrum, respectively.

The numerical scheme of stationary wave spectral transformation is analyzed in Chapter 3. Based on Noda's numerical procedures, the non-homogeneous terms which are the effect of the wind generation and bottom friction are also added to be solved. Shoaling and refraction are well handled in the model. In low fequency components, the influence of the bottom friction is found to be important in shallow water since the long wave component has already felt the bottom. However, in high frequency components, energy generation or transfer are more important than the bottom friction. In the steady local wind generation, the short wave component exceeds the maximum wave steepness and follow the breaking criterion of Kitaigorodskii's shallow water equilibrium energy spectrum. Whereas the long wave component has not reached the maximum wave steepness and continues to grow until the total energy spectrum reaches the depth-limited wave condition.

The numerical scheme of non-stationary wave spectral transformation is analyzed in chapter 4. The

problem is solved by using the two-step Lax-Wendroff scheme. Numerical verification is based on an example which has the same type as the energy transport equation. The exact solution and the approximate solution agree very well (no more than 2%). It shows that the present numerical scheme can handle both transient equations (one is the wave conservation equation and the other is the energy transport equation). The characteristics of the wave spectral transformation, in which the variation of wave component at the boundary affects far locations, are shown in the example of monochromatic wave in one and two dimensions. The effect which the propagation velocity of long wave is faster than that of short wave is clearly revealed.

Based on the linear assumption, the random wave model for non-stationary wave spectral transformation is discussed in Chapter 5. The problem is handled by developing three separate models; 1) swell wave model handles the offshore wind variation without local wind generation, 2) wind wave model handles the local wind generation, 3) hybrid wave model linearly combines the swell wave model and wind wave model to predict a real ocean wind waves. The numerical results show

reasonably agreement with the North Sea field data except the wave components at high and low frequency. This is likely to be a consequence of the non-linear wave-wave interactions which is not considered in this model and of the assumed constancy of the Kitaigorodskii's " B " constant for the equilibrium condition.

Wave spectral transformation in shallow water is important for the study of analyzing and predicting wave conditions in nearshore zone due to hurricanes or storms sweeping through offshore region. In the present model, only the linear problem is considered. Ideally, the non-linear wave-wave interaction terms should be included. But, it has not been done so for two practical reasons as follows:

1) Lack of suitable model. Phillips (1960) made the first investigation of nonlinear resonant interactions among particular groups of wave components. Hasselmann, in a series of three papers (1962,1963a and 1963b) studied the rate of energy exchange in a random wave field. He assumed that the probability density distribution of the surface displacement is normal and calculated the net rate of energy exchange from one wave to its wave components in the resonant tetrad.

Unfortunately, the results he got are neither mathematically smooth nor stable. Barnett (1968) modified Hasselmann's parameterized function in a manner that will increase the calculation speed but the result is only an approximation. Based on the narrow band spectrum, Longuet-Higgins (1976) and Fox (1976) applied the evolution of wave packets in three dimensions to the Hasselmann's resonant energy transfer result. The simplification improved calculation speed and stability. All the above studies are restricted to deepwater waves. Herterich and Hasselmann (1980) modified Longuet-Higgins results for the computation of the rate of wave energy transfer in finite depth water for a narrow band spectrum. However, their results cannot be applied to shallow water areas where the kh value is between 0.3 and 0.7. Resio (1981) modified Hasselmann's(1976) parameterized function to be a new parameterization. The result is still not applicable because it is restricted to deepwater waves.

2) Lengthy computation. The numerical program would have become unwieldily complicated at this stage that would submerge us in numerical manipulation.

Actually, it is a drawback to omit the non-linear wave-wave interaction terms which by many

researchers are regarded as an important parameter in shallow water. Therefore, a more extensive study should account for the effects of non-linear wave-wave interations.

REFERENCES

Barnett, T. P., "On the generation, dissipation and prediction of ocean wind waves," J. Geophys. Res., 73, 513-530, 1968.

Blackman, R. B. and J. W. Tukey, "The measurement of power spectra," Dover Publication, New York, 1958.

Bretschneider, C. L. and R. O. Reid, "Changes in wave height due to bottom friction, percolation, and refraction," Tech. Memo., Beach Erosion Board, U. S. Army Corps of Engineers, No. 45, pp36, 1954.

Burling, R. W., "The spectrum of waves at short fetches," Dtsch. Hydrogr. Zr., XII, 45-117, 1959.

Cavaleri, L. and P. M. Rizzoli, "Wind wave prediction in shallow water: theory and application," J. Geophys. Res., 86(c11), 10961-10973, 1981.

Cooley, J. W. and J. W. Tukey, "An algorithm for the machine calculation of complex fourier series," Math. of Computation, V. 19(99), 297-301, 1965.

Collins, J. I., "Prediction of shallow water spectra," J. Geophys. Res., 77(15), 2693-2707, 1972.

Dingler, J. R., "Wave-formed ripples in near shore sands," Ph.D. Dissertation, U.C. San Diego, 1975.

Divoky, D. et al., "Breaking waves on gentel slopes," J. Geophys. Res., 75, 1681-1692, 1970.

Fox, M. J. H., "On the non-linear transfer of energy in the peak of a gravity-wave spectrum, II," Proc. Roy. Soc., A348, 467-483, 1976.

Friedrichs, K. O., "Water waves on a shallow sloping beach," Comm. Pure and Appl. Math., 1, 109-134, 1948.

Gelci, R., J. Cazale, Vassal, "Utilisation des diagrams de propagation a la provision entergitique de

le houle," Bulletin d'Information du Commite Central d'Oceanographic et d'Etude des Cotes, VIII, NO. 4, 169-187, 1956.

Groves, G. W. and J. Melcer, "On the propagation of ocean waves on a sphere," Geofisica Internacional, 4, NO. 1, 77-93, 1961.

Gunther, H., W. Rosenthal, T. J. Weare, B. A. Worthington, K. Hasselmann and J. A. Ewing, "A hybrid paramatrical wave prediction model," J. Geophys. Res., 84(c6), 5727-5738, 1979.

Hasselmann, K., "Gudegleichungen der seegangsvoraussage," Schiffstechnik, 7, 191-195, 1960.

Hasselmann, k., "On the nonlinear energy transfer in a gravity-wave spectrum, part 1, general theory," J. Fluid Mech., 12, 481-500,1962.

Hasselmann, K., "On the nonlinear energy transfer in a gravity-wave spectrum, part 2, conservation theorems; wave-particle anology; irreversibility," J. Fluid Mech., 15,273-281,1963a.

Hasselmann, K., "On the nonlinear energy transfer in a gravity-wave spectrum, part 3, evaluation of the energy flux and swell-sea interaction for a Neumann spectrum," J. Fluid Mech., 15,385-398,1963b.

Hasselmann, K. and J. I. Collins, "Spectral dissipation of finite-depth gravity waves due to bottom friction," J. Mar. Res., 26, 1-12, 1968.

Hasselmann, K., T. P. Barnett, E. Bouws, H. Carlson, D. E. Cartwright,K. Enke, J. A. Ewing, H. Giennapp, D. E. Hasselmann, P. Kruseman, A. Meersburg, P. Muller, D. J. Olbers, K. Richter, W. Sell and H. Walden, "Measurements of wind-wave growth and swell decay during the Joint North Sea Wave Project (JONSWAP)," Deut. Hydrogr. Zeit., Suppl. A, 8, 12, 1973.

Hasselmann, K., D. B. Ross, P. Muller and W. Sell, "A parametric wave prediction model," J. Phys. Oceanogr., 6, 200-228, 1976.

Herterich, K., and K. Hasselmann, "A similarity relation for the non-linear energy transfer in a finite-depth gravity-wave spectrum," J. Fluid Mech., 97, 215-224,1980.

Hicks, B. L., "The energy spectrum of small wind waves," C.S.L. Rep. M-92, pp88, Univ. of Ill., Urbana, Ill., 1960.

Hsiao, S. V. and O. H. Shemdin, "Bottom dissipation in finite-depth water waves," proc. 16th Int. Conf. Coastal Eng., 434-448, 1978.

Ijima, T., "The properties of ocean waves on the Pacific coast and the Japan Sea coast of Japan," Transportation Tech. Res. Inst. (Japan), Rept.No. 25, 1957.

Jonsson, I. G., "Friction factor diagram for oscillatory boundary layers," Prog. Rep., Coastal Eng. Lab., Tech. Univ. Denm., NO. 10, 10-21, 1965.

Karlsson, T., "Refraction of continuous ocean wave spectra," J. Waterways, Harbors and Coastal Eng. Div., ASCE, WW4, 437-448, 1969.

Kinsman, B., "Surface waves at short fetch and low wind speed: a field study," Tech. Rep., NO. 19, Chesapeake Bay Inst., The Johns Hopkins University, 1-169, 1960.

Kitaigorodskii, S. A., et al., "On Phillips theory of equilibrium range in the spectra of wind generated gravity waves," J. Phys. Oceanogr., Vol. 5, 410-420, 1975.

Krasitskiy, V. P., "Toward a theory of transformation of the spectrum on refraction of wind waves". Izv. Atmosph. Oceanic Phys., 10(1), 72-82, 1974.

Long, R. B. and K. Hasselmann, "A variational technique for extracting directional spectra from multi-components wave data," J. Phys. Oceanogr., 9, 373-381, 1979.

Longuet-Higgins, M. S., "The refraction of sea waves

in shallow water," J. Fluid Mech., Vol. 1, Part 2, 163-176, 1956.

Longuet-Higgins, M. S., "On the transformation of a continuous spectrum by refraction," Proc. Camb. Phil. Soc., 53, 226-229, 1957.

Longuet-Higgins, M. S. and R. W. Stewart, "Changes in the form of short gravity waves on long waves and tidal currents," J. Fluid Mech., 8, 565-583, 1960.

Longuet-Higgins, M. S. and R. W. Stewart, "The changes in amplitude of short gravity waves on steady non-uniform currents," J. Fluid Mech., 10, 529-549, 1961.

Longuet-Higgins, M. S., D. E. Cartwright and N. D. Smith, "Observations of the directional spectrum of sea waves using the motions of a floating buoy in ocean wave spectra," 111-131, Prentice-Hall, New York, 1963.

Longuet-Higgins, M. S., "On the nonlinear transfer of energy in the peak of a gravity-wave spectrum: a simplified model," Proc. Roy. Soc., A347, 311-328, 1976.

Miles, J. W., "On the generation of surface waves by shear flows," J. Fluid Mech., 3, 185-204, 1957.

Miles, J. W., "On the generation of surface waves by shear flows," Part II, J. Fluid Mech., 6, 568-582, 1959a.

Miles, J. W., "On the generation of surface waves by shear flows," Part III, J. Fluid Mech., 6, 583-598, 1959b.

Miles, J. W., "On the generation of surface waves by shear flows," Part IV, J. Fluid Mech., 13, 433-448, 1962.

Nielsen, P., "A note on wave ripple geometry," Prog. Rep., Inst. Hydrodyn. and Hydraulic Eng., Tech. Univ. Denm., No. 43, 17-22, 1977.

Noda, E. K., C. J. Sonu, V. C. Rupert, and J. I. Collins, "Nearshore circulations under sea breeze

conditions and wave-current interactions in the surf zone," Tetra Tech Report, TC-149-4, Feb. 1974.

Ou, Shan-Hwei, "The equilibrium range in the frequency sepctra of the wind generated gravity waves," Proc. 4th Conf. on Ocean Eng. in the R. O. C., Sept. 1980.

Phillips, O. M., "On the generation of waves by turbulent wind," J. Fluid Mech., 2, 417-445, 1957.

Phillips, O. M., "The equilibrium range in the spectrum of wind generated waves," J. Fluid Mech. 4, 426-434, 1958.

Phillips, O. M., "On the dynamics of unsteady gravity waves of finite amplitude," J. Fluid Mech., 9, 193-217, 1960.

Phillips, O. M., "The dynamics of the upper ocean," Cambridge University Press, London, 1966.

Pierson, W. J.(ed.), "The directional spectrum of a wind generated sea as determined from data obtained by the stereo wave observation project," Coll. Engrg., N.Y.U. , Met. Pap. 2, NO. 6, 1962.

Priestley, J. T., "Correlation studies of pressure fluctuations on the ground beneath a turbulent boundary layer," Nat. Bur. Stds. Rpt. 8942, Nat. Bur. Stds., 1-92, 1965.

Putnam, J. A. and J. W. Johnson, "The dissipation of wave energy by bottom friction," Trans. Amer. Geophys. Union, 30, 67-74, 1949.

Resio, D. T., "The estimation of wind wave generation in a discrete model," J. Phys. Oceanogr. vol 11, pp. 510-525, 1981.

Richtmyer, R. O. and K. W. Morton, "Difference Methods for initial-value problems," Wiley(Interscience), New York, 1967.

Shiau, J. C. and H. Wang, "Wave energy transformation over irregular bottom," J. Waterways, Port, coastal and Ocean Div., ASCE, 103(WW1), 57-68,

1977.

Snodgrass, F. E., G. W. Groves, K. F. Hasselmann, G. R. Miller, W. H. Munk and W. H. Powers, "Propagation of ocean swell across the Pacific," Phil. Trans. Roy. Soc., London A, 259, NO. 1103, 431-497, 1966.

Snyder, R. L. and C. S. Cox, "A field study of the wind generation of ocean waves," J. Mar. Res., 24, NO. 2, 141-178, 1966.

Stoker, J. J., "Surface waves in water of variable depth," Quarterly of Appl. Math., Vol. 5, 1-54, 1947.

Thornton, E. B., "Rederivation of the saturation range in the frequency spectrum of wind generated gravity waves," J. Phys. Oceanogr., Vol. 7, 137-140, 1977.

Van Ieperen, M. P., "The bottom friction of the sea-bed off Melkbosstrand, South Africa: a comparison of a quadratic with a linear friction model," Dtsch. Hydrogr. Zr., 28, 72-88, 1975.

Vincent, I. R., et al., "Depth limited significant wave height," CERC Misc. Rep., in press, 1981.

Vincent, L. V., "Shallow-water wave modeling," 1st Int. Conf. on met. and air-sea interaction in the coastal zone, Hague, May 1982.

Wang, H., H. H. Dette and Y. H. Chen, "nearshore data from North Sea during MARSEN I September - December, 1979," Ocean Eng. Rep. No. 24, Dept. of Civil Eng., Univ. of Delaware, Dec. 1980.

Wang, H. and W. C. Yang, "Wave spectral transformation measurements at Sylt, North Sea," Coastal Eng., Vol. 5, 1-34, 1981.

Yang, C. Y. and Y. H. Chen, "Transformation of random wave spectrum on beaches," J. the Eng. Mech. Div., Vol. 105, No. Em4, 1979.

Distribution

Office of Naval Research
Coastal Science Program
Code 42205
Arlington, VA 22217

Defense Documentation Center
Cameron Station
Alexandria, VA 22314

Director, Naval Research Lab.
ATTN: Technical Information Officer
Washington, D. C. 20375

Director
Office of Naval Research Branch Office
1030 East Green Street
Pasadena, CA 91101

Chief of Naval Research
Code 100M
Office of Naval Research
Arlington, VA 22217

Office of Naval Research
Operational Applications Division
Code 200
Arlington, VA 22217

Office of Naval Research
Scientific Liaison Officer
Scripps Institution of Oceanography
La Jolla, CA 92093

Director Naval Research Laboratory
ATTN: Library, Code 2628
Washington, D. C. 20375

ONR Scientific Liaison Group
American Embassy - Room A-407
APO San Francisco, CA 96503

Commander
Naval Oceanographic Office
ATTN: Library, Code 1600
Washington, D. C. 20374

Naval Oceanographic Office
Code 3001
Washington, D. C. 20374

Chief of Naval Operations
OP 987P1
Department of the Navy
Washington, D. C. 20350

Oceanographer of the Navy
Hoffman II Building
200 Stovall Street
Alexandria, VA 22322

Naval Academy Library
U. S. Naval Academy
Annapolis, MD 21402

Commanding Officer
Naval Coastal Systems Laboratory
Panama City, FL 32401

Director
Coastal Engineering Research Center
U. S. Army Corps of Engineers
Kingman Building
Fort Belvoir, VA 22060

Officer in Charge
Environmental Research Prodctn Felty.
Naval Postgraduate School
Monterey, CA 93940

Director
Amphibious Warfare Board
U. S. Atlantic Fleet
Naval Amphibious Base
Norfolk, Little Creek, VA 23520

Commander, Amphibious Force
U. S. Pacific Fleet
Force Meteorologist
Comphibpac Code 25 5
San Diego, CA 93155

Librarian, Naval Intelligence
Support Center
4301 Suitland Road
Washington, D. C. 20390

Commanding Officer
Naval Civil Engineering Laboratory
Port Hueneme, CA 93041

Chief, Wave Dynamics Division
USAE-WES
P. O. Box 631
Vicksburg, MS 39180

Commandant
U. S. Coast Guard .
ATTN: GECV/61
Washington, D. C. 20591

Office of Research and Development
%DS/62
U. S. Coast Guard
Washington, D. C. 20591

National Oceanographic Data
Center %D764
Environmental Data Services
NOAA
Washington, D. C. 20235

Prof. Dr. Fuehrboeter
Lehrstuhl F. Hydromechanik U. Kuestenw
Technische Hochschule Braunschweig
Beethovenstrasse 51A
D-3300 Braunschweig, West Germany

Prof. Dr. Walter Hansen
Direktor D. Instituts F. Meereskunde
Universitaet Hamburg
Heimhuderstrasse 71
D-2000 Hamburg 13, West Germany

Prof. Dr. Klaus Hasselmann
Institut F. Geophysik
Universitaet Hamburg
Schleuterstrasse 22
D-2000 Hamburg 13, West Germany

Coastal Studies Institute
Louisiana State University
Baton Rouge, LA 70803

Dr. Edward Thornton
Department of Oceanography
Naval Postgraduate School
Monterey, CA 93940

Dr. Douglas I. Inman
University of California A-009
Shore Processes Laboratory
La Jolla, CA 92093

Dr. Bruce Heyden
Dept. of Environmental Sciences
University of Virginia
Charlottesville, VA 22903

SECURITY CLASSIFICATION OF THIS PAGE (When Data Entered)

REPORT DOCUMENTATION PAGE		READ INSTRUCTIONS BEFORE COMPLETING FORM
1. REPORT NUMBER ONR TR No. 10	2. GOVT ACCESSION NO.	3. RECIPIENT'S CATALOG NUMBER
4. TITLE (and Subtitle) Wave Spectral Transformation in Shallow Water		5. TYPE OF REPORT & PERIOD COVERED Technical 6. PERFORMING ORG. REPORT NUMBER
7. AUTHOR(s) Yun-Hai Chen and Hsiang Wang		8. CONTRACT OR GRANT NUMBER(s) N00014-81-K-0297
9. PERFORMING ORGANIZATION NAME AND ADDRESS		10. PROGRAM ELEMENT, PROJECT, TASK AREA & WORK UNIT NUMBERS
11. CONTROLLING OFFICE NAME AND ADDRESS		12. REPORT DATE June 1982 13. NUMBER OF PAGES 147
14. MONITORING AGENCY NAME & ADDRESS(if different from Controlling Office)		15. SECURITY CLASS. (of this report) 15a. DECLASSIFICATION/DOWNGRADING SCHEDULE

16. DISTRIBUTION STATEMENT (of this Report)

This report has been approved for public release and sale, its distribution is unlimited.

17. DISTRIBUTION STATEMENT (of the abstract entered in Block 20, if different from Report)

18. SUPPLEMENTARY NOTES

19. KEY WORDS (Continue on reverse side if necessary and identify by block number)

Wave spectral transformation, wave refraction, wave shoaling, wave breaking, wave generation, wave dissipation

20. ABSTRACT (Continue on reverse side if necessary and identify by block number)

A numerical model was developed to compute the shallow water wave spectral transformation for the stationary and non-stationary cases. The physical processes simulated in the model are wave refraction and shoaling computed by conservation of energy flux considerations, and wind generation, bottom dissipation and wave breaking computed by source and sink mechanisms. The results of the numerical modeling were compared with data from the North Sea.

DD FORM 1 JAN 73 1473 EDITION OF 1 NOV 65 IS OBSOLETE

Unclassified

SECURITY CLASSIFICATION OF THIS PAGE (When Data Entered)